# 学位論文

# Design of an anti-cancer drug screening model combined with three-dimensional cell culture and drug release system

（3 次元細胞培養と薬物放出システムを組み合わせた抗がん剤スクリーニングモデルの創製）

2021 年 3 月

新居　輝樹

# CONTENTS

## Abbreviation

| | |
|---|---|
| 2D | Two-Dimensional |
| 3D | Three-Dimensional |
| A | Adenosine |
| αMEM | Alpha Minimum Essential Medium |
| α-SMA | Alpha-Smooth Muscle Actin |
| CAF | Cancer-Associated Fibroblasts |
| DDS | Drug Delivery System |
| DDW | Double-Distilled Water |
| ECM | Extracellular Matrix |
| ELISA | Enzyme-Linked Immunosorbent Assay |
| EMT | Epithelial-Mesenchymal Transition |
| FCS | Fetal Calf Serum |
| GM | Gelatin Hydrogel Microspheres |
| HPLC | High Performance Liquid Chromatography |
| LPS | Lipopolysaccharide |
| MEM | Minimum Essential Medium |
| MMP | Matrix Metalloproteinase |
| MSC | Mesenchymal Stem Cells |
| PBS | Phosphate Buffered-Saline |
| PFT | Pifithrin-Alpha |
| PLGA | Poly (Lactic-*Co*-Glycolic Acid) |
| PVA | Poly (Vinyl Alcohol) |
| RPMI 1640 | Roswell Park Memorial Institute Medium-1640 |
| RT-PCR | Real-Time Polymerase Chain Reaction |
| TAM | Tumor-Associated Macrophages |

| | |
|---|---|
| TGF-β1 | Transforming Growth Factor-β1 |
| VEGF | Vascular Endothelial Growth Factor |

# Chapter 1
# General introduction

## 1.1. The concept of regenerative medicine

The basic concept of regenerative medicine is to achieve the regeneration and repairing of damaged or injured tissues by utilizing the natural healing potential of the body itself. Regenerative medicine consists of regenerative therapy and regenerative research. Regenerative therapy is to treat patients through the *in vivo* enhancement of cell activity which physiologically bases on the natural healing potential. Regenerative research is positioned as the scientific support for the regeneration therapy of the next generation. Drug discovery is defined as regenerative research. The therapeutic efficacy, metabolism, or toxicology of drugs are efficiently evaluated by taking advantage of activated cells [1]. To enhance cell activity, two methodologies have been recently noted. One is to utilize three-dimensional (3D) cell culture technologies. Cells are usually cultured in a two-dimensional (2D) system, with a plate or dish. However, the functions of cells cultured in the 2D system are lower than those of body cells because cells tend to interact with each other for the enhancement of their own activities in the body [2-5]. Due to the difference in the cell condition, the drug effect evaluated by the *in vitro* drug screening is not always the same as that in the pre-clinical or clinical study, which leads to the failure of drug research and development [6, 7]. The comparison of cancer cell culture between 2D and 3D systems is shown in Table 1.1.

Table 1.1. Comparison of cancer cells culture between 2D and 3D systems

| Points compared | Culture system | |
|---|---|---|
| | 2D | 3D |
| Cost | Low | High |
| Cell proliferation | High | Low |
| Cell differentiation | Low | High |
| Reproducibility | Good | Poor |
| *In vivo* imitation | Limited | Versatile |
| Cell-cell interaction | Low | High |
| Cell morphology change | Low | High |
| Diverse polarity | Loss | Diverse |
| ECM synthesis | Low | High |
| Drug sensitivity | High (in contrast to *in vivo*) | Low (Same as *in vivo*) |

The other methodology to enhance cell functions is the active utilization of biomaterials. Cell culture is often performed on the dish or plate which is mainly composed of polystyrene. This condition of an artificial environment is quite different from the *in vivo* body environment of cancer cells, and consequently, the drug effect or cytotoxicity evaluation is technologically limited. Biomaterials that are composed of cell-friendly

components are effective in enhancing cell activity or functions. The interaction with biomaterials will enable cells to enhance their proliferation, differentiation, and biological functions, leading to the realization of cancer cell-environment interaction. Biomaterials classify into natural biomaterials derived from animals or plants and synthetic biomaterials artificially prepared. Natural biomaterials are composed of polysaccharide (amylose, cellulose, alginate, chitosan, or hyaluronic acid), peptide (collagen or gelatin), nucleic acid, or polyhydroxyalkanoates. Since the degradative enzyme and metabolic system have already existed in the body, most natural biomaterials can enzymatically be degraded. Because the components constitute the cancer environment as the ECM and contribute to cancer diseases, natural biomaterials are often used to design the 3D culture system of cancer cells. Although natural biomaterials are of high biocompatible, there are some limitations of immunogenicity or homogeneity to use. To avoid the issues, synthetic biomaterials are used. Synthetic biomaterials are mainly degraded non-enzymatically based on simple hydrolysis. There are some merits of synthetic biomaterials, such as the characteristics control, the high stiffness, and the clarity of properties.

## 1.2. Purposes and contents of this study

In this study, 3D cell aggregates combined with biomaterials were prepared for drug screening. Among the biomaterials, gelatin hydrogel microspheres (GM) were used. GM incorporation into the cell aggregates allows cells to supply oxygen and nutrients because a water phase of GM matrices is a pathway to permeate oxygen or nutrients.

Chapter 2 is a section on the optimization of the mixing ratio of cells and GM. Because the number of microspheres would be one of the most important factors contributing to the oxygen and nutrient permeation for cell aggregates. Shaking culture methods are also often introduced in cell culture to improve the cell viability and functions because the oxygen and nutrient permeation is expected by the dynamic motion of the medium. Here, the influence of the two factors, the shaking culture, and the amount of GM, on the biological functions of cell aggregates were evaluated. At the smaller ratio of microspheres to cells, the viability of cell aggregates under the shaking culture was significantly higher than that of static culture. On the other hand, there was no significant difference in the viability between them at a higher ratio. GM are enabled to enhance ATP and mitochondrial activities of cell aggregates under the shaking culture. The effect was high at the smaller microspheres/cells ratio. It is concluded that the shaking culture was promising to allow cells to enhance their activities.

Chapter 3 is the design of a cancer invasion model based on an interaction between cancer cells and 3D cancer-associated fibroblasts (CAF) aggregates. The strength of this study is to incorporate GM containing pifithrin-α (PFT) of a p53 inhibitor (GM-PFT) with the CAF aggregates. When the cancer cells were co-cultured with the CAF aggregates incorporating GM-PFT, the invasion rate of cancer cells was

significantly high compared with CAF aggregates or CAF aggregates incorporating GM with or without the same dose of free PFT as well as two-dimension cultured CAF with or without the same does of PFT. Besides, an inhibitor of matrix metalloproteinase decreased the cancer invasion rate for the CAF aggregates incorporating GM-PFT. It is concluded that the interaction between cancer cells and CAF aggregates incorporating GM-PFT of biological activation needs to realize the invasion of cancer cells even *in vitro*. This study is the first report to create an invasion model *in vitro* by taking advantage of a combined 3D culture system and the DDS technology.

Chapter 4 is the design of a cancer invasion model where the cancer invasion rate can be regulated *in vitro*. CAF aggregates incorporating GM containing various concentrations of transforming growth factor-β1 (TGF-β1) (CAF-GM-TGF-β1) were prepared. The expression level of alpha-smooth muscle actin (α-SMA) for CAF increased with an increase in the TGF-β1 concentration. When co-cultured with various types of CAF-GM-TGF-β1, the cancer invasion rate was well correlated with the α-SMA level. It is conceivable that the TGF-β1 concentration could modify the level of CAF activation, leading to the invasion rate of cancer cells. In addition, at the high concentrations of TGF-β1, the effect of a matrix metalloproteinase (MMP) inhibitor on the cancer invasion rate was observed. The higher invasion rate would be achieved through higher MMP production. The present model is promising to realize the cancer invasion whose rate can be modified by changing the TGF-β1 concentration.

Chapter 5 is the design of a cancer invasion model by making use of CAF or tumor-associated macrophages (TAM) and GM for the sustained release of drugs. The GM containing adenosine (A) (GM-A) were prepared and cultured with TAM to obtain 3D TAM aggregates incorporating GM-A

(3D TAM-GM-A). When co-cultured with HepG2 liver cancer cells in an invasion assay, the 3D TAM-GM-A promoted the invasion rate of cancer cells. In addition, the E-cadherin expression level decreased to a significantly great extent compared with that co-cultured with TAM aggregates incorporating GM, whereas the significantly higher expression of N-cadherin and Vimentin was observed. This indicates that the epithelial-mesenchymal transition event was induced. Following a co-culture of mixed 3D CAF-GM-TGF-β1 and 3D TAM-GM-A and every HepG2, MCF-7 breast cancer cells, or WA-hT lung cancer cells, the invasion rate of every cancer cells enhanced depending on the mixing ratio of 3D TAM-GM-A and 3D CAF-GM-TGF-β1. This model is a promising 3D culture system to evaluate the invasion ability of various cancer cells *in vitro*.

# Chapter 2
# Influence of shaking culture on the biological functions of cell aggregates incorporating gelatin hydrogel microspheres

## 2.1. Introduction

Cells are often cultured in two-dimensional (2D) systems such as a dish or plate, and the 2D culture systems are known as conventional cell culture. It is easy to culture and to observe cells under the 2D systems. However, the 2D cell culture systems are not suitable for researches of cell proliferation, cell differentiation, regenerative medicine, and drug discovery because the 2D systems are quite different from the inner body and the local environment. In the body tissues, most cells tend to form cell aggregates, resulting in enhanced cell differentiation [2], metabolic activity [3], cell-cell interaction [4], and production of extracellular matrix proteins [5]. Therefore, recently, the development of three-dimensional (3D) cell culture technologies has been reported to mimic the local environment of cells in living tissues [8-11]. However, there are some disadvantages of the 3D cell culture systems. For example, little oxygen and nutrients are supplied to cells present in the center of cell aggregates during the growth of cell aggregates, resulting in cell death. Therefore, it is impossible to culture cell aggregates over a long time period because of cell death [12, 13]. However, to investigate cell proliferation or differentiation, it is necessary to culture cell aggregates over a long time period. To tackle this serious problem, cell aggregates incorporating hydrogel materials have been developed, resulting in protected cells aggregated from the lack of oxygen and nutrients in the long-term culture [14]. Gelatin, which is recognized as a biodegradable biomaterial, is used for many fields such as medical, pharmaceutical, and

cosmetic applications [15-35]. In this study, gelatin was selected because it is easy to form a hydrogel and its biosafety has been proven [15].

Shaking culture methods are often used in cell culture to enhance biological functions such as improvement of cell availability [36], promotion of bone proliferation from mesenchymal stem cells (MSC) [37], and release of more types of proteins from MSC [38]. Because the shaking culture methods supply more oxygen and nutrients to cells compared with the static culture methods. However, the influence of shaking culture on the biological functions of cell aggregates incorporating gelatin hydrogel microspheres has been never investigated. The objective of this study is to investigate the influence of shaking culture on the biological functions of cell aggregates. Following MC3T3-E1 cells were cultured with gelatin hydrogel microspheres at different mixing ratios of microspheres/cells under the static or shaking culture, the sizes, morphologies, ATP, mitochondrial activities, and oxygen concentration of cell aggregates were evaluated.

## 2.2. Methods

### 2.2.1. Preparation of gelatin hydrogel microspheres

Gelatin hydrogel microspheres (GM) were prepared by the chemical crosslinking of gelatin in a water-in-oil emulsion state according to the method previously reported [27]. Briefly, an aqueous solution (20 ml) of 10 wt % gelatin (isoelectric point 5.0, weight-averaged molecular weight = 100,000, Nitta Gelatin Inc., Osaka, Japan) was preheated at 40 ºC, followed by stirring at 300 rpm for 10 min to prepare the water-in-oil emulsion. The emulsion temperature was decreased at 4 ºC for the natural gelation of gelatin solution to obtain non-crosslinked hydrogel microspheres. The resulting gelatin hydrogel microspheres were washed three times with cold acetone in combination with centrifugation (5,000 rpm, 4 ºC, 5 min) to completely exclude the residual oil. Then, GM were fractionated by size using sieves with apertures of 32 and 53 μm (Iida Seisakusho Ltd, Osaka, Japan) and air dried at 4 ºC. Then, non-crosslinked and dried GM (200 mg) were treated in a vacuum oven at 140 ºC to allow to dehydrothermally crosslink for 72 hr. The picture of GM in the swollen state was taken with a microscope (BZ-X710, KEYENCE Ltd, Osaka, Japan). The size of 100 microspheres for each sample was measured using the computer program Image J (NIH Inc., Bethesda, USA) to calculate the average diameters.

### 2.2.2. Cell culture experiments

MC3T3-E1 cells of a pre-osteoblast line derived from mouse (KAC Co., Ltd., Kyoto, Japan) were cultured in alpha minimum essential medium (αMEM) (Invitrogen Inc., Carlsbad, USA) supplemented with 10 vol % fetal calf serum (FCS) (Thermo Inc. Waltham, USA), penicillin (50 U/mL), and streptomycin (50 U/mL) (standard medium) and cultured at 37 ºC in a 95 %

air - 5 % carbon dioxide atmosphere. The culture medium was changed every 2 days and the confluent cells were subcultured through trypsinization.

2.2.3. Preparation of cell aggregates incorporating various amounts of gelatin hydrogel microspheres and their culture under shaking or static culture

A poly (vinyl alcohol) (PVA) sample (the degree of polymerization = 1,800 and the saponification = 88 mole %) kindly supplied from Unichika (Tokyo, Japan) was dissolved in phosphate-buffered solution (PBS) (pH 7.4, 1wt %). The PVA solution was added to each well of the round-bottomed (U-bottomed) 96-well culture plate (100 μl/well) and incubated at 37 ºC for 15 min. Then, the solution was removed by aspiration and the wells washed twice with PBS (100 μl/well). Gelatin microspheres dehydrothermally crosslinked for 72 hr and MC3T3-E1 cells were separately suspended in the standard medium. After the suspensions of GM (0 or $1\times10^3$, $2\times10^3$, $3\times10^3$, and $4\times10^3$ microspheres/ml, 50 μl) and cell suspensions ($2\times10^4$ cells/ml, 100 μl) were mixed, the mixture was added to the wells coated. After 2 days (cell aggregates were formed), some samples were cultured by an orbital shaker (Bellco, Inc. California, USA) at 30 rpm until over the periods of 21 days, and then the medium was changed on the first day and every 3 days until the end of experiments. Experiments for each sample were performed three wells independently unless otherwise mentioned.

2.2.4. Morphologies and size of cell aggregates incorporating various amounts of gelatin hydrogel microspheres under shaking or static culture

To investigate the influence of the amounts of GM incorporated under

the shaking culture on the morphologies and size of cell aggregates in the long-term culture, the morphologies and the size of cell aggregates were evaluated. The pictures of cell aggregates without GM or with various amounts of GM incorporated under the shaking or static culture were taken with a microscope (CKX41, Olympus Ltd, Tokyo, Japan). The size of cell aggregates was measured using the computer program Image J (NIH Inc., Bethesda, USA) to calculate the average diameter.

2.2.5. Evaluation of ATP activity of cell aggregates under shaking or static culture

The ATP activity of cell aggregates was determined by using KATAMARI ATP assay kit TM (FUJIFILM Wako Pure Chemical Co. Ltd, Osaka, Japan) 7, 14, and 21 days after incubation.

2.2.6. Evaluation of mitochondrial activity of cell aggregates under shaking or static culture

At different time intervals, cell aggregates were taken into 2 ml of the tube, and 400 µl of the medium was added. Then, 40 µl of WST-8 [2-(2-methoxy-4-nitrophenyl)-3-(4-nitrophenyl)-5-(2,4-disulfophenyl)-2H-tetrazolium, monosodium salt] (Nacalai tesque Inc, Kyoto, Japan) was added to each tube, and the tubes were incubated for further 4 hr to allow the mitochondria of cells to reduce the yellow MTT into dark-blue formazan crystals. The absorbance of individual wells (100 µl) was measured at 450 nm using a microplate reader (F-2000, HITACHI Ltd, Tokyo, Japan). The mitochondrial activity per cell of cell aggregates was calculated as the mitochondrial activity per cell of cell aggregates without GM 7 days after incubation under the static culture of 1.

2.2.7. Measurement of oxygen concentration of cell aggregates under shaking or static culture

The oxygen concentration of cell aggregates incorporating GM was measured by using an $O_2$ sensor probe (Fibox4, TITEC Co., Saitama, Japan). Cell aggregates 14 days after incubation were sensed by the sensor probe (the diameter of 200 μm) as carefully as possible not to break or miss cell aggregates (on the dish), and then oxygen concentration was measured. One unit of cell aggregates was used per the measurement.

2.2.8. Statistical analysis

All the statistical data were expressed as the mean ± standard error of the mean (SEM). The data were analyzed by t-test or Tukey's test to determine the statistical significance of difference between experimental results which was accepted at the $p$ value of $<0.05$.

## 2.3. Results

### 2.3.1. Characterization of gelatin hydrogel microspheres

Figure 2.1 shows the microscopic pictures of GM. The GM were spherical and had a smooth surface. The size of microspheres in the swollen condition was 50.5 ± 6.7 μm.

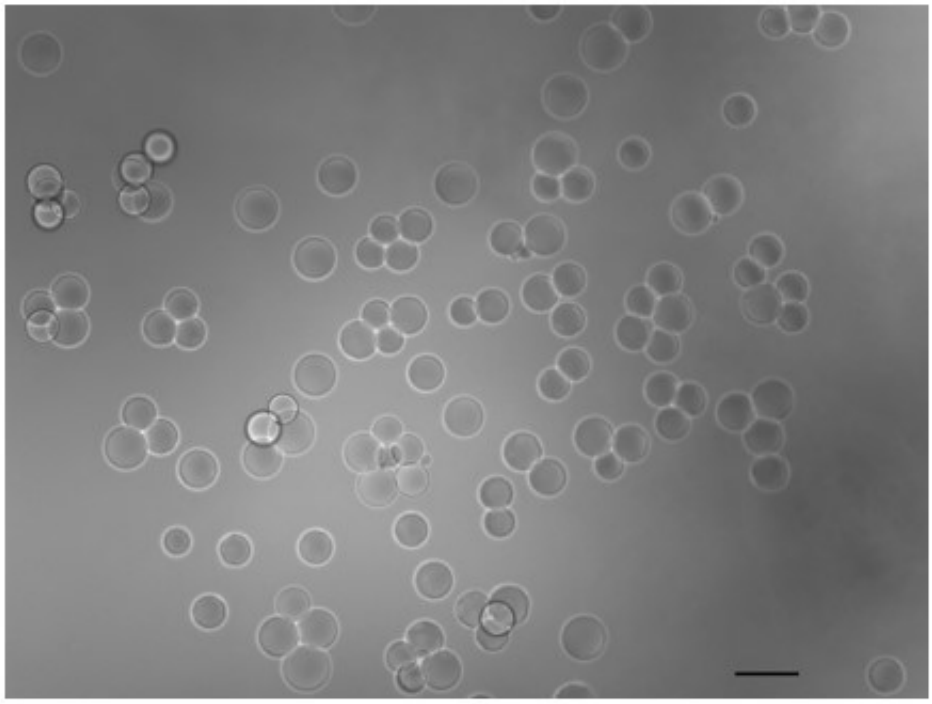

Figure 2.1. Microscopic picture of GM dispersed in water. The GM were dehydrothermally crosslinked for 72 hr at 140 ºC. Scale bar; 100 μm.

### 2.3.2. Culture of cell aggregates incorporating various amounts of gelatin hydrogel microspheres under shaking or static culture

Figures 2.2A-E shows that the light microscopic pictures of MC3T3-E1 cell aggregates 7, 14, and 21 days after incubation with various amounts of GM incorporated under the shaking or static culture. Figure 2.2F shows the size of cell aggregates 7, 14, and 21 days after incubation without GM or with various amounts of GM incorporated. The size of cell aggregates

increased upon increasing the amount of GM in the cell aggregates. At the same amount of GM, the size of cell aggregates did not change, irrespective of the culture condition. However, the size of cell aggregates incorporating GM 21 days after incubation was small compared with that 7 and 14 days. GM looked to be present in the cell aggregates 60 days after incubation (data not shown).

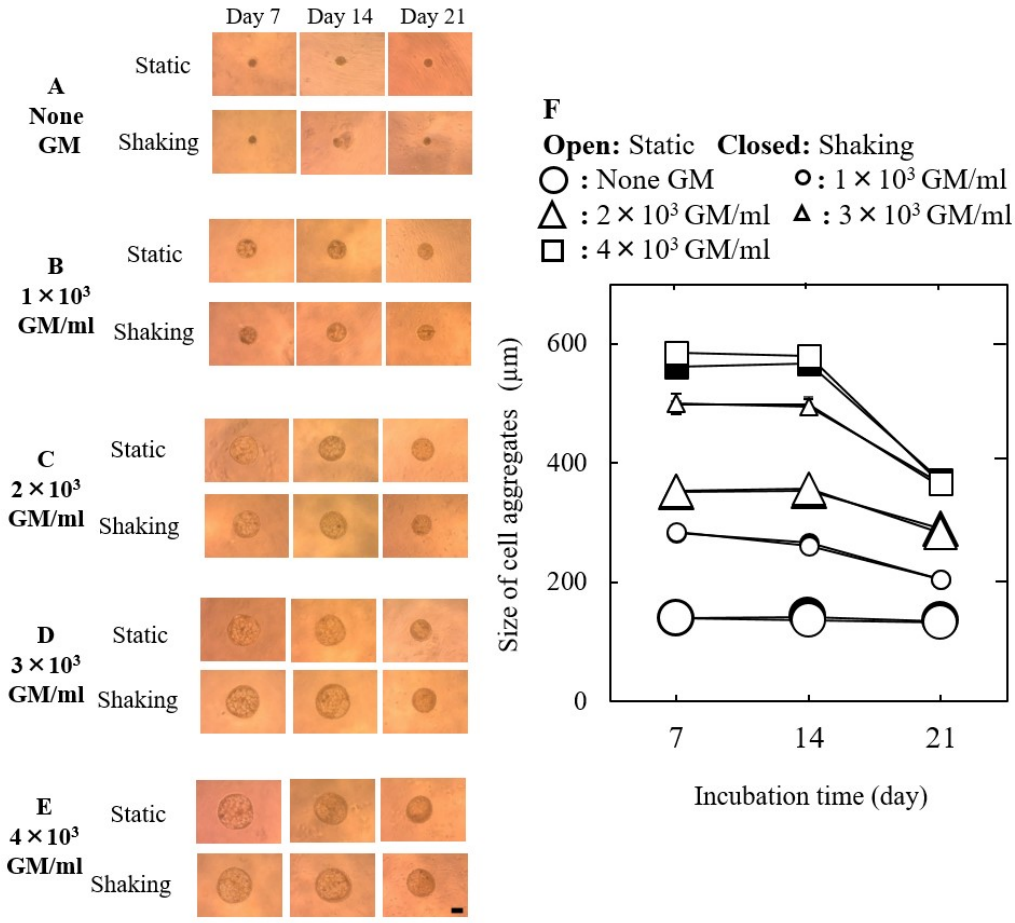


Figure 2.2. Light microscope pictures of MC3T3-E1 cell aggregates 7, 14, and 21 days after incubation without GM (A) or with $1\times10^3$(B), $2\times10^3$(C), $3\times10^3$(D), and $4\times10^3$ GM/ml (E) under the static culture or shaking culture. Scale bar; 200 μm. (F) The sizes of MC3T3-E1 cell aggregates 7, 14, and 21 days after incubation without GM (○, bigger size) and incorporating $1\times10^3$

(○, smaller size), $2\times10^3$ (△, bigger size), $3\times10^3$ (△, smaller size), and $4\times10^3$ GM/ml (□) under the static culture, or without GM (●, bigger size) and with $1\times10^3$ (●, smaller size), $2\times10^3$ (▲, bigger size), $3\times10^3$ (▲, smaller size), and $4\times10^3$ GM/ml (■) under the shaking culture.

2.3.3. ATP activity of cell aggregates incorporating gelatin hydrogel microspheres under shaking or static culture

Figure 2.3 shows the ATP activity of cell aggregates 7, 14, and 21 days after incubation with various amounts of GM under the shaking or static culture. When cell aggregates incorporating 0 or $1\times10^3$ and $2\times10^3$ microspheres/ml of GM were prepared, the ATP activity of cell aggregates 7, 14, and 21 days after incubation under the shaking culture was higher than that under the static culture (Figures 2.3A-3C). However, when cell aggregates incorporating $3\times10^3$ and $4\times10^3$ microspheres/ml of GM were prepared, the ATP activity was not significantly different from that under the static culture, irrespective of the culture period (Figures 2.3D and 2.3E). In addition, the ATP activity of cell aggregates incorporating $3\times10^3$ and $4\times10^3$ microspheres/ml of GM 21 days after incubation was low compared with that 7 and 14 days later (Figures 2.3D and 2.3E). Moreover, the ATP activity of cell aggregates incorporating GM was much higher than that of GM-Free culture (Figure 2.3F).

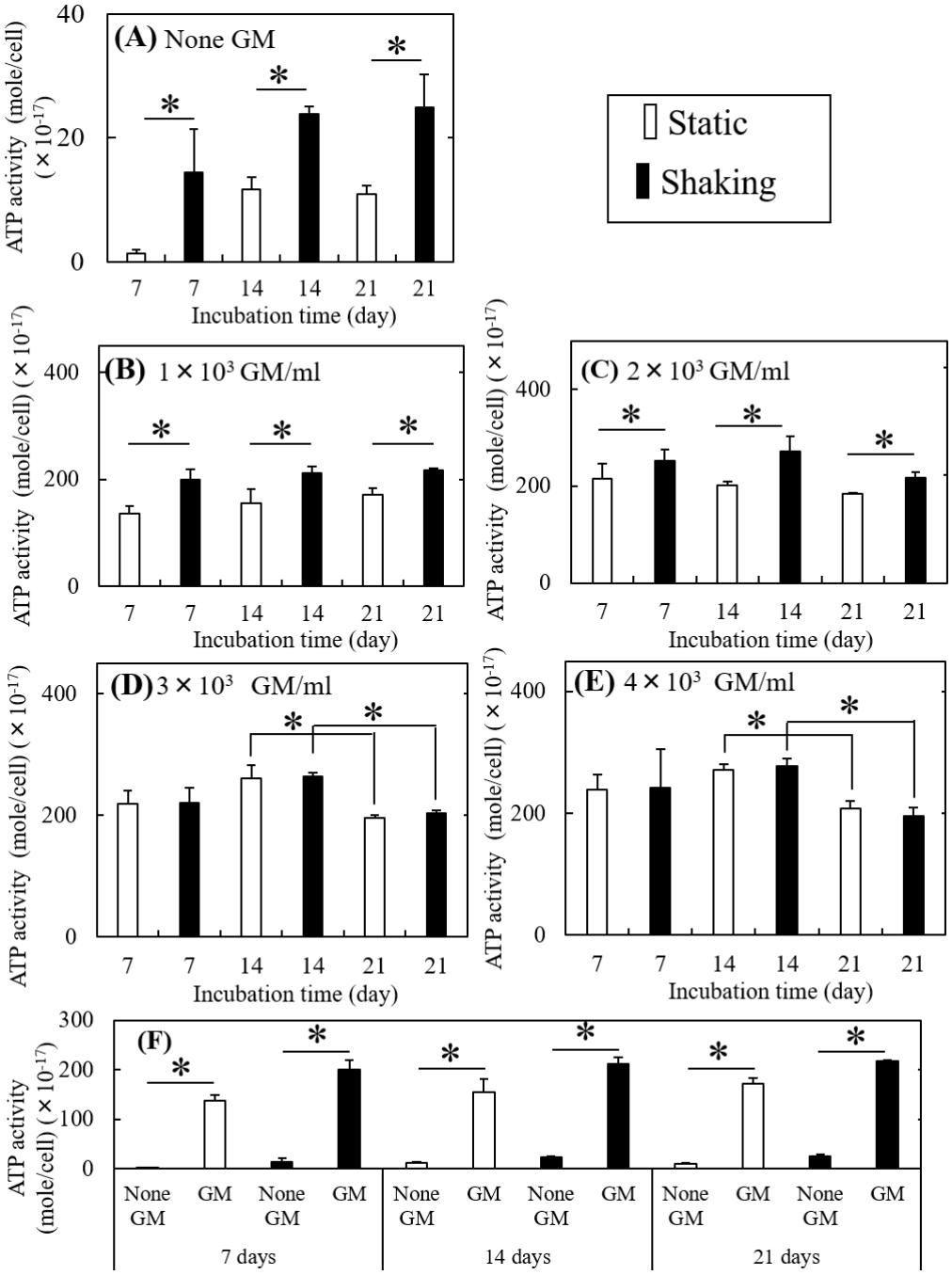


Figure 2.3. ATP activity of MC3T3-E1 cells in cell aggregates without (A) or with 1 × $10^3$ (B), 2 × $10^3$ (C), 3 × $10^3$ (D), and 4 × $10^3$ GM/ml (E) of GM 7, 14, and 21 days after incubation under the static (□) or shaking culture (■). $p < 0.05$; significant against ATP activity between the two groups. (F) ATP activity of MC3T3-E1 cells in cell aggregates without or with

$1 \times 10^3$ GM/ml of GM 7, 14, and 21 days after incubation under the static (□) or shaking culture (■). $p < 0.05$; significant against ATP activity between the two groups.

2.3.4. Mitochondrial activity of cell aggregates incorporating gelatin hydrogel microspheres under shaking or static culture

Figure 2.4 shows the mitochondrial activity of cell aggregates 7, 14, and 21 days after incubation with various amounts of GM under the shaking or static culture. The tendency was similar to that of ATP activity (Figure 2.3A-2.3E). When cell aggregates incorporating 0 or $1\times10^3$ and $2\times10^3$ microspheres/ml of GM were prepared, the mitochondrial activity of cell aggregates 7, 14, and 21 days after incubation under the shaking culture was higher than that under the static culture (Figures 2.4A-2.4C). However, when cell aggregates incorporating $3\times10^3$ and $4\times10^3$ microspheres/ml of GM were prepared, the mitochondrial activity of cell aggregates was not significantly different from that under the static culture, irrespective of the culture period (Figures 2.4D and 2.4E). Moreover, the mitochondrial activity of cell aggregates incorporating $4\times10^3$ microspheres/ml of GM 21 days after incubation was low compared with that 7 and 14 days later (Figure 2.4E). However, the mitochondrial activity of cell aggregates incorporating GM was not always higher than that of GM-free culture (Figure 2.4F).

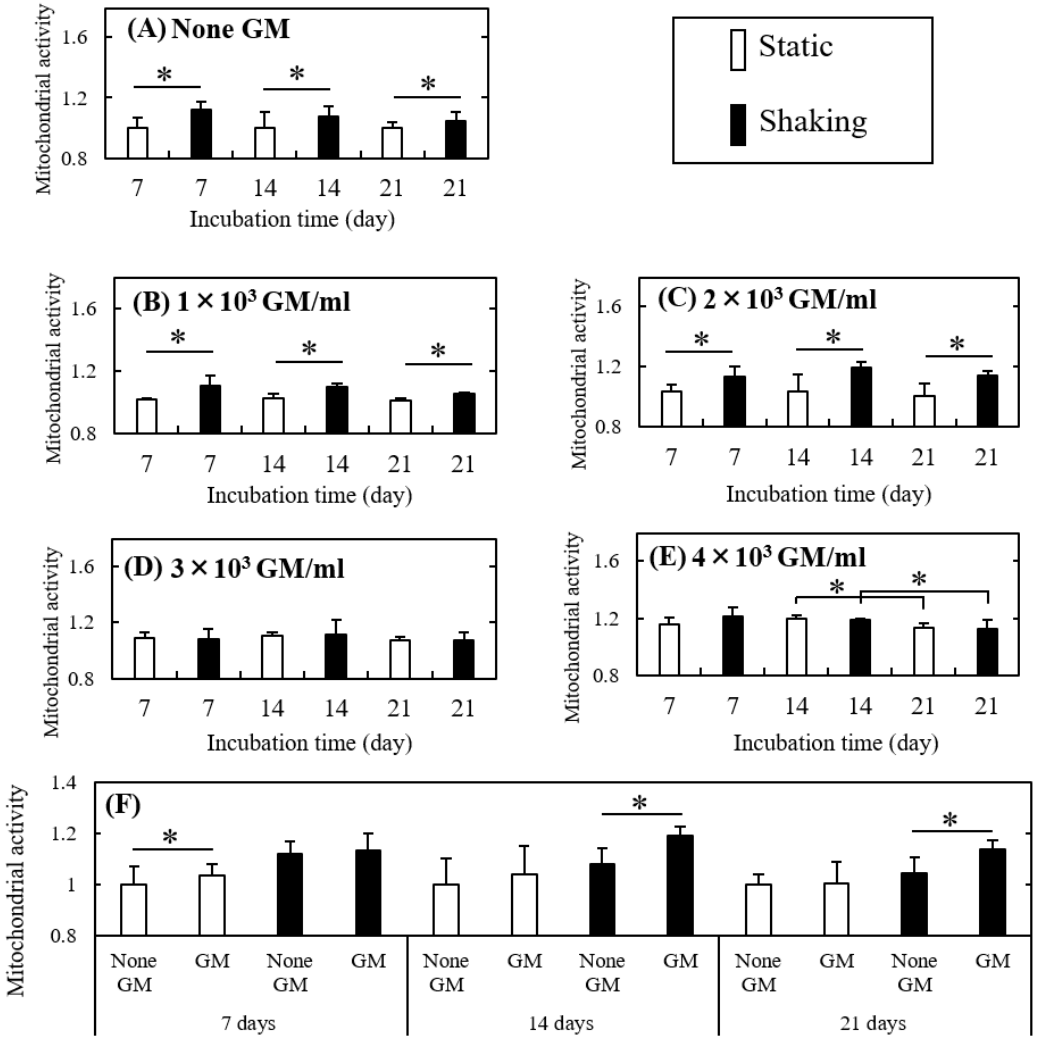


re 2.4. Mitochondrial activity of MC3T3-E1 cells in cell aggregates without (A) or with 1 × $10^3$ (B), 2 × $10^3$ (C), 3 × $10^3$ (D), and 4 × $10^3$ GM/ml (E) of GM 7, 14, and 21 days after incubation under the static (□) or shaking culture (■). $p < 0.05$; significant against mitochondrial activity between the two groups. (F) Mitochondrial activity of MC3T3-E1 cells in cell aggregates without or with 2 × $10^3$ GM/ml of GM 7, 14, and 21 days after incubation under the static (□) or shaking culture (■). $p < 0.05$; significant against mitochondrial activity between the two groups.

2.3.5. The oxygen concentration of cell aggregates incorporating gelatin hydrogel microspheres under shaking or static culture

Figure 2.5 shows that the relative oxygen concentration of the cell aggregates incorporating $1\times10^3$ (A) and $4\times10^3$ (B) microspheres/ml of GM 14 days after incubation under the shaking or static culture. The oxygen concentration of cell aggregates incorporating $1\times10^3$ microspheres/ml of GM 14 days after incubation under the shaking culture was higher than that under the static culture (Figure 2.5A). However, the oxygen concentration of cell aggregates incorporating $4\times10^3$ microspheres/ml of GM under the shaking culture was not significantly different from that under the static culture (Figure 2.5B).

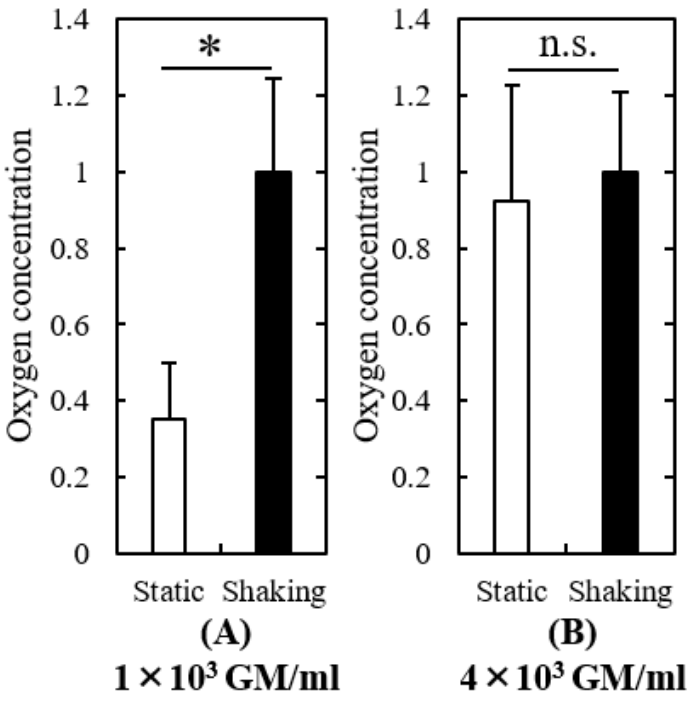


Figure 2.5. Relative oxygen concentration of MC3T3-E1 cell aggregates incorporating $1 \times 10^3$ (A) and $4 \times 10^3$ GM/ml (B) of GM 14 days after incubation under the static (□) or shaking culture (■). $p < 0.05$; significant against oxygen concentration between the two groups.

## 2.4. Discussion

Gelatin hydrogel microspheres (GM) enable the cells to improve their viability and functions in cell aggregates. Preparation of cell aggregates incorporating microspheres such as gelatin, poly (lactic-co-glycolic acid) (PLGA), and alginate has been reported [16, 18, 39-41]. Among these materials, in this study, gelatin was selected because of a cell adhesion ability. In addition, the oxygen and nutrient permeation through the water phase of gelatin hydrogel microspheres is expected [41]. Among the properties of the microspheres, the mixing ratio of microspheres to cells was focused because the number of microspheres would be one of the most important factors contributing to the oxygen and nutrient permeation for cell aggregates. Shaking culture methods are also often introduced in cell culture to improve the cell viability and functions because the oxygen and nutrient permeation is expected by the dynamic motion of the medium [36-38]. Here, the influence of the two factors, the shaking culture, and GM, on the biological functions of cell aggregates were evaluated.

In the previous study, the GM incorporation for MCT3T3-E1 cell aggregates was characterized to optimize [41]. In this study, the effect of culture procedures on the functions was evaluated. Therefore, the same MC3T3-E1 cell line was used. In this study, the GM with diameters of 32-53 μm were used (Figure 2.1). This is because the size range of GM is demonstrated to be appropriate to form cell aggregates [41]. In addition, the GM dehydrothermally crosslinked for 72 hr were used. The previous study demonstrates that the crosslinking condition was suitable for this purpose although the crosslinking extent of GM increased with an increase in the crosslinking time [41].

Various types of cell aggregates incorporating GM by changing the

mixing ratio of GM to cells under the shaking or static culture were prepared. The cell aggregates were formed only for the U-bottomed well, in contrast to the flat-bottomed one. It is conceivable that a U-shaped bottom well allows cells to accumulate in the center of the well. As a result, the frequency of cell-cell contact would increase, resulting in the better formation of cell aggregates [14]. In addition, cell aggregates with or without the GM incorporation were heavy enough to spontaneously sink the bottom of each well. Even if the shaking was added, only the culture medium would be moved. The number of GM did not significantly affect the formation of cell aggregates. However, cell aggregates were not formed when cells were prepared with more than $4\times10^3$ microspheres/ml of GM (i.e. cells: GM = 10: 1) (data not shown). This proportion would be an upper limit to form cell aggregates incorporating GM because cell-cell interaction would be weaker in the presence of too much GM. In addition, the culture condition (shaking or static culture) did not significantly affect the size and morphologies of cell aggregates incorporating the same number of GM (Figure 2.2). However, the mixing ratio of GM to cells affected the size and morphologies. The increased ratio of GM to cells increased both of them (Figure 2.2). It is possible that considering the amount of GM, the size of cell aggregates is modified. The size of cell aggregates incorporating GM 21 days after incubation was small compared with that 7 and 14 days, irrespective of the number of GM or the culture conditions. GM were seen within cell aggregates clearly 7 and 14 days after incubation, but the frame of GM within cell aggregates 21 days after incubation was unclear because of their degradation (Figures 2.2B-2.2E). The degradation of GM would make the size of cell aggregates smaller. Moreover, it seems that GM existed in cell aggregates 60 days after incubation because the size of cell

aggregates was about 250 μm (> 150 μm: the size of cell aggregates without GM) (data not shown). The results suggest that the GM degradation is one of the important factors to form cell aggregates. For drug discovery or regenerative medicine using cell aggregates for a longer time period, GM with a slower degradation should be used. GM of slower degradation could be prepared for longer time periods of crosslinking [41]. For the drug discovery, cell aggregates for about 2 weeks or longer would need to survive. On the other hand, for the application to tissue regeneration, longer time periods would be needed although it depends on the therapeutic purpose. The time period needed to maintain the functions should be optimized in terms of the application.

ATP and mitochondrial activities of cell aggregates were investigated as a measure of biological functions (Figures 2.3 and 2.4). The amounts of ATP per cell were calculated by dividing the number of cells into cell aggregates. ATP activity is often evaluated as a metabolic level of cells [42]. However, it is suggested that the level of ATP activity does not always indicate the metabolism of mitochondria. The active glycolysis may make ATP activity higher. To evaluate the metabolic functions of cell aggregates, the ATP and mitochondrial activities of cell aggregates were measured. First, when cell aggregates were prepared without GM, the ATP activity was much lower than that of cell aggregates incorporating GM, irrespective of the culture conditions (Figure 2.3F). It is demonstrated that when the amounts of ATP and mitochondrial activities are higher, biological functions are higher [42]. The results strongly support the previous studies. GM enable to facilitate to supply oxygen and nutrients to cells, which leads to making cells alive [14]. However, the mitochondrial activity of cell aggregates incorporating GM was not always high compared with that of aggregates without GM (Figure

2.4F). The reason is not clear at present. Furthermore, when cell aggregates without or with lower amounts of GM ($1\times10^3$ and $2\times10^3$ microspheres/ml) were prepared under the shaking culture, the ATP and mitochondrial activities of cell aggregates were significantly different from that under the static culture (Figures 2.3A-2.3C and 2.4A-2.4C). It is suggested that shaking culture is the most important factor when the influence of GM on cell aggregates is lower. However, in case of cell aggregates incorporating larger amounts of GM ($3\times10^3$ and $4\times10^3$ microspheres/ml), the ATP and mitochondrial activities of cell aggregates were not significantly different between the static and shaking culture (Figures 2.3D, 2.3E, 2.4D, and 2.4E), and the difference between static and shaking culture decreased upon increasing the amounts of GM (Figures 2.3A-2.3C and 2.4A-2.4C). Taken together, it is highly conceivable that the influence of GM on the biological functions of cell aggregates was stronger than under the shaking culture. The tendency of mitochondrial activity was similar to that of ATP activity. Furthermore, ATP activities of cell aggregates incorporating larger amounts of GM ($3\times10^3$ or $4\times10^3$ microspheres/ml) and mitochondrial activities of cell aggregates incorporating larger amounts of GM ($4\times10^3$ microspheres/ml) 21 days after incubation were low compared with those 7 and 14 days later because of degradation of GM (Figures 2.3D, 2.3E, and 2.4E). Furthermore, the ATP and mitochondrial activities of cell aggregates incorporating various amounts of GM under the shaking culture at 5-20 rpm were not significantly different (data not shown). This indicates that when the shaking speed was lower, the shaking culture is not always an important factor to affect the functions of cell aggregates. However, the effect of the shaking culture on the biological functions of cell aggregates incorporating GM at 20-30 rpm was observed (Figures 2.3 and 2.4). At the shaking rate of

more than 30 rpm, a leakage of culture medium from each well was observed in the experimental system of this study. In addition, to evaluate the effect of the number of GM or the shaking culture on the oxygen supply to cell aggregates, the oxygen concentration of the cell aggregates incorporating a lower ($1\times10^3$ microspheres/ml) or larger ($4\times10^3$ microspheres/ml) amount of GM 14 days after incubation under the shaking or static culture was measured (Figure 2.5). The relative oxygen concentration of cell aggregates incorporating $1\times10^3$ microspheres/ml of GM under the shaking culture was higher than that under the static culture (Figure 2.5A). However, the concentration of cell aggregates incorporating $4\times10^3$ microspheres/ml of GM under the shaking culture was not significantly different from that under the static culture (Figure 2.5B). The findings support the results of ATP or mitochondrial activities (Figures 2.3 and 2.4). A more effective allowance of oxygen supply to cells was likely observed for the lower amount of GM incorporated. On the other hand, when a larger amount of GM was incorporated into cell aggregates, enough oxygen would be supplied, irrespective of the culture conditions. However, there is one point to be considered in this study. It is unclear the distance which the probe can reach in cell aggregates. Therefore, the relative oxygen concentration was introduced (Oxygen concentration of cell aggregates under the shaking culture = 1).

It was demonstrated that the shaking culture enables to facilitate to supply oxygen or nutrients of culture medium into cells, which leads to enhancing the biological function [36]. On the other hand, it is reported that there is a relationship between the biological functions of cells and the supply of oxygen or nutrients [14]. Considering the findings, it is likely that the shaking culture enables to supply the oxygen and nutrients into cell

aggregates, leading to an enhanced cell function. In addition, oxygen and nutrients would be permeated through the water phase of GM matrices [14, 41]. However, the shaking culture did not improve the biological functions of cell aggregates incorporating a large amount of GM. This may be explained in terms of the amount of GM incorporated. Since the GM are present in the cell aggregates at a large enough volume, the water phase necessary for oxygen and nutrient supply would be large enough for cell functions in aggregates [14, 41, 43]. As the result, the shaking of medium may not affect the cell functions very much.

Recently, the cell transplantation of cell aggregates has been reported and increasingly noted to enhance their viability and therapeutic efficacy [44, 45]. It is needed to improve the efficiency of cell therapy such as the incorporation of growth factors into GM [41]. Furthermore, the shaking culture should be introduced to enhance the biological functions of cell aggregates and mimic the body environment of the blood circulation. Thus, a combination of biomaterials and shaking culture is important to improve the efficacy of tissue regeneration or drugs.

# Chapter 3

# A cancer invasion model combined with cancer-associated fibroblasts aggregates incorporating gelatin hydrogel microspheres containing a p53 inhibitor

## 3.1. Introduction

Tumor tissues are composed of cancer cells and many stromal cells, such as cancer-associated fibroblasts (CAF), vascular endothelial cells, smooth muscle cells, or immune cells. Among the stromal cells, CAF are the major components [46, 47]. CAF of large spindle-shaped cells are perpetually activated and do not undergo apoptosis [48]. In addition, recently, the crosstalk between cancer cells and CAF has been investigated to clearly demonstrate that the interaction plays a key role in the cancer events of the progression [49-51], the invasion [52-54], and the metastasis [55-57]. For the cancer invasion, matrix metalloproteinase (MMP), which is secreted by cancer cells or CAF, plays a key role in the remodeling of the extracellular matrix. MMP can selectively degrade collagen type IV and laminin, which are important components of the basement membrane. Therefore, a high level of MMP production by the interaction promotes the invasiveness of cancer cells because of the degradation of the basement membrane (Figure 3.1) [58-61].

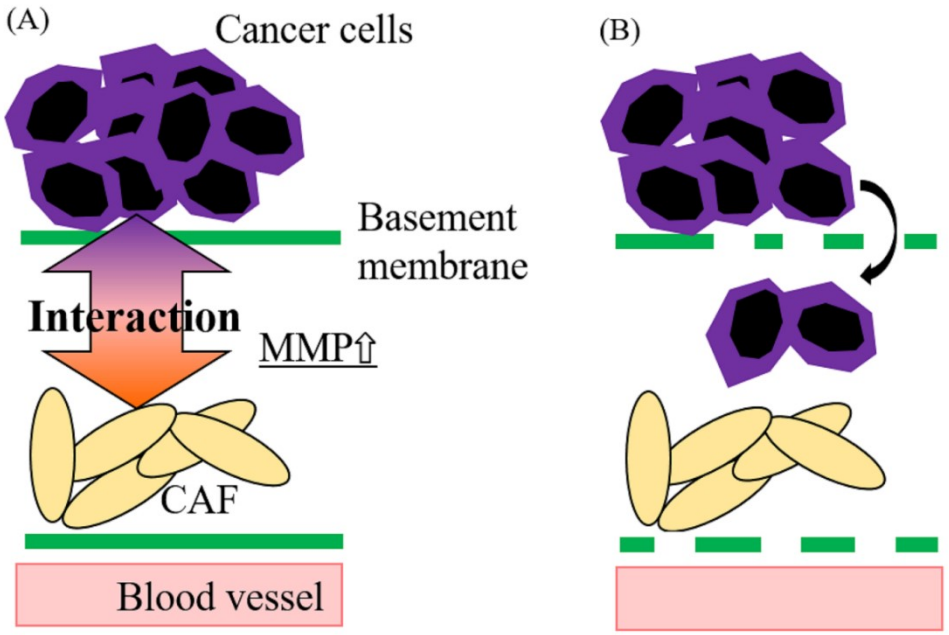


Figure 3.1. Characterization of cancer invasion by the interaction between cancer cells and CAF in vivo. (A) In tumor sites, cancer cells usually attached to the basement membrane as an alternative of epithelial cells. Interaction between cancer cells and CAF (in stromal cells) leads to an accelerated MMP production. (B) Cancer cells start to penetrate through the basement membrane degraded by MMP produced. This process of cancer invasion is one of the important points to consider the therapeutic efficacy of tumor therapy because of the consequent metastasis and final poor mortality rates.

Recently, it is well recognized that drugs to target CAF or the interaction between cancer cells and CAF would be effective in cancer treatment [46, 47, 62, 63]. Based on the reasons, CAF are important cells to study the cancer characteristics while a co-culture of cancer cells and CAF is necessary to simulate the *in vivo* environment of tumor tissues *in vitro*.

Cell culture of three-dimension (3D) is an important method to mimic

the body environment [64]. In the body tissue, most cells tend to form aggregates, and the aggregation permitted cells to enhance their biological functions, such as proliferation, cell-cell interaction, and metabolic activity [2, 3, 5, 10, 11, 65]. However, cells present in the center of cell aggregates rapidly die because of poor oxygen and nutrient supplies [12, 66]. To tackle this problem, gelatin hydrogel microspheres (GM) were incorporated into cell aggregates to demonstrate the cell viability for a long-time period [14]. Furthermore, the GM incorporation allowed cells to supply oxygen and nutrients while GM could release growth factors or drugs to improve cell survival and functions [24-31]. In other words, GM are widely used in the field of drug delivery system (DDS), which is well known as the technology and methodology to enhance drug effects or reduce the side effects. The GM are promising in regenerative medicine or drug discovery based on DDS technology [19-23].

Recently, 3D aggregates of cancer cells and CAF have been reported to mimic real cancer tissues [67-69]. Some researches report the deposition of biomolecular onto the matrices for the improvement of cell distribution, function, signaling, or interventions based on the tumor-stromal interaction [67, 70, 71]. The 3D engineered model will be useful for anti-cancer drug screening. However, few researches have been reported on the combined 3D model and DDS for the drugs to activate cancer cells or CAF. It is important to enhance the biological functions of CAF by the controlled drug release to closely mimic the event of tumor sites because CAF are always activated in the tumor sites. In this study, 3D CAF aggregates incorporating GM capable of drug release were prepared. The alpha-smooth muscle actin (α-SMA) expression level (the most widely used marker for CAF) was measured for the CAF activation level. As the drug, pifithrin-α (PFT) which is an

inhibitor to suppress the gene function of p53, was used because it has been reported that the inactivate or mutate the p53 gene can lead to the activation of CAF although the mechanism is not completely clear in biology. In addition, to investigate the effect of the interaction between cancer cells and CAF on the cancer invasion *in vitro*, the invasion assay was performed. Furthermore, the inhibitor of MMP (marimastat) was used to evaluate the effect of MMP secretion on the cancer invasion level.

## 3.2. Methods

### 3.2.1. Preparation of gelatin hydrogel microspheres

Gelatin hydrogel microspheres (GM) were prepared by the chemical crosslinking of gelatin in a water-in-oil emulsion state according to the method previously reported [27]. Briefly, an aqueous solution (20 ml) of 10 wt % gelatin (isoelectric point 5.0, weight-averaged molecular weight = 100,000, Nitta Gelatin Inc., Osaka, Japan) was preheated at 40 ºC, followed by stirring at 300 rpm for 10 min to prepare the water-in-oil emulsion. The emulsion temperature was decreased at 4 ºC for the natural gelation of gelatin solution to obtain non-crosslinked hydrogel microspheres. The resulting gelatin hydrogel microspheres were washed three times with cold acetone in combination with centrifugation (5,000 rpm, 4 ºC, 5 min) to completely exclude the residual oil. Then, GM were fractionated by size using sieves with apertures of 32 and 53 μm (Iida Seisakusho Ltd, Osaka, Japan) and air dried at 4 ºC. Then, non-crosslinked and dried GM (200 mg) were treated in a vacuum oven at 140 ºC to allow to dehydrothermally crosslink for 72 hr. The picture of GM in the swollen state was taken with a microscope (BZ-X710, KEYENCE Ltd, Osaka, Japan). The size of 100 microspheres for each sample was measured using the computer program Image J (NIH Inc., Bethesda, USA) to calculate the average diameters.

### 3.2.2. Preparation of gelatin hydrogel microspheres containing pifithrin-α

Pifithrin-α (PFT) (FUJIFILM Wako Pure Chemical Co. Ltd, Osaka, Japan) was dissolved in DDW to give a concentration of 20, 100, and 500 μg/ml. The PFT solution (20 μl) was dropped into 2 mg of freeze-dried GM, followed by leaving at 37 $^{o}$C overnight for the impregnation of PFT into the GM to prepare GM containing PFT (GM-PFT). The PFT solution was

completely absorbed into the GM through the impregnation process because the solution volume was much less than theoretically required for the equilibrated swelling of GM.

3.2.3. Drug release profile from gelatin hydrogel microspheres

GM-PFT (2mg) were incubated in phosphate-buffered solution (PBS) (pH 7.4, 1 wt %). At each time point, the buffer was removed and replaced with fresh PBS. After 24 hr, PBS was replaced with collagenase. PFT concentration released from GM was measured using High performance liquid chromatography (HPLC, SIL-20A prominence, SPD-20A prominence, LC-20AD prominence, CTO-10ASvp, DGU-20$A_3$ prominence, Shimadzu) at 208 nm with ODS column (STR ODS-M, size: 4.6 mm × 150 mm, Shinwa Chemical Industries Ltd., Kyoto, Japan). The mobile phase consisted of DDW and acetonitrile with a volume ratio of 2:8.

3.2.4. Degradation of gelatin hydrogel microspheres

As well as the drug release profile, 2 mg of GM-PFT was incubated in PBS. At each time point, the buffer was removed and replaced with fresh PBS. After 24 hr, PBS was replaced with collagenase. The degradation of GM-PFT was measured using Micro BCA™ Protein Assay Kit (Thermo Inc. Waltham, USA).

3.2.5. Cell culture experiments

WA-hT cells of human small cell lung carcinoma cell line (RIKEN, Japan) and WA-mFib cells of the small cell lung cancer-associated fibroblasts (CAF) cell line in minimum essential medium (MEM) (Sigma-Aldrich Co. LLC. St. Louis, USA) supplemented with 10 vol % fetal

calf serum (FCS) (Thermo Inc. Waltham, USA), penicillin (50 U/mL), and streptomycin (50 U/mL) (standard medium) and cultured at 37 $^{O}$C in a 95 % air - 5 % carbon dioxide atmosphere.

3.2.6. Preparation of various types of cancer-associated fibroblasts aggregates

A Poly (vinyl alcohol) (PVA) sample (the degree of polymerization = 1,800 and the saponification = 88 mole %) kindly supplied from Unichika (Tokyo, Japan) was dissolved in PBS. The PVA solution was added to each well of the round-bottomed (U-bottomed) 96-well culture plate (200 µl/well) and incubated at 37 $^{O}$C for 15 min. Then, the solution was removed by aspiration and the wells washed twice with PBS (200 µl/well). GM, GM-PFT, and CAF were separately suspended in the standard medium. After the suspensions of GM or GM-PFT ($2\times10^3$ microspheres/ml, 100 µl), and CAF suspensions ($2.0\times10^4$ cells/ml, 100 µl) were mixed, the mixture was added to the wells coated. After 7 days (CAF aggregates were formed), CAF aggregates were cultured by an orbital shaker (Bellco, Inc. California, USA) at 30 rpm to enhance the biological functions until over the time periods of 15 days [72], and then the medium was changed on the first day and every 3 days until the end of experiments. In terms of the addition of free PFT (10 % amounts of PFT) into solution form every day, culture was performed until 10 days. Because after 10 days, the total amount of PFT added to CAF aggregates would be the theoretically same as that of PFT release group. The pictures of the various types of CAF aggregates were taken with a microscope (CKX41, Olympus Ltd, Tokyo, Japan). The size of various types of CAF aggregates was measured by using the computer program Image J (NIH Inc., Bethesda, USA) to calculate the average

diameter. Figure 3.2 shows the illustration of experimental samples applied in the U-bottomed well.

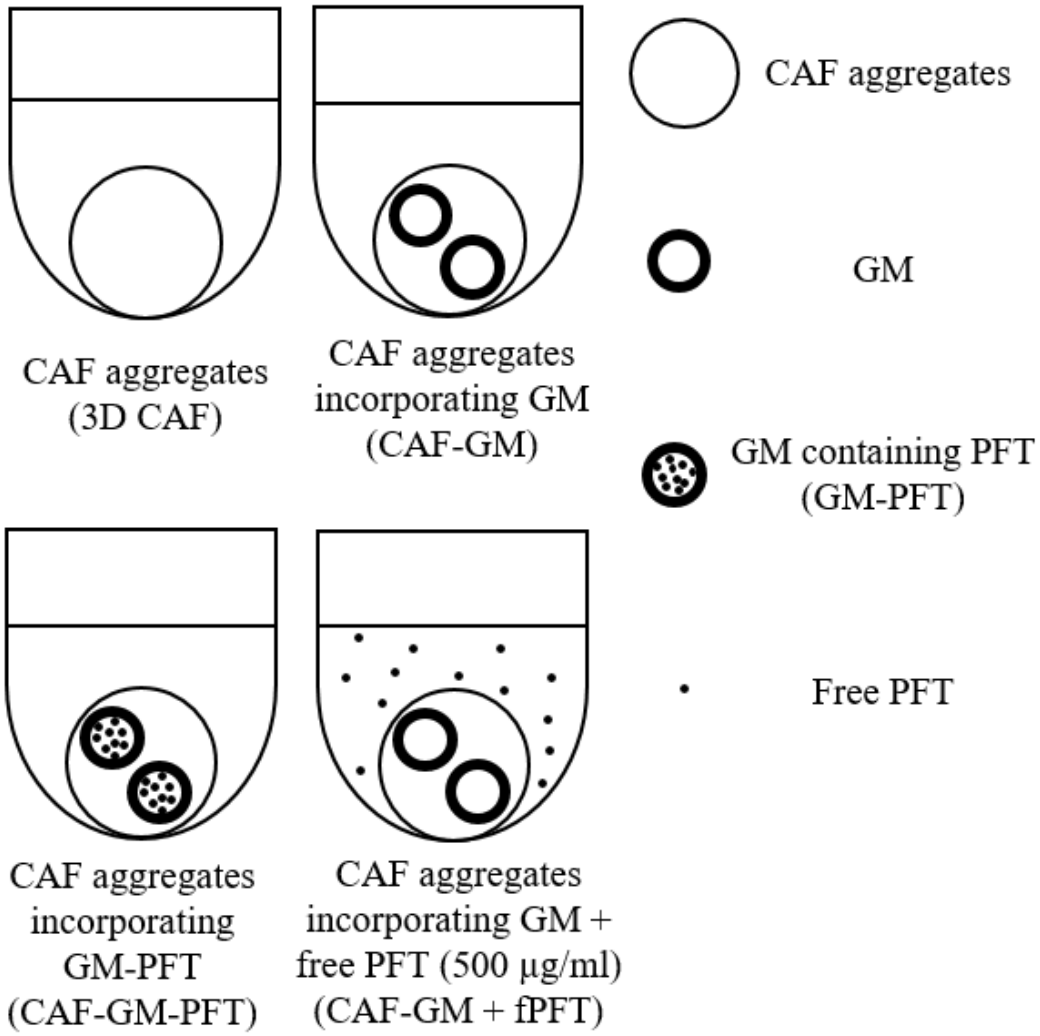


Figure 3.2. Preparation of CAF aggregates (3D CAF), CAF aggregates incorporating GM (CAF-GM), CAF aggregates incorporating GM-PFT (CAF-GM-PFT), and CAF aggregates incorporating GM in the presence of free PFT (500 µg/ml) addition (CAF-GM + fPFT).

### 3.2.7. Cell number

To evaluate the cell number in CAF aggregates without (3D CAF) or

with GM (CAF-GM) and GM-PFT containing various concentrations of PFT (CAF-GM-various concentrations of PFT) 5, 10, and 15 days after incubation, each sample was taken into a microtube. After centrifuge, the culture medium was carefully removed and the samples were washed with 200 µl of PBS. After removing PBS, 200 µl of collagenase was added and samples were incubated at 37 $^{O}$C for 30 min to degrade GM or GM-PFT. Then, 50 µl of trypsin was added and samples were incubated at 37 $^{O}$C for 30 min and pipetted every 5 min to facilitate the dissociation of the aggregates. The enzyme action was stopped by the addition of 50 µl of culture medium. The total cell number was measured using Countess (Thermo Inc. Waltham, USA).

3.2.8. Alpha-smooth muscle actin expression level

To evaluate the effect of PFT release on the CAF functions, alpha-smooth muscle actin (α-SMA) expression level for the 2D CAF, 2D CAF + fPFT, and various types of CAF aggregates were measured by using Enzyme-Linked ImmunoSorbent Assay (ELISA).

3.2.9. Invasion assay

To evaluate the crosstalk between various types of CAF and cancer cells, a cancer invasion assay was performed by using Cytoselect 96 well invasion assay (Cell Biolabs, Inc., San Diego, USA). In brief, 150 µl of CAF suspension ($8.0 \times 10^5$ cells/well in medium containing FCS) or various types of CAF aggregates (the same cell number of CAF suspension) were added (150 µl) into the tubes. The tubes were centrifuged and the supernatant was removed. Then, 800 µg/ml of marimastat or standard medium was added (150 µl) to the tubes, and the suspensions were plated to

the well of the feeder tray. After the membrane chamber was placed into the feeder tray, cancer cell suspension ($2.0 \times 10^5$ cells/well in FCS free medium) was added (100 μl) to the membrane chamber. The samples were incubated for 24 hr. After completely dislodge the cancer cells from the underside of the membrane, a Lysis Buffer dye solution was added. Then, the fluorescent intensity was measured in a fluorescence spectrometer (F-2000, HITACHI Ltd, Tokyo, Japan) at excitation and emission wavelengths of 480 and 520 nm, respectively. The invasion rate of cancer cells was calculated as follows: the number of cancer cells in the underside of the membrane was divided by $2.0 \times 10^5$. Furthermore, the culture medium was collected, and then the secretion level of MMP-2 was measured by ELISA.

3.2.10. Statistical analysis

All the data were statistically analyzed and expressed as the mean ± the standard error of the mean. The data were analyzed by student t-test to determine the statistically significant difference while the significance was accepted at $p < 0.05$. Experiments for each sample were performed three times independently unless otherwise mentioned.

## 3.3. Results

### 3.3.1. Observation of GM

Figure 3.3 shows the microscopic pictures of GM. The GM were spherical and had a smooth surface. The size of GM in the swollen condition ranged 51.25 ± 7.28 μm.

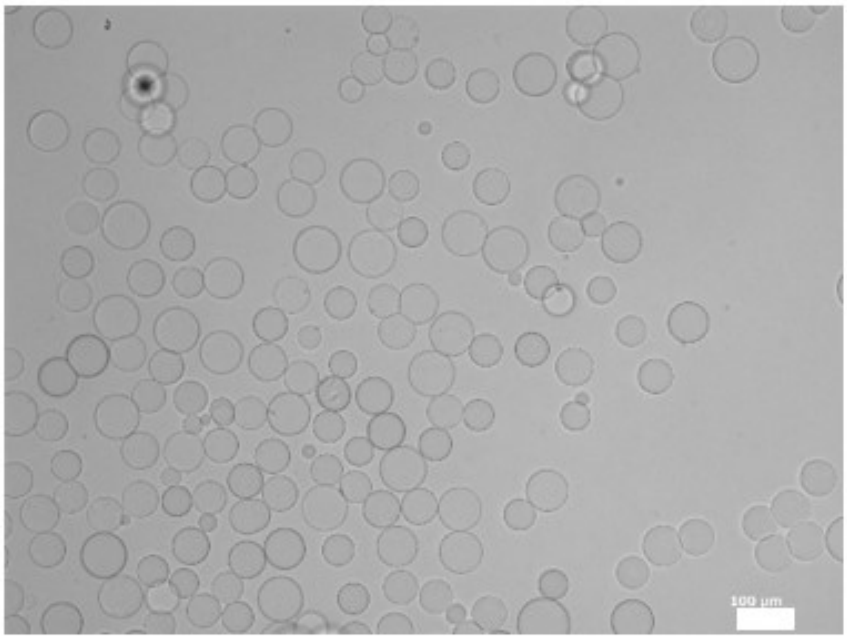


Figure 3.3. A light microspheres photograph of GM dispersed in water. Scale bar; 100 μm.

### 3.3.2. Drug release characterization of GM-PFT

Figure 3.4A shows the PFT release profile from GM-PFT. When GM-PFT was incubated into PBS, a slow release of PFT was observed. By the addition of collagenase, PFT was rapidly released. Figure 3.4B shows the degradation profile of GM-PFT. The profile was similar to that of PFT release. There was a correlation between the two-time profiles. The

coefficient of determination was about 0.96 (Figure 3.4C).

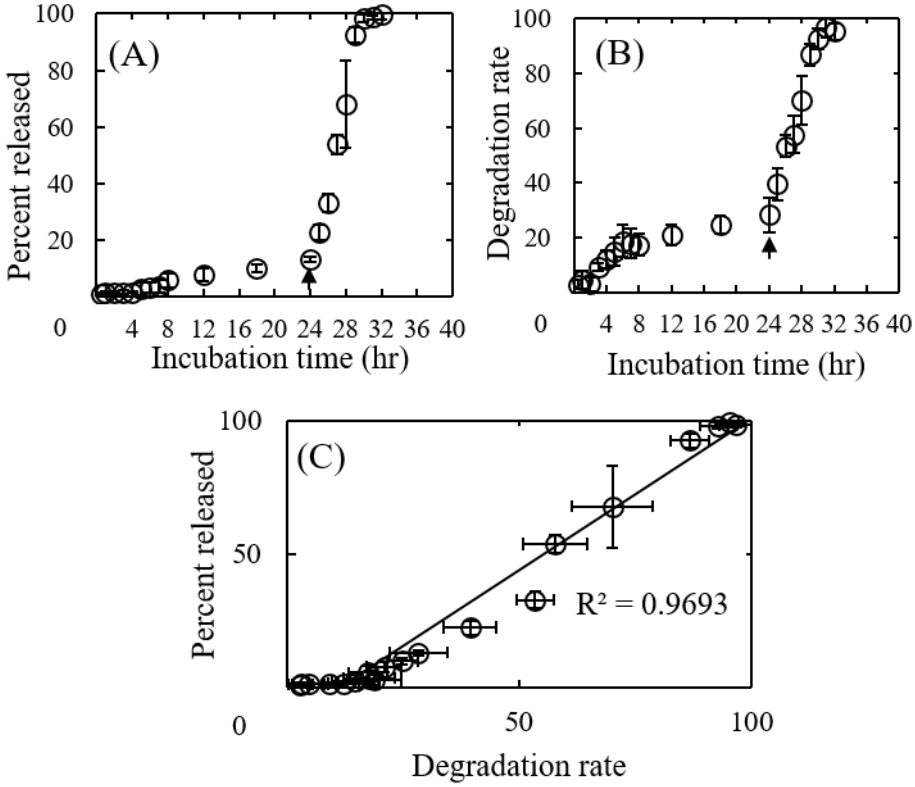


Figure 3.4. (A) *In vitro* time profile of PFT from GM-PFT in PBS. Collagenase was added into PBS at 24 hr indicated by the arrow. (B) Degradation profile of GM in PBS and then collagenase. (C) Relationship between PFT release and GM degradation profile.

3.3.3. Observation of various types of CAF aggregates

Figure 3.5 shows the light microscopic pictures of 3D CAF, CAF-GM, and CAF aggregates incorporating GM-PFT containing 500 μg/ml PFT (CAF-GM-500 μg/ml PFT) 5, 10, and 15 days after incubation, or that of 3D CAF and CAF-GM with free PFT addition 5 and 10 days after incubation. The size of 3D CAF or CAF-GM did not change, irrespective of free PFT

addition (Figure 3.5). The tendency was similar in terms of the PFT concentration (data not shown). However, the size of CAF-GM and CAF-GM-PFT 15 days after incubation was small compared with that after 10 days (Figure 3.5).

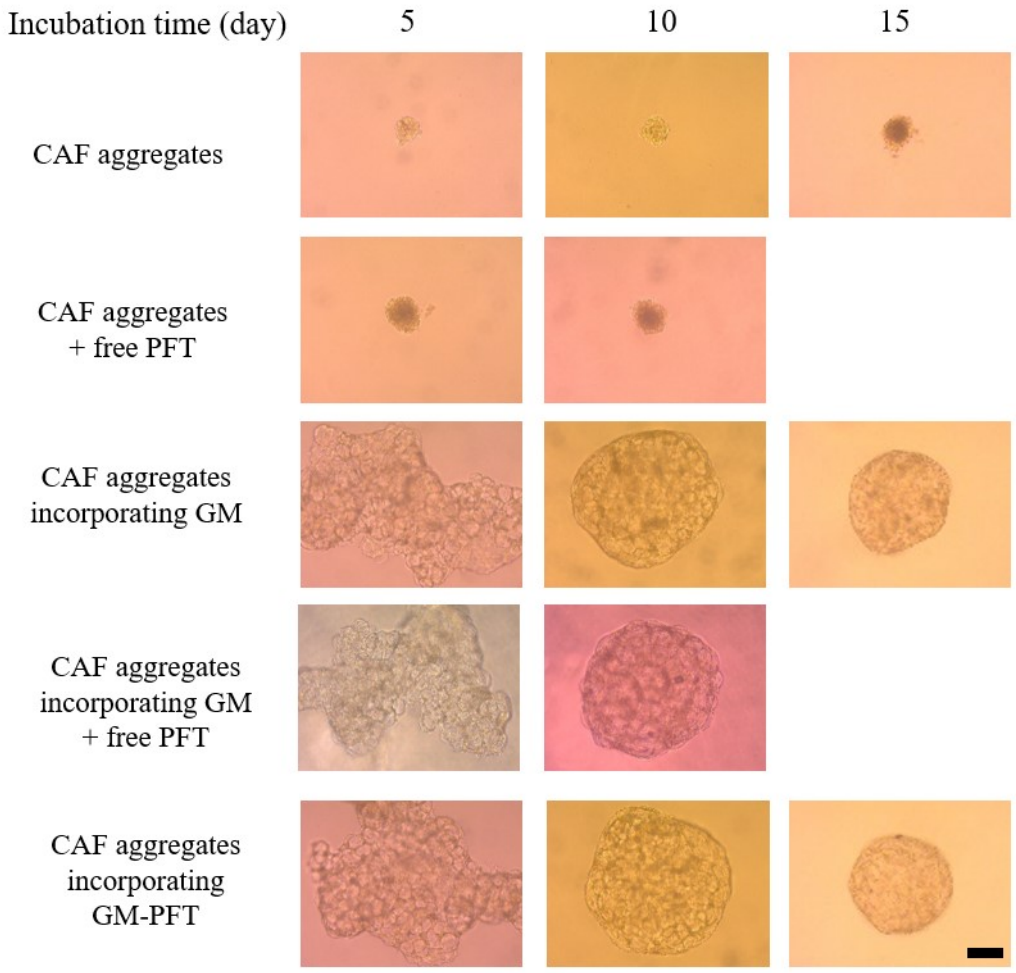


Figure 3.5. Light microscope photographs of 3D CAF, CAF-GM, and CAF-GM-500 μg/ml PFT 5, 10, and 15 days after incubation. Light microscope photographs of 3D CAF + fPFT and CAF-GM + fPFT 5 and 10 days after incubation. Scale bar; 200 μm.

### 3.3.4. Cell proliferation of various types of CAF aggregates

Figure 3.6 shows the cell number in various types of CAF aggregates. The cell number in 3D CAF was significantly lower than that in GM incorporation group. The cell number in 3D CAF 5 days after incubation was not significantly different from that 10 or 15 days later. In terms of GM or GM-various concentrations of PFT incorporation, the cell number 10 days after incubation was larger than that 5 days later. However, there was no difference in the cell number between 10 and 15 days after incubation. In addition, the cell number did not depend on the PFT concentration or free PFT addition.

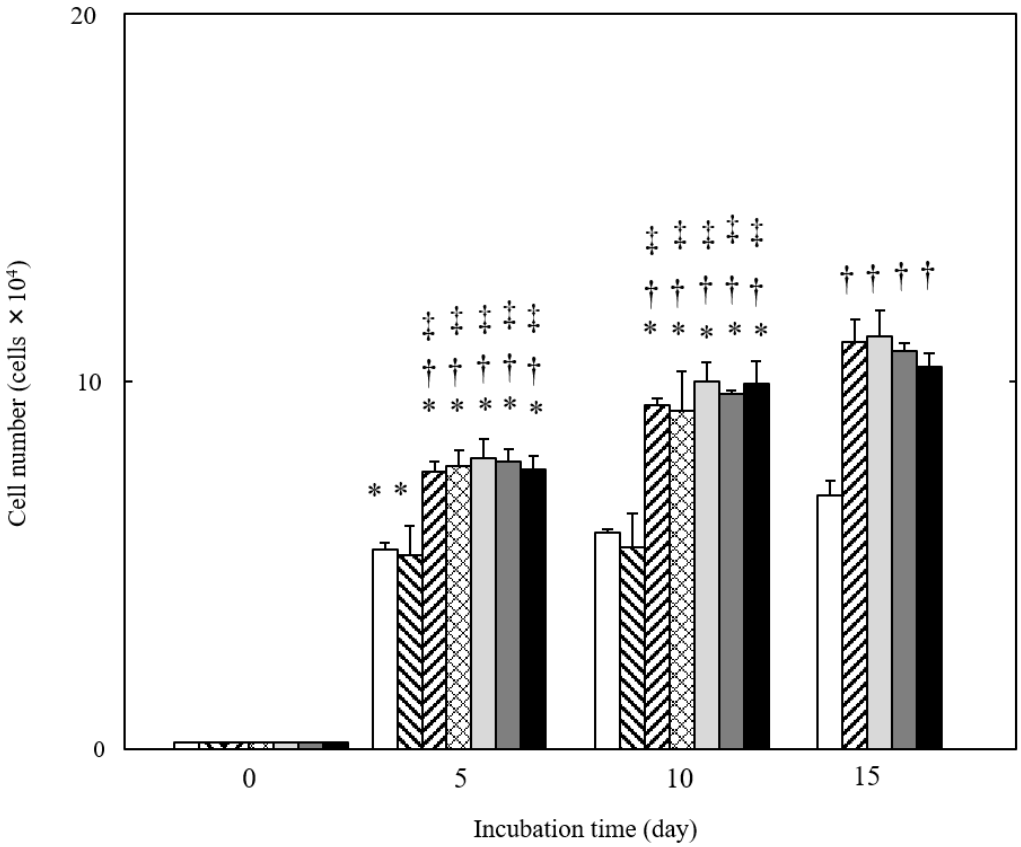


Figure 3.6. Cell number in 3D CAF (□) or CAF-GM (▨) and CAF-GM-PFT containing 20 μg/mL (▩), 100 μg/mL (▩), and 500 μg/mL (■) PFT 5, 10, and 15 days after incubation. Cell number in 3D CAF+fPFT (▨) and CAF-GM+fPFT (▨) 5 and 10 days after incubation. *$p < 0.05$; significant

difference against the cell number for the same condition of CAF 5 days before. $^{\dagger}p < 0.05$; significant difference against the cell number for 3D CAF at the corresponding time. $^{\ddagger}p < 0.05$; significant difference against the cell number for 3D CAF+fPFT at the corresponding time.

### 3.3.5. Measurement of α-SMA expression

To evaluate the effect of PFT on the activation of CAF aggregates, the alpha-smooth muscle actin (α-SMA) expression level was measured. Figure 3.7 shows the α-SMA expression level for 2D CAF, 3D CAF CAF-GM, and CAF-GM-various concentrations of PFT 5, 10, and 15 days after incubation. In terms of free PFT addition, the α-SMA expression level was evaluated until 10 days. The α-SMA expression level among all types of CAF aggregates was not significantly different 5 days after incubation. In addition, at each incubation time, the α-SMA expression level for CAF-GM, CAF-GM-20, and 100 μg/ml PFT did not change. However, the α-SMA expression level for CAF-GM-500 μg/ml PFT 10 and 15 days after incubation was high compared to that for the other types of CAF aggregates. In addition, the α-SMA expression level for 3D CAF was much lower than that of GM or GM-PFT incorporation groups 10 and 15 days after incubation. The α-SMA expression level for CAF-GM-500 μg/ml PFT 10 days after incubation was high compared to that for CAF-GM + fPFT (500 μg/ml). The tendency was observed only for CAF-GM-500 μg/ml PFT. In addition, the α-SMA expression level for 3D CAF was much higher than that for 2D CAF, irrespective of free PFT addition.

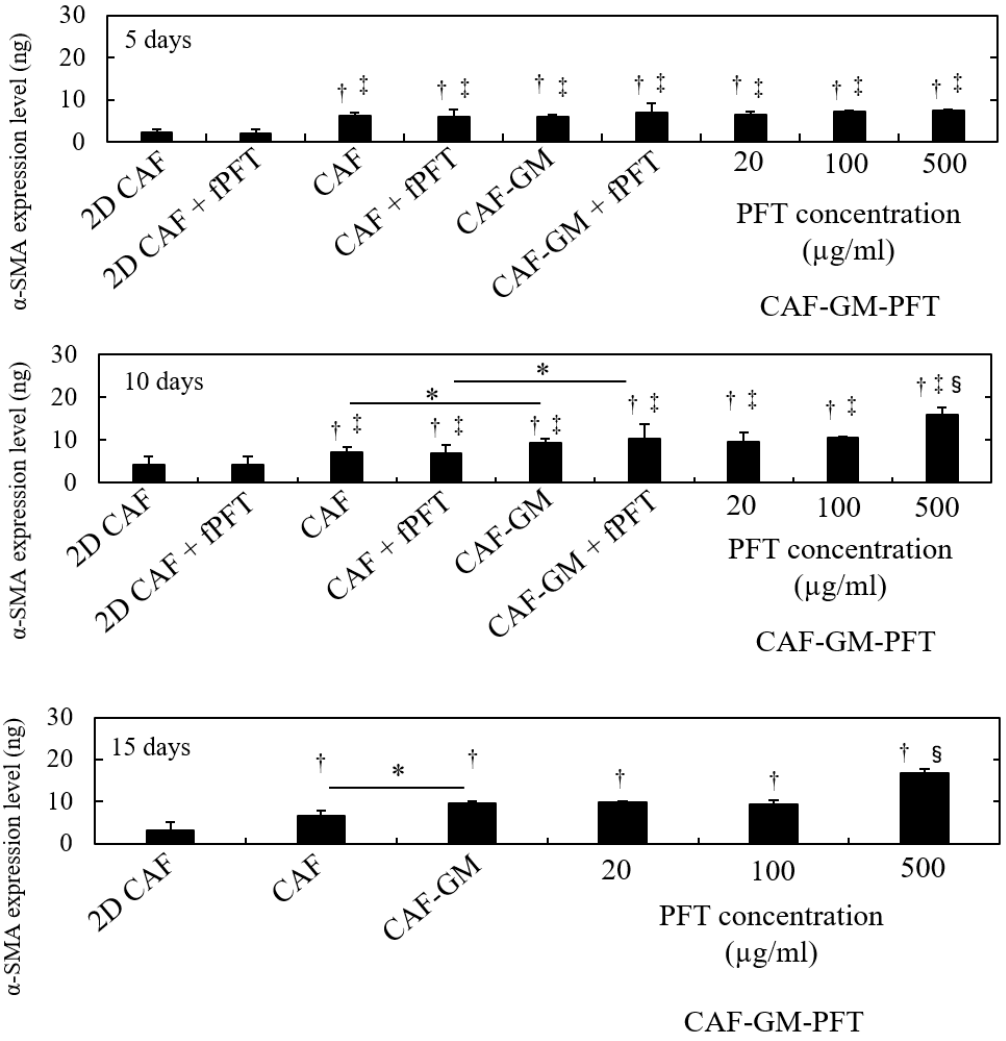


Figure 3.7. α-SMA expression level for 2D CAF, 3D CAF, CAF-GM, and CAF-GM-PFT containing 20 μg, 100 μg, and 500 μg/ml PFT 5, 10, and 15 days after incubation. α-SMA expression level for 2D CAF + fPFT, 3D CAF + fPFT, and CAF-GM + fPFT 5 and 10 days after incubation. *$p< 0.05$; significant difference between the two groups. $^{\dagger}p< 0.05$; significant difference against α-SMA expression level for 2D CAF at the corresponding time. $^{\ddagger}p< 0.05$; significant difference against α-SMA expression level for 2D CAF + fPFT at the corresponding time. $^{\S}p< 0.05$; significant difference against α-SMA expression level for other groups at the corresponding time.

3.3.6. Measurement of cancer invasion rate and secretion level of MMP-2

Figure 3.8 shows the invasion rate of cancer cells by co-culture with various types of CAF. The invasion rate of cancer cells by co-culture with CAF-GM-500 μg/ml PFT was high compared to that of other groups. The addition of marimastat (800 μg/ml: $IC_{50}$ for cancer cells) reduced the invasion rate of cancer cells only when co-cultured with CAF-GM-500 μg/ml PFT. As shown in Figure 3.9, the secretion level of MMP-2 from the CAF-GM-500 μg/ml PFT and cancer cells was much higher than other groups. Only when co-culture with the CAF-GM-500 μg/ml PFT, the secretion level of MMP-2 was significantly higher than other groups and was reduced by the marimastat.

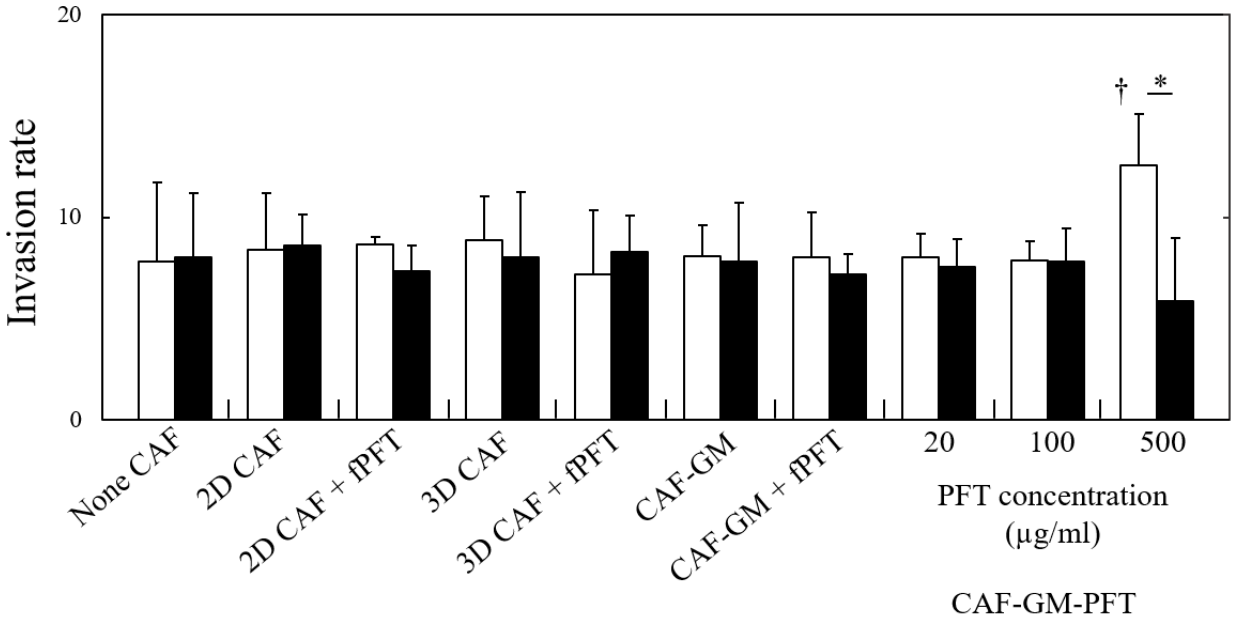


Figure 3.8. Invasion rate of cancer cells without CAF or by co-culture with 2D CAF, 2D CAF + fPFT, 3D CAF, 3D CAF + fPFT, CAF-GM, CAF-GM + fPFT, and CAF-GM-PFT containing 20 μg, 100 μg, and 500 μg/ml PFT.

Control (□) and MMP inhibitor addition culture (■). *$p$< 0.05; significant difference between the two groups. †$p$< 0.05; significant difference against invasion rate for other control groups.

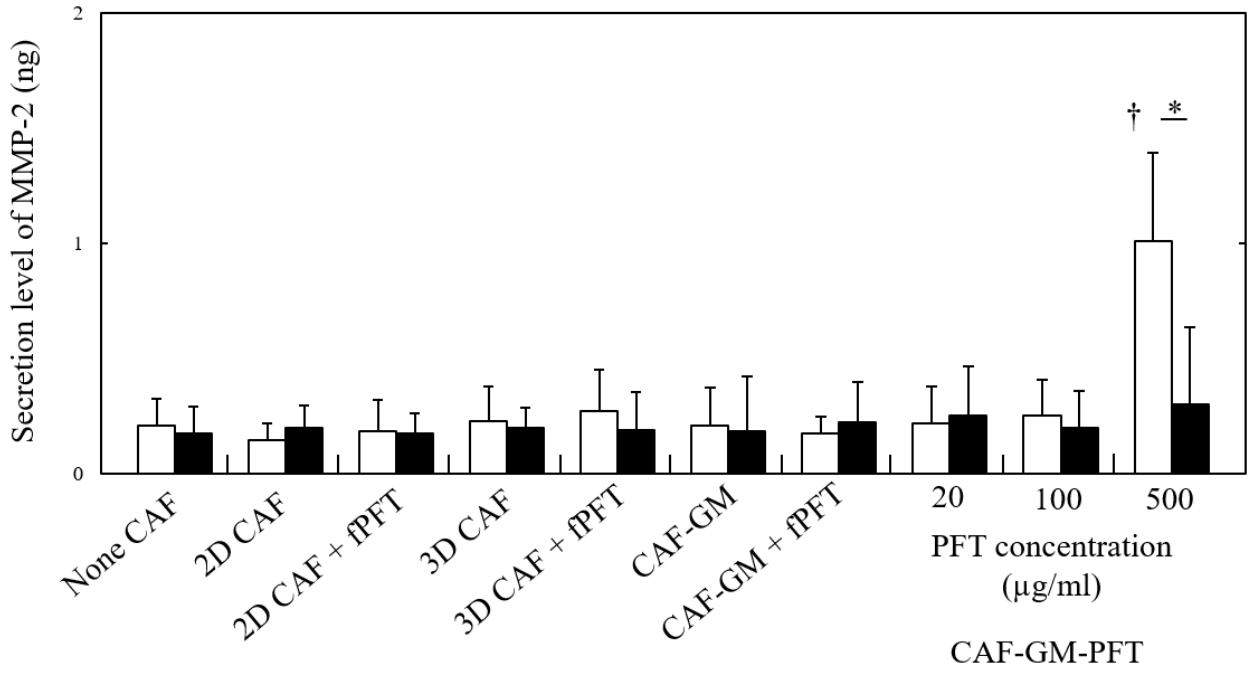


Figure 3.9. Secretion level of MMP-2 without CAF or by co-culture with 2D CAF, 2D CAF + fPFT, 3D CAF, 3D CAF + fPFT, CAF-GM, CAF-GM + fPFT, and CAF-GM-PFT containing 20 μg, 100 μg, and 500 μg/ml PFT. Control (□) and MMP inhibitor addition culture (■). *$p$< 0.05; significant difference between the two groups. †$p$< 0.05; significant difference against secretion level of MMP-2 for other control groups.

### 3.4. Discussion

The purpose of this study is to mimic the real tumor microenvironment and cancer invasion behavior *in vitro*. *In vivo*, it has been reported that p53 inhibition factors were secreted from cancer cells and the stromal cells such as CAF or the factors were released from the vessel, leading to the sustained CAF activation. The mechanism may not completely be understood in biology [46, 73-75]. On the other hand, it is difficult to control the real body environment or situation *in vitro* at present. Therefore, the gelatin hydrogel microspheres (GM) which are capable of p53 inhibitor slow release are prepared. GM with diameters of 32-53 μm were used in this study (Figure 3.2). This is because the size range of GM is demonstrated to be suitable to form cell aggregates. In addition, the previous study demonstrates that the dehydrothermal crosslinking for 72 hr allowed GM to incorporate into cell aggregates although the crosslinking extent of GM increased with an increase in the crosslinking time [41]. It has been also characterized to optimize the cell aggregates incorporating GM in terms of cell activities to conclude that the cells/GM mixing ratio of 10:1 was appropriate to form cell aggregates incorporating GM [72]. This study also indicates that the ATP activity of CAF aggregates increased with an increase in the number of GM incorporated (data not shown).

It is apparent from the time profile of drug release and GM degradation (Figure 3.4) that the drug is released from GM-PFT not by the drug diffusion, but by the association with the degradation of GM. This mechanism of matrix-degradation-based drug release characterization is advantageous in terms of the drug release regulation [27, 76, 77]. The PFT release profile did not change, irrespective of the PFT concentration (data not shown). It is possible that the number of gelatin molecules is large

enough to associate with PFT molecules. From the results of PFT release profile (Figure 3.4A), about 10 % of PFT was released for 1 day. Based on this, 10 % of the total amounts of PFT was added in the solution form every day as a control group. The size of CAF-GM-PFT did not change, irrespective of the PFT concentration, upon comparing the same time (Figure 3.5). However, the size of CAF-GM or CAF-GM-PFT 15 days after incubation was small compared with that after 10 days (Figure 3.5). This can be explained in terms of GM degradation. The previous study demonstrates that a decrease in the size of cell aggregates incorporating GM leads to reduce the biological functions of cell aggregates [72]. Based on this, in this study, CAF aggregates were cultured at the longest for 15 days.

The incorporation of GM or GM-PFT affected the increase in the cell number in CAF aggregates (Figure 3.6). The cell number in CAF-GM was larger than that in the GM-Free group. It is likely that the GM presence gave cells in the aggregates a good condition of enhanced oxygen or nutrient permeability and concentration, resulting in an enhanced cell number in CAF aggregates. However, the cell number in CAF-GM-PFT did not depend on the PFT concentration. These results are supported by the pictures in Figure 3.5. The findings indicate that the PFT release did not affect the cell proliferation of CAF aggregates. During the initial 10 days, the cell number in CAF-GM or CAF-GM-PFT increased, but not after 10 days. Considering the degradation of GM or GM-PFT in the aggregates for 10 days, it is conceivable that the GM lost results in the deteriorated condition of oxygen and nutrient in aggregates, leading to reduced or stopped cell growth. This can be controlled by changing the time period of GM degradation. To evaluate the effect of PFT on the activation of CAF aggregates, first, the α-SMA expression level for CAF-GM or CAF-GM-various concentrations of

PFT (20, 100, and 500 μg/ml) (Figure 3.7). To identify CAF, α-SMA which is known as a specific marker for myofibroblasts, is a widely used marker as a measure of CAF activation [46, 78, 79]. The activation level of CAF is very important because the activation of CAF is enabled CAF to enhance the interaction with cancer cells, which contributes to cancer progression, invasion, and metastasis, through the secretion of various growth factors, cytokines, and chemokines [46, 47]. The α-SMA expression level of various types for CAF aggregates 5 days after incubation was not significantly different. However, 10 and 15 days after incubation, the α-SMA expression level for CAF aggregates was significantly low compared with that of CAF-GM. As demonstrated by the previous study, GM facilitate supplying oxygen and nutrients to cells, which leads to increased survival of cells and the consequent biological activation [41]. The α-SMA expression level for CAF-GM-500 μg/ml PFT was significantly high compared with that of the other CAF aggregates. This indicates that 500 μg/ml PFT was suitable to enhance the functions of CAF aggregates. Next, the effect of PFT release to CAF aggregates on the CAF functions was considered. The α-SMA expression level for CAF-GM-500 μg/ml PFT was significantly different from that for CAF-GM + fPFT 10 days after incubation. The biological activation of PFT for CAF functions more effectively than the only addition of free PFT into the medium from outside of CAF-GM. The effect of the addition of free PFT into the medium on the activation of 2D CAF or 3D CAF was not observed. In addition, the α-SMA expression level for 2D CAF was significantly lower than that of 3D CAF 5, 10, and 15 days after incubation. This may be explained in terms of cellular interaction. It is suggested that the better interaction of 3D cell-cell contact allows cells to enhance their function. It has been reported that the cell functions were

determined by not a cell but a unit of the cells [2-5]. The 3D cell culture technology is essential to enhance the cell functions.

Figure 3.8 shows the invasion rate of cancer cells by co-culture with various types of CAF. The invasion assay is usually performed by using a transwell via the basement membrane. For example, to evaluate the cancer invasion ability or the effect of the gene or the regents on the cancer invasion, the cell invasion assay kit was utilized [80-83]. In tumor sites, although cancer cells usually attached to the basement membrane as an alternative of epithelial cells, cancer cells started to penetrate through the basement membrane when cancer cells gained the invasiveness. Therefore, the culture condition in this study (cancer cells on the basement membrane, CAF under the basement membrane) would mimic the inner state of cancer cells in cancer sites. The mixing ratio of cancer cells and CAF of 1:4 was used. This is because it has reported that the numbers of CAF are about second, three, or four times as much as that of cancer cells although the ratio depends on the cancer type [67]. The invasion rate of cancer cells only by co-culture with CAF-GM-500 μg/ml PFT was significantly higher than that with other groups. From the results, it is possible that the CAF-GM-500 μg/ml PFT simulates the cancer microenvironment better than other groups. Interestingly, when cancer cells were cultured without CAF, the invasion rate was not significantly different from that with them. It is well known that invasion tends to occur with CAF existence because of the interaction between cancer cells and CAF *in vivo* [46]. It is conceivable that the activation of CAF as much as possible is needed to occur the interaction between them *in vitro*. To further evaluate the interaction between cancer cells and CAF, the addition assay of marimastat, an inhibitor of matrix metalloproteinase (MMP), was performed (Figure 3.8, closed bar). As a

result, the cancer invasion rate was significantly inhibited only by co-culture with CAF-GM-500 μg/ml PFT. In addition, the level of MMP-2 secreted from the CAF-GM-500 μg/ml PFT was significantly higher than that of other groups (Figure 3.9). Moreover, the inhibition effect of marimastat on the MMP-2 secretion was seen only for the CAF-GM-500 μg/ml PFT group (Figure 3.9). However, the MMP-9 secretion was not observed for all of the groups (data not shown). Among the MMPs, it has been reported that MMP-2 and 9 selectively degrade type IV collagen and laminin, which mainly are composed in the basement membrane, and contribute to the cancer invasion. The expression of larger amounts of MMP-2 and 9 is demonstrated in several cancers. Taken together, the two types of MMPs were focused. MMP-9 is also activated by MMP-3 and MMP-13 [46]. MMP-3 and 13 were not evaluated because MMP-9 is not secreted higher. In addition, the MMP inhibition did not affect the CAF function (data not shown). Taken together, it is likely that the efficient interaction between cancer cells and CAF with a high activity allowed cancer cells to achieve their invasion behavior even *in vitro* via the MMP-2 system (Figure 3.10). This study is the first report to create an invasion model *in vitro* by taking advantage of a combined 3D culture system and the DDS technology.

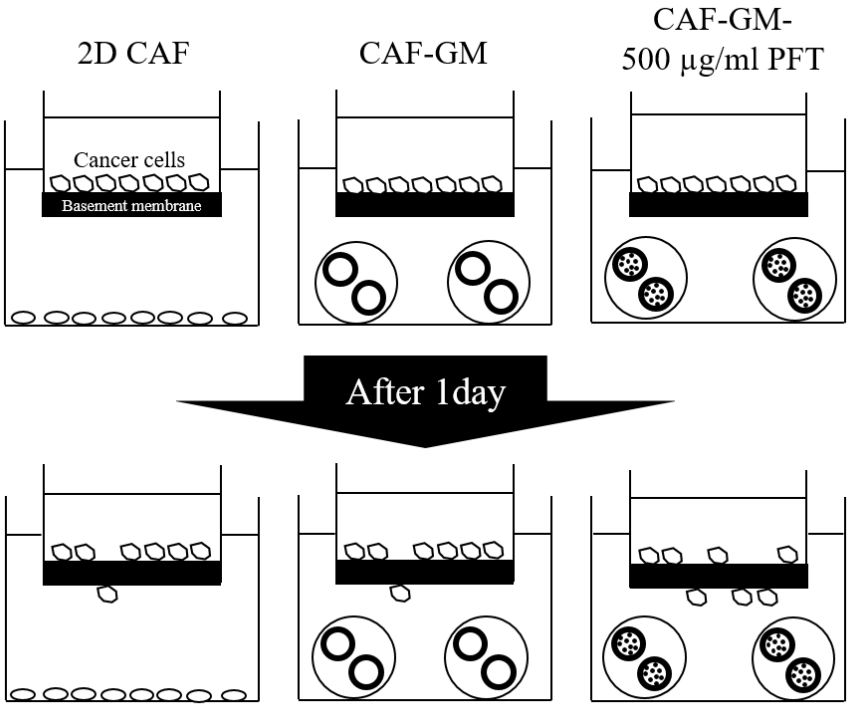


Figure 3.10. Result illustration of cancer invasion model based on a combination of 3D cell culture and DDS technology. The cancer invasion rate was low in the conventional model (with 2D CAF or CAF-GM) because the cancer local environment is different from that of *in vivo* tumor microenvironment, leading to the lower MMP secretion. The present cancer invasion model would be an effective tool to evaluate the ability of cancer invasion *in vitro* because this invasion model enables cancer cells to give a microenvironment similar to *in vivo*.

# Chapter 4

# A cancer invasion model of cancer-associated fibroblasts aggregates combined with TGF-β1 release system

## 4.1. Introduction

Recently, it has been gotten harder and harder to perform animal experiments for the evaluation of biological mechanisms, drug effects, and drug toxicology because of ethical issues [84, 85]. For example, animal experiments for cosmetic research and development have been prohibited since 2013 in Europe [86, 87]. Based on this situation, animal-free experiments have been carried out extensively. As alternative animal models, some cell culture systems to mimic the *in vivo* environment have been developed [88-90]. Among the systems, there are many research reports on three-dimensional (3D) cell culture, such as cell aggregates, spheroids, or organoids [72, 91-95]. In the body tissue, cells 3D interact with each other, leading to an enhanced extracellular matrix production, cytokine secretion, metabolic activity, and proliferation or differentiation [2-4, 65]. Therefore, as one experimental trial, cell aggregates would be effective in mimicking the body system for biological research or drug discovery [5]. However, as the size of cell aggregates becomes large, oxygen or nutrient supplies into the cells present in cell aggregates are too poor to survive and maintain the biological activities of cells [12, 66]. In addition, it is also difficult to culture the cell aggregates for a long time period which is necessary for the *in vitro* performance of drug discovery. As one trial to tackle this issue, gelatin hydrogel microspheres (GM) were incorporated into the cell aggregates because the oxygen and nutrients can be permeated through the water phase of GM for their supply to cells [14].

Moreover, it has been demonstrated that the GM can control release growth factors (e.g. basic fibroblast growth factor, transforming growth factor-β (TGF-β), or platelet-derived growth factor) or drugs (e.g. a p53 inhibitor), which is effective in enhancing the cell viability and functions [24-31, 96, 97]. Based on these findings, it is experimentally confirmed that cell aggregates incorporating GM containing the growth factors or drugs are promising in drug screening or regenerative medicine [20, 72, 97-101].

Cancer invasion is one of the problems to be solved in cancer therapy because the cancer invasion leads to cancer metastasis, which often causes finally poor mortality rates [102]. Recently, it has been demonstrated that cancer cells do not have a great ability in themselves to promote the invasion and that stromal cells support their invasion [48, 97, 103, 104]. Among the stromal cells, cancer-associated fibroblasts (CAF) play major roles to promote cancer invasion through the interaction with cancer cells [46]. It is reported that the cancer invasion rate by co-cultured or existence with CAF is significantly higher than that of CAF-free culture *in vitro* or *in vivo* [52-57]. Although several factors are secreted by the interaction, matrix metalloproteinase (MMP) is essential for the cancer invasion because MMP has an ability to degrade the basement membrane [46, 58, 60]. Based on the findings, it has been noted that the cancer invasion therapy to target CAF or the research of interaction between cancer cells and CAF would be effective [46, 62, 63, 97, 105, 106]. In addition, growth factors also have an important influence in promoting the cancer invasion while they are physiologically secreted from several cells of cancer cells, CAF, and endothelial cells. The previous study has revealed that CAF stimulated by TGF-β1 increase the cancer invasion rate in a population study [107]. TGF-β1 is one of the important growth factors for interaction between

cancer cells and CAF via MMP, leading to the cancer invasion as shown in Figure 4.1 [107-109].

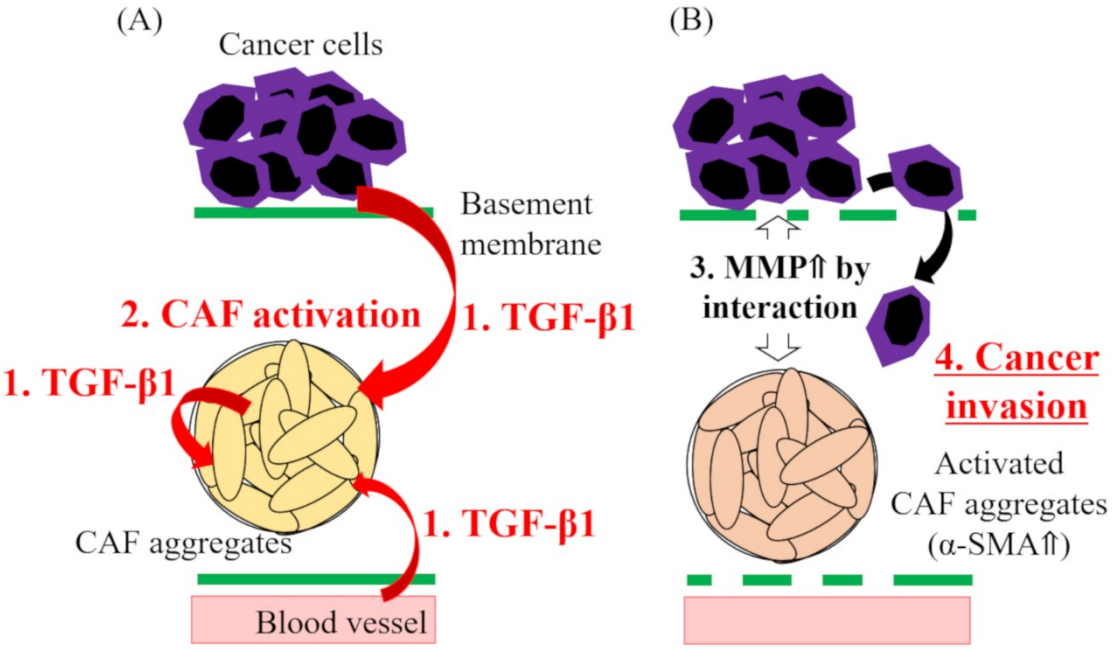


Figure 4.1. Characterization of cancer invasion by the cell culture system of interaction between cancer cells and CAF. (A) TGF-β1 secreted from cancer cells, endothelial cells, or CAF aggregates are able to stimulate or activate CAF aggregates. (A higher α-SMA expression level for CAF). (B) Cancer cells and activated CAF sustainably interact with each other, leading to an accelerated MMP production. MMP could degrade the basement membrane, resulting in an enhanced cancer invasion.

The objective of this study is to design a cancer invasion model where the cancer invasion rate can be regulated by changing the concentration of TGF-β1. To replicate the cancer invasion via CAF activation by TGF-β1, first, CAF aggregates incorporating GM capable of TGF-β1 controlled release were prepared. Then, alpha-smooth muscle actin (α-SMA) for the CAF aggregates was measured to investigate the CAF activation level by

changing the concentration of TGF-β1. An invasion assay was performed to evaluate the cancer invasion rate by co-cultured of cancer cells with various CAF aggregates incorporating GM containing TGF-β1. The effect of an MMP inhibition treatment on the secretion level of MMP and the cancer invasion rate were examined.

## 4.2. Methods

### 4.2.1. Preparation of gelatin hydrogel microspheres

Gelatin hydrogel microspheres (GM) were prepared by the chemical crosslinking of gelatin in a water-in-oil emulsion state according to the method previously reported [27]. Briefly, an aqueous solution (20 ml) of 10 wt % gelatin (isoelectric point 5.0, weight-averaged molecular weight = 100,000, Nitta Gelatin Inc., Osaka, Japan) was preheated at 40 ºC, followed by stirring at 300 rpm for 10 min to prepare the water-in-oil emulsion. The emulsion temperature was decreased at 4 ºC for the natural gelation of gelatin solution to obtain non-crosslinked hydrogel microspheres. The resulting gelatin hydrogel microspheres were washed three times with cold acetone in combination with centrifugation (5,000 rpm, 4 ºC, 5 min) to completely exclude the residual oil. Then, GM were fractionated by size using sieves with apertures of 32 and 53 μm (Iida Seisakusho Ltd, Osaka, Japan) and air dried at 4 ºC. Then, non-crosslinked and dried GM (200 mg) were treated in a vacuum oven at 140 ºC to allow to dehydrothermally crosslink for 72 hr. The picture of GM in the swollen state was taken with a microscope (BZ-X710, KEYENCE Ltd, Osaka, Japan). The size of 100 microspheres for each sample was measured using the computer program Image J (NIH Inc., Bethesda, USA) to calculate the average diameters.

### 4.2.2. Preparation of GM-TGF-β1

Recombinant human TGF-β1 (R&D Systems, Inc., Minneapolis, USA) was dissolved in double-distilled water (DDW) to give a solution at TGF-β1 concentration of 10, 100, 500, 1000, and 5000 μg/ml. The TGF-β1 solution (20 μl) was dropped into 2 mg of freeze-dried GM, followed by leaving at 37 $^{o}$C overnight for the impregnation of TGF-β1 into the GM to prepare

GM containing TGF-β1 (GM-TGF-β1). GM-TGF-β1 containing 10, 100, 500, 1000, and 5000 μg/ml TGF-β1 were named GM-10TGF-β1, GM-100TGF-β1, GM-500TGF-β1, GM-1000TGF-β1, and GM-5000TGF-β1, respectively. The TGF-β1 solution was completely absorbed into the GM through the impregnation process because the solution volume was much less than theoretically required for the equilibrated swelling of GM.

4.2.3. Evaluation of *in vitro* TGF-β1 release

GM-5000TGF-β1 (2 mg) were incubated in 9.57 mM phosphate-buffered saline solution (PBS, pH 7.4). At each point, the buffer was removed and replaced with fresh PBS. After 24 hr, PBS was replaced with collagenase. TGF-β1 concentrations released from GM were measured using a human TGF-β1 ELISA kit (Proteintech Inc., Rosemont, USA).

4.2.4. Cell culture experiments

WA-hT cells of human small cell carcinoma cell line (RIKEN, Japan) and WA-mFib cells of cancer-associated fibroblasts (CAF) cell line derived WA-hT were cultured in minimum essential medium (MEM) (Sigma-Aldrich Co. LLC. St. Louis, USA) supplemented with 10 vol % fetal calf serum (FCS) (Thermo Inc. Waltham, USA), penicillin (50 U/mL), and streptomycin (50 U/mL) (standard medium) and cultured at 37 $^{O}$C in a 95 % air - 5 % carbon dioxide atmosphere.

4.2.5. Preparation of various CAF aggregates

A Poly (vinyl alcohol) (PVA) sample (the degree of polymerization = 1,800 and the saponification = 88 mole %) kindly supplied from Unichika (Tokyo, Japan) was dissolved in PBS (1 wt %). The PVA solution was added

to each well of round-bottomed (U-bottomed) 96-well culture plate (200 μl/well) and incubated at 37 $^{O}$C for 15 min. Then, the solution was removed by aspiration and the wells washed twice with PBS (200 μl/well). GM, various GM-TGF-β1, and CAF suspensions were separately suspended in the standard medium. After the suspensions of GM ($2\times10^3$ microspheres/ml, 100 μl) and various GM-TGF-β1 ($2\times10^3$ microspheres/ml, 100 μl) were prepared, CAF suspensions ($2.0\times10^4$ cells/ml, 100 μl) were mixed. The mixtures were added to the wells coated. As a control group, CAF aggregates incorporating GM by addition of free TGF-β1 solution (5000 μg/ml) into the culture medium were cultured. The addition schedule is followed: 20 % of TGF-β1 amount contained in GM was added when the culture was started. After 7 days, 20 % of TGF-β1 amount was added on day 7, 8, 9, and 10 for 4 days (Figure 4.2B). In addition, the CAF aggregates were not cultured 10 days later because the amount of TGF-β1 added into the culture medium was higher than that of TGF-β1 contained in GM. The pictures of the various types of CAF aggregates were taken with a microscope (CKX41, Olympus Ltd, Tokyo, Japan). The size of CAF aggregates was measured using the computer program Image J (NIH Inc., Bethesda, USA) to calculate the average diameter. CAF aggregates incorporating GM, GM-10TGF-β1, GM-100TGF-β1, GM-500TGF-β1, GM-1000TGF-β1, and GM-5000TGF-β1 were named CAF-GM, CAF-GM-10TGF-β1, CAF-GM-100TGF-β1, CAF-GM-500TGF-β1, CAF-GM-1000TGF-β1, and CAF-GM-5000TGF-β1, respectively (Figure 4.2A). In addition, CAF-GM by the addition of free TGF-β1 solution was named CAF-GM + fTGF-β1.

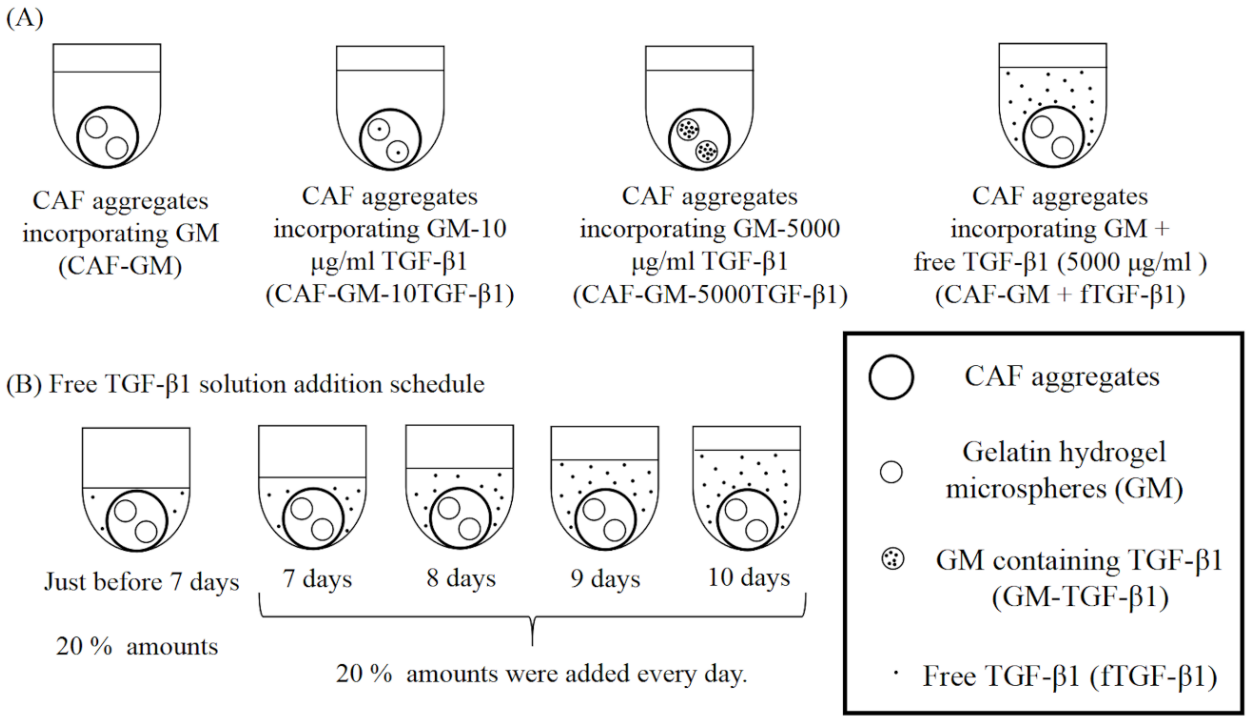


Figure 4.2. (A) Preparation of CAF aggregates incorporating GM (CAF-GM), CAF aggregates incorporating GM containing various concentrations (10, 100, 500, 1000, and 5000 μg/ml) of TGF-β1 (CAF-GM-10TGF-β1, CAF-GM-100TGF-β1, CAF-GM-500TGF-β1, CAF-GM-1000TGF-β1, and CAF-GM-5000TGF-β1), and CAF aggregates incorporating GM in the presence of free TGF-β1 (CAF-GM + fTGF-β1). (B) Time schedule of free TGF-β1 solution addition in the culture medium. When the culture was started, 20 % of total TGF-β1 amounts were added. After 7 days after incubation, 20 % of the total amounts were added on day 7, 8, 9, and 10. The total amount of TGF-β1 added was the same as that of TGF-β1 incorporated 10 days after incubation.

### 4.2.6. Evaluation of cell number

To evaluate the cell number in CAF-GM, various CAF-GM-TGF-β1, and CAF-GM + fTGF-β1, CAF aggregates were taken into a microtube. After

their centrifugation, the culture medium was carefully removed and the CAF aggregates were washed with 200 µl of PBS. After removing PBS, 200 µl of collagenase was added and samples were incubated at 37 $^{o}$C for 30 min to allow to completely degrade GM. Then, 50 µl of 2.5 g/l-trypsin and 1 mmol/l-EDTA solution (Nacali tesque, Inc., Kyoto, Japan) was added and samples were incubated at 37 $^{o}$C for 30 min while they were pipetted every 5 min to facilitate the dissociation of CAF aggregates. The enzyme action was stopped by the addition of 50 µl of culture medium. The total cell number per cell aggregates was measured.

4.2.7. Evaluation of α-SMA expression level

To evaluate the level of alpha-smooth muscle actin (α-SMA) expression, various types of CAF aggregates were measured by using alpha-smooth muscle actin ELISA kit (NBP2-66429) (Novus Biologicals, LLC, New York, USA). The α-SMA expression level was calculated by dividing the total cell number.

4.2.8. Invasion assay

To evaluate the cancer invasion ability by co-culture of cancer cells with various types of CAF aggregates, the cancer invasion assay was performed by using Cytoselect 96 well invasion assay (Cell Biolabs, Inc., San Diego, USA). In brief, 150 µl of CAF aggregates (10 days after incubation) was added (150 µl) into the tubes. The tubes were centrifuged and the supernatant was removed. Then, 800 µg/ml of an MMP inhibitor or standard medium was added (150 µl) to the tubes, and the suspensions were plated to the well of feeder tray. After the membrane chamber was placed into the feeder tray, the cancer cell suspension (100 µl, $2.0 \times 10^5$ cells/well

in FCS-free medium) was added to the membrane chamber. The samples were incubated for 24 hr. After completely dislodging the cancer cells from the underside of the membrane, the lysis buffer dye solution was added. Then, the fluorescent intensity was measured in a fluorescence spectrometer (F-2000, HITACHI Ltd, Tokyo, Japan) at excitation and emission wavelengths of 480 and 520 nm, respectively. Calculation of cancer invasion rate was followed: Cell number of cancer cells in underside of the membrane was divided by $2.0 \times 10^5$ cells. Moreover, the culture medium was collected, and then the amount of MMP-2 secreted was measured by total MMP-2 quantikine ELISA kit (MMP200) (R&D Systems, Inc., Minneapolis, USA).

4.2.9. Statistical analysis

All the data were statistically analyzed and expressed as the mean ± the standard error of the mean. The data were analyzed by student t-test or Tukey's test to determine the statistically significant difference while the significance was accepted at $p < 0.05$. Experiments for each sample were performed three wells independently unless otherwise mentioned.

## 4.3. Results

### 4.3.1. Morphology of GM

Figure 4.3 shows the microscope picture of GM. The GM were spherical and had a smooth surface. The size in the swollen condition ranged 46.5 ± 5.18 μm.

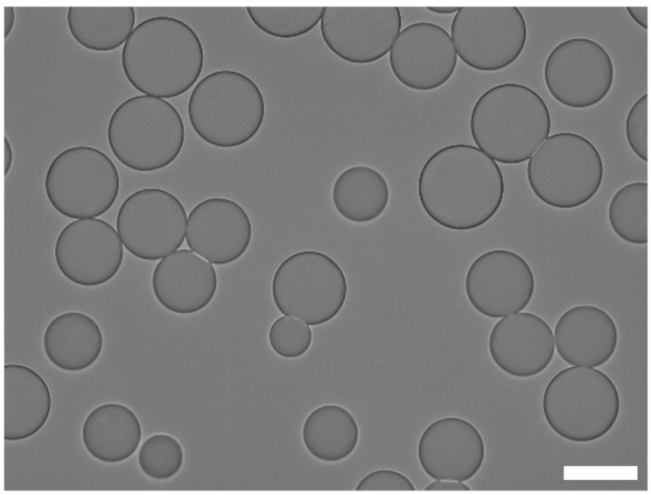

Figure 4.3. A light microscope photograph of GM dispersed in the water. Scale bar; 50 μm.

### 4.3.2. Time profile of TGF-β1 release from GM-TGF-β1

Figure 4.4 shows the TGF-β1 release profile from GM-TGF-5000β1. When GM-5000TGF-β1 were incubated into PBS, an initial slow release of TGF-β1 was observed. On the other hand, TGF-β1 was released with time by the addition of collagenase.

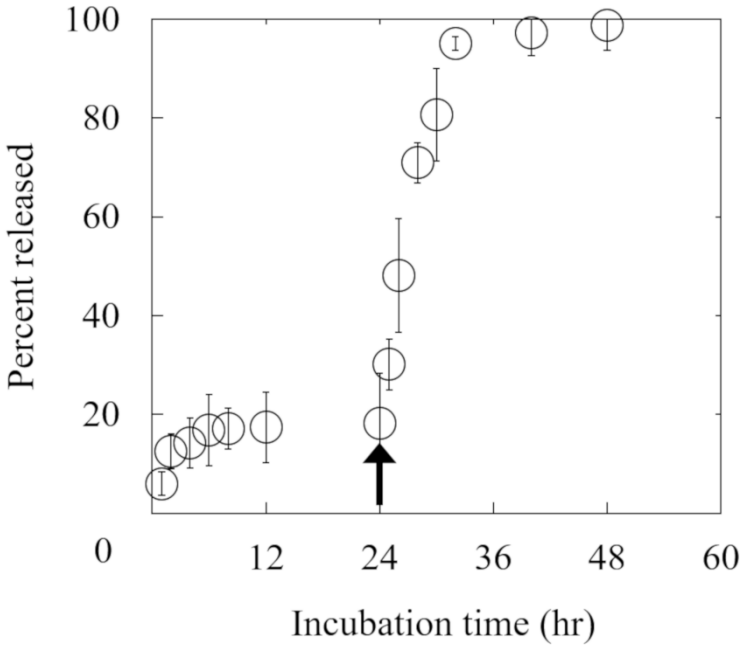


Figure 4.4. *In vitro* time profile of TGF-β1 from GM-5000TGF-β1. Collagenase was added into PBS at 24 hr indicated by the arrow.

4.3.3. Characterization of CAF-GM, CAF-GM-TGF-β1, and CAF-GM + fTGF-β1

Figure 4.5 shows the light microscope pictures of CAF-GM, CAF-GM-TGF-β1, and CAF-GM + fTGF-β1. All types of CAF aggregates were formed 7 days after incubation. The TGF-β1 presence, the TGF-β1 concentrations, and the addition of free TGF-β1 solution did not affect the morphology or size of aggregates (Figures 4.5 and 4.6). In addition, the size of CAF aggregates 15 days after incubation was significantly smaller than that 10 days later.

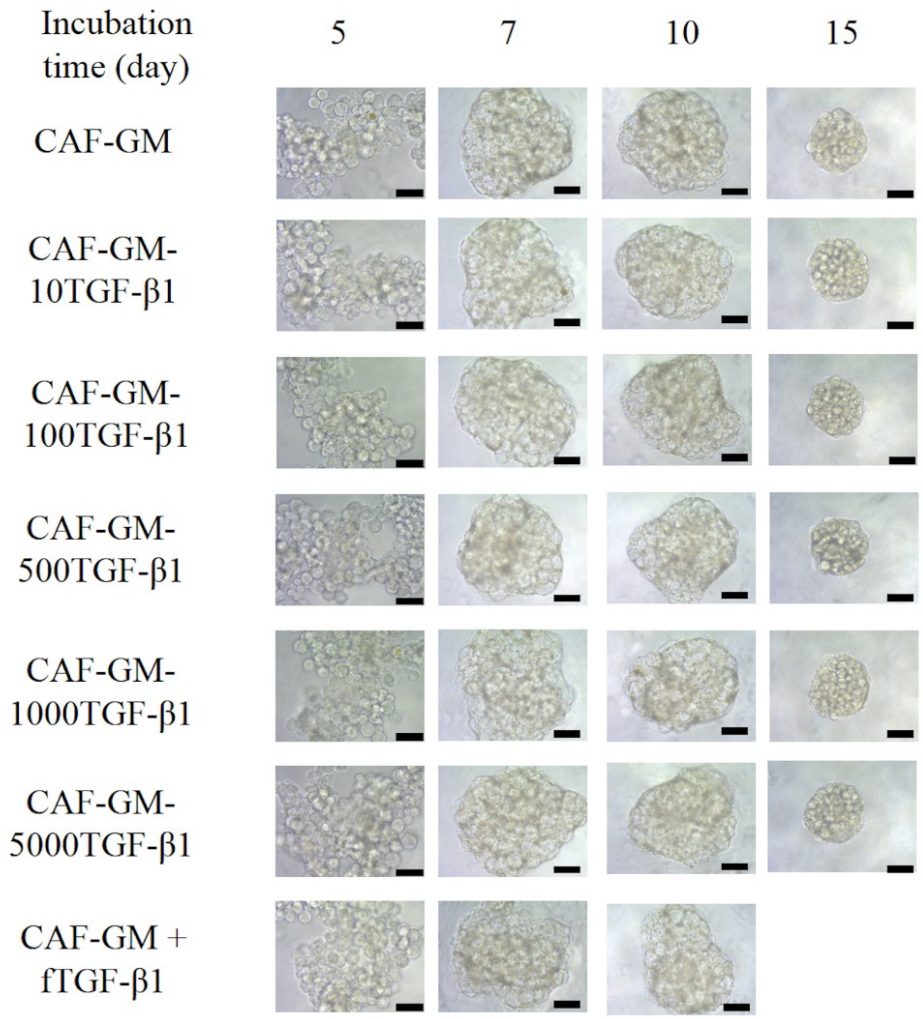


CAF-GM + fTGF-β1 were not cultured 10 days later because the amount of TGF-β1 added into the culture medium was higher than that of TGF-β1 contained in GM.

Figure 4.5. Light microscope photographs of CAF-GM, CAF-GM-10TGF-β1, CAF-GM-100TGF-β1, CAF-GM-500TGF-β1, CAF-GM-1000TGF-β1, and CAF-GM-5000TGF-β1 5, 7, 10, and 15 days after incubation or that of CAF-GM + fTGF-β1 5, 7, and 10 days after incubation. Scale bar; 200 μm.

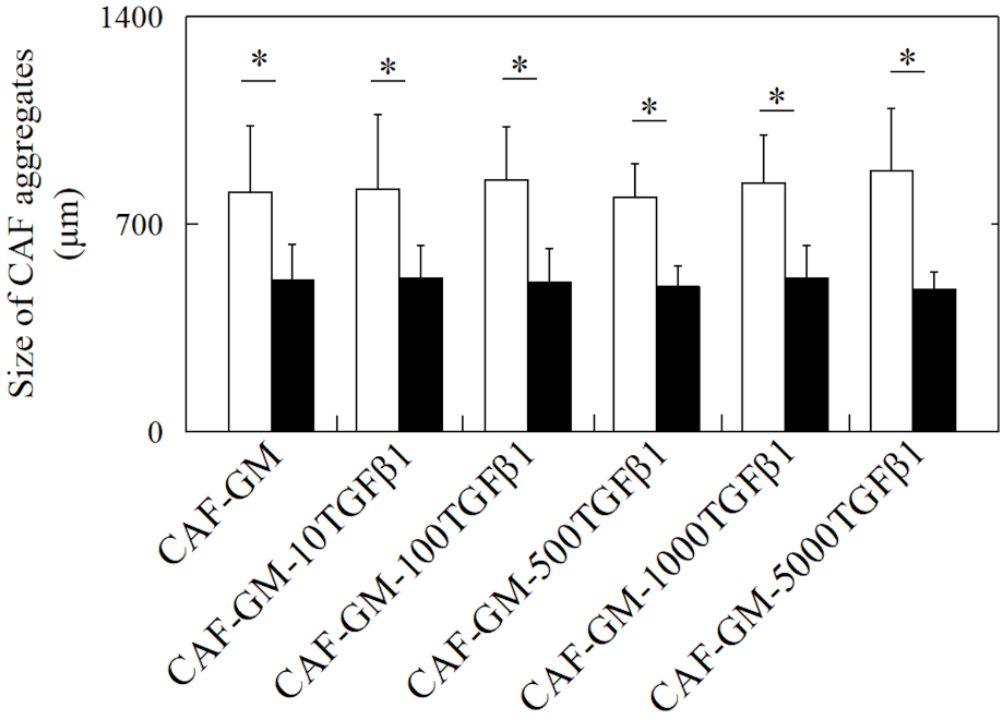


Figure 4.6. Size of CAF aggregates for CAF-GM, CAF-GM-10TGF-β1, CAF-GM-100TGF-β1, CAF-GM-500TGF-β1, CAF-GM-1000TGF-β1, and CAF-GM-5000TGF-β1 groups 10 (□), and 15 days after incubation (■). *$p$< 0.05; significant difference between the two groups.

4.3.4. Cell number in CAF-GM, various types of CAF-GM-TGF-β1, and CAF-GM + fTGF-β1

Figure 4.7. shows the cell number for CAF-GM, CAF-GM-TGF-β1, and CAF-GM + fTGF-β1. TGF-β1 presence, the TGF-β1 concentrations, and the addition of free TGF-β1 solution did not affect the cell number. In addition, the cell number 10 days after incubation was significantly higher than that 5 days later.

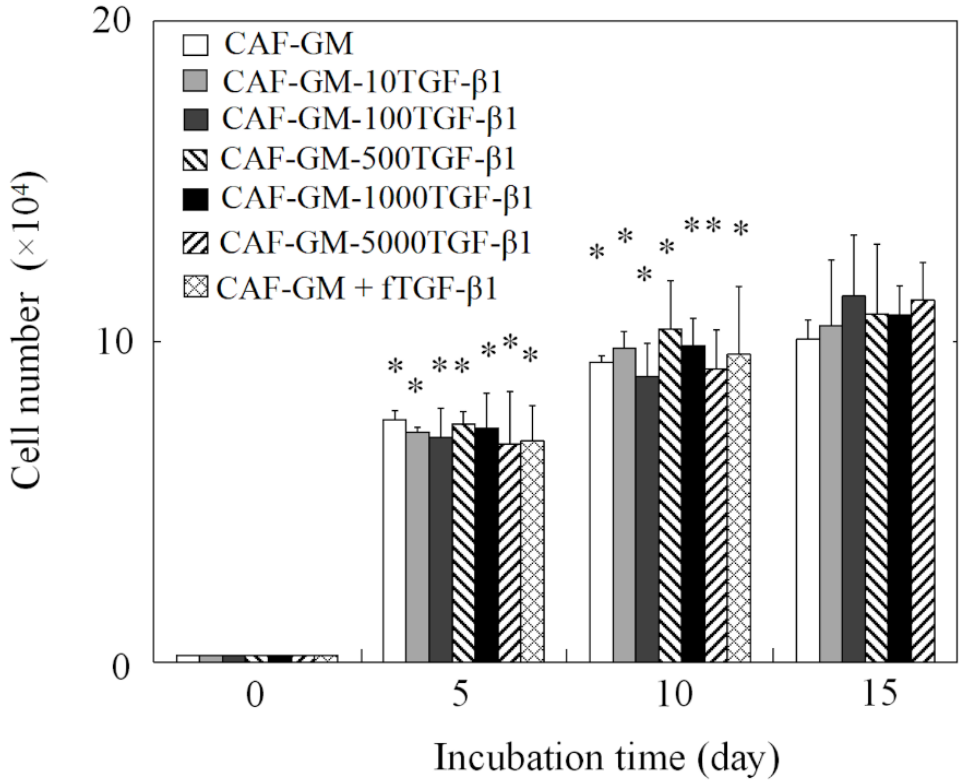


Figure 4.7. Cell number of CAF aggregates for CAF-GM, CAF-GM-10TGF-β1, CAF-GM-100TGF-β1, CAF-GM-500TGF-β1, CAF-GM-1000TGF-β1, and CAF-GM-5000TGF-β1 groups 5, 10, and 15 days after incubation or CAF-GM + fTGF-β1 5 and 10 days after incubation. *$p$< 0.05; significant difference against the cell number for the same condition of CAF 5 days before.

4.3.5. α-SMA expression level of CAF-GM, various types of CAF-GM-TGF-β1, and CAF-GM + fTGF-β1

To evaluate the effect of TGF-β1 on the CAF activation, the α-SMA expression level was measured 5, 10, and 15 days after incubation (Figure 4.8). There was no significant difference in the α-SMA expression level among all types of CAF 5 days after incubation. However, 10 and 15 days

after incubation, the α-SMA expression level for CAF-GM-500TGF-β1 was significantly higher than that for CAF-GM, CAF-GM-10TGF-β1, and CAF-GM-100TGF-β1. Although the α-SMA expression level for CAF-GM-1000TGF-β1 was significantly higher than that for CAF-GM-500TGF-β1, there was no significant difference between the CAF-GM-1000TGF-β1 and CAF-GM-5000TGF-β1. In addition, the α-SMA expression level for CAF-GM + fTGF-β1 was not significantly different from that for CAF-GM, CAF-GM-10TGF-β1, or CAF-GM-100TGF-β1 5 and 10 days after incubation.

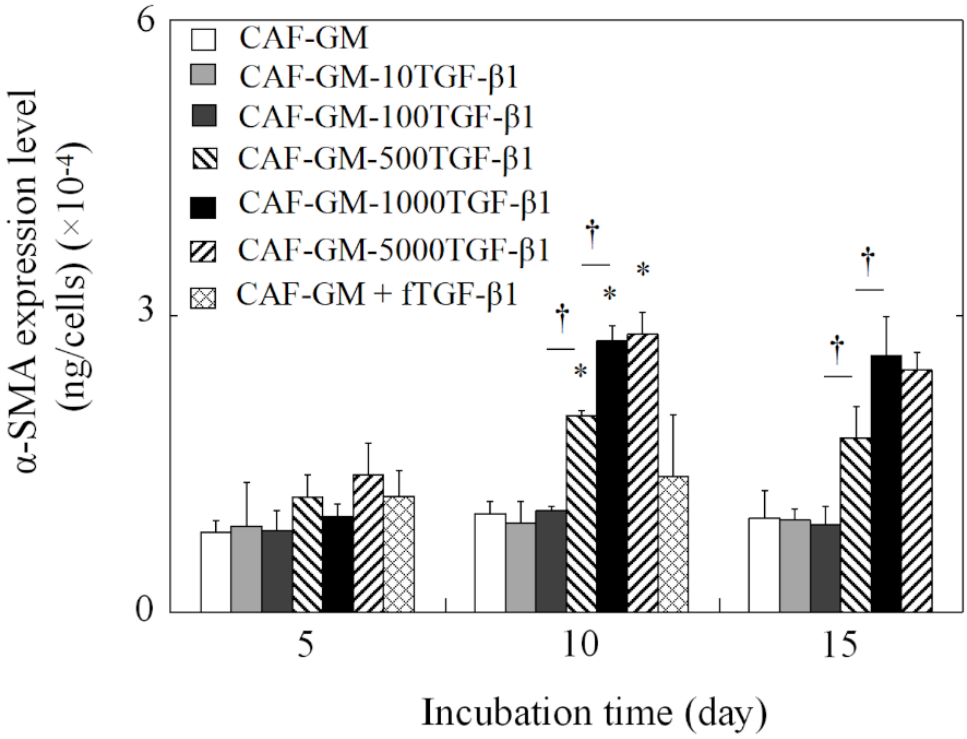


Figure 4.8. α-SMA expression level of CAF aggregates for CAF-GM, CAF-GM-10TGF-β1, CAF-GM-100TGF-β1, CAF-GM-500TGF-β1, CAF-GM-1000TGF-β1, and CAF-GM-5000TGF-β1 groups 5, 10, and 15 days after incubation or CAF-GM + fTGF-β1 5 and 10 days after incubation. *$p$< 0.05; significant difference against the α-SMA expression level for the same condition of CAF 5 days before. †$p$< 0.05; significant difference between the two groups.

4.3.6. Invasion assay

Figure 4.9A shows that the invasion rate of cancer cells by co-cultured with CAF-GM, various CAF-GM-TGF-β1, and CAF-GM + fTGF-β1. Figure 4.9B shows that the correlation between the invasion rate and α-SMA expression level. The coefficient of determination was about 0.87. In

addition, Figure 4.9C shows that the correlation between the invasion rate and the TGF-β1 concentration. The coefficient of determination was about 0.96. Figure 4.10 shows the invasion rate of cancer cells by MMP inhibitor. The invasion rate of cancer cells by co-cultured with CAF-GM-500TGF-β1, CAF-GM-1000TGF-β1, and CAF-GM-5000TGF-β1 decreased by MMP inhibitor. However, the effect of MMP inhibitor was not observed in CAF-GM, CAF-GM-10TGF-β1, CAF-GM-100TGF-β1, and CAF-GM + fTGF-β1. Moreover, the secretion level of MMP-2 had an important role in the cancer invasion rate (Figure 4.11).

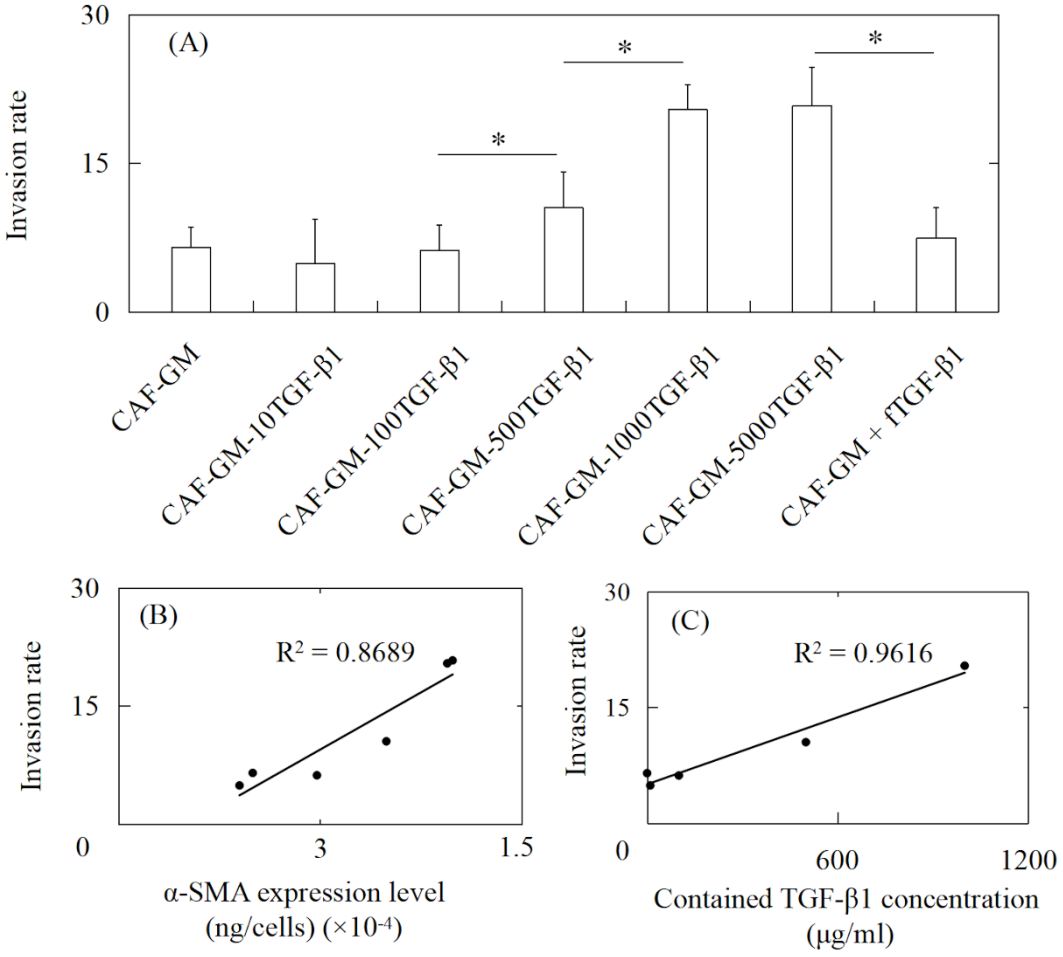


Figure 4.9. (A) Invasion rate of cancer cells by co-cultured with CAF-GM, CAF-GM-10TGF-β1, CAF-GM-100TGF-β1, CAF-GM-500TGF-β1, CAF-GM-1000TGF-β1, CAF-GM-5000TGF-β1, and CAF-GM + fTGF-β1 groups 1 days after incubation. *$p$< 0.05; significant difference between the two groups. (B) Correlation between the α-SMA expression level and the invasion rate. (C) Correlation between the TGF-β1 concentration and the invasion rate.

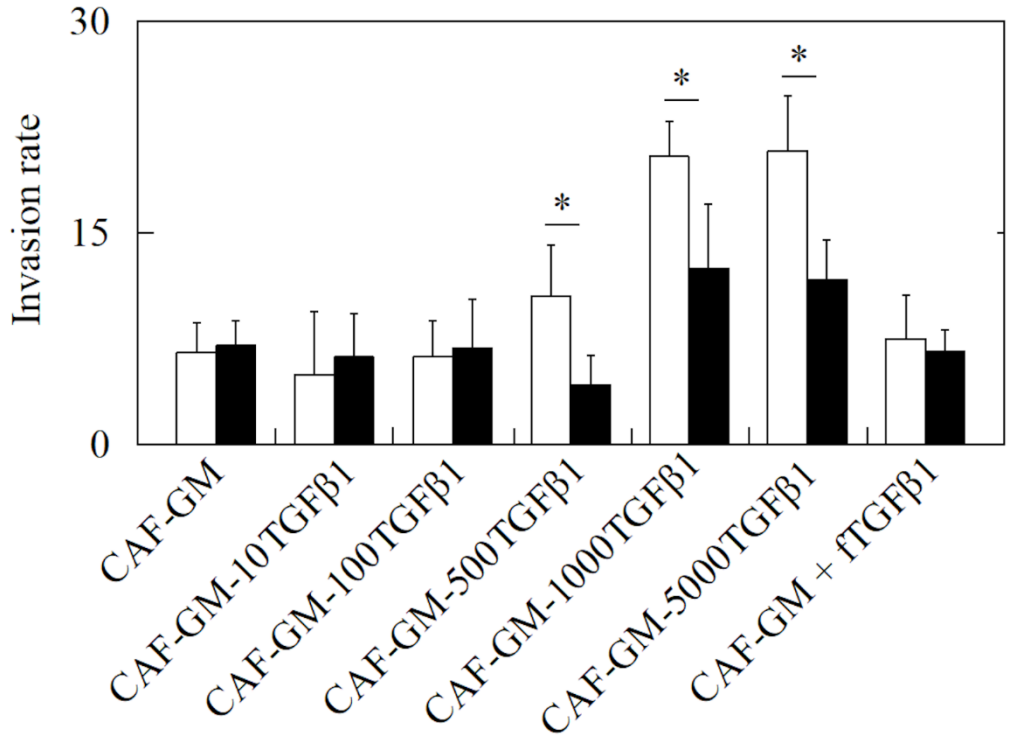


Figure 4.10. Invasion rate of cancer cells by co-cultured with CAF-GM, CAF-GM-10TGF-β1, CAF-GM-100TGF-β1, CAF-GM-500TGF-β1, CAF-GM-1000TGF-β1, CAF-GM-5000TGF-β1 groups, and CAF-GM + fTGF-β1 1 days after incubation: culture without (□) or with MMP inhibitor addition (■). *$p$< 0.05; significant difference between the two groups.

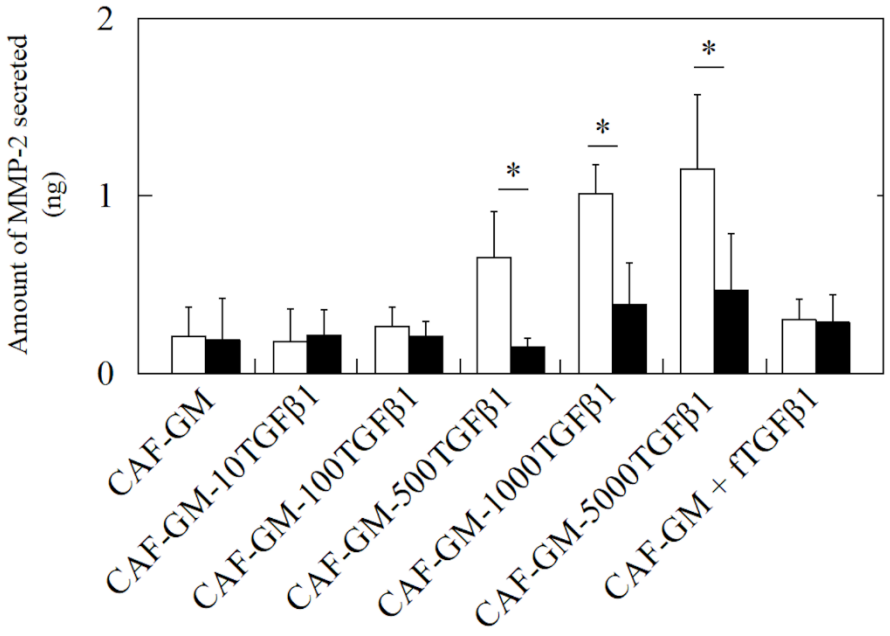


Figure 4.11. Amount of MMP-2 secreted by co-cultured with CAF-GM, CAF-GM-10TGF-β1, CAF-GM-100TGF-β1, CAF-GM-500TGF-β1, CAF-GM-1000TGF-β1, CAF-GM-5000TGF-β1, and CAF-GM + fTGF-β1 groups 1 days after incubation: culture without (□) and with MMP inhibitor addition (■). *$p$< 0.05; significant difference between the two groups.

### 4.4. Discussion

For the combination with cell aggregates, various microspheres of gelatin [72, 76, 110], poly (lactic-*co*-glycolic acid) (PLGA) [77, 111-113], and alginate [114, 115] were investigated. Among these materials, in this study, gelatin was used because of the high cell adhesiveness or lower cytotoxicity [15-17]. GM used in this study were of 32-53 μm in diameter dehydrothermally crosslinked for 72 hr. Because the previous study demonstrates that GM with this property is good for the purpose of cell aggregates incorporating GM [41]. In terms of the mixing ratio of cells to GM, 10:1 was selected because this mixing ratio was appropriate to form the cell aggregates incorporating GM [72]. In addition, in this study, two-dimensional (2D) CAF and CAF aggregates without GM were not prepared as controls. Because the biological functions of 2D CAF and CAF aggregates without GM were found to be much lower than that of CAF-GM due to the lower cell-cell contact and rapid cell death, respectively [97].

In the previous study, the proliferation of bone marrow stem cells was improved based on the TGF-β1 controlled release from GM-TGF-β1 [96]. TGF-β1 slow release from GM-TGF-β1 can enhance cell activity or functions. However, the effect of the TGF-β1 controlled release from GM-TGF-β1 on the CAF functions has not been studied. From the TGF-β1 release profile, about 20 % of TGF-β1 total amount was initially released from GM-TGF-β1 in PBS. The previous studies revealed that TGF-β1 could be controlled release from GM [96]. By the addition of collagenase, TGF-β1 was released with time. It is likely that TGF-β1 was released as the gelatin degradation of GM by collagenase. In addition, the TGF-β1 concentration did not affect the drug release profile (data not shown). The number of gelatin molecules would be large enough to molecularly associate with

TGF-β1.

To claim the advantageous effect of TGF-β1 release “inside” CAF aggregates, free TGF-β1 solution was daily added into the CAF-GM culture medium. To this end, it is important to determine the addition schedule considering the release profile. From Figure 4.4, 20 % of the total TGF-β1 amount contained was initially released in PBS, followed by the controlled TGF-β1 release as the result of GM degradation with time was observed. Based on the release profile, at the starting point of culture, 20 % of the total TGF-β1 amount was added into the culture medium. After CAF-GM were formed (7 days), 20 % of the total TGF-β1 amount was added every day (Figure 4.2B). Because it has been reported that cell aggregates produce the enzyme, cytokine, or chemokine much more efficiently than non-aggregated cells [2, 3, 5]. At 10 days, the amount of free TGF-β1 solution is the same as that of TGF-β1 contained. The total amount of TGF-β1 solution would not be lower than that of TGF-β1 released from GM-TGF-β1. Taken together, the effect of TGF-β1 released in CAF aggregates 10 days after incubation could be evaluated. It is no doubt that the time schedule of TGF-β1 addition does not always simulate that of TGF-β1 released from GM-TGF-β1.

It is apparent from Figures 4.5-4.7, the TGF-β1 present, TGF-β1 concentrations, and the addition of free TGF-β1 solution did not affect the morphology, size, and cell number. Although the reason is not clear at present, the previous study suggests that the characterization of GM did not affect these parameters [41, 72]. The size of CAF aggregates 15 days after incubation was smaller than that 10 days because of the GM degradation (Figures 4.5 and 4.6). The previous study demonstrates that the GM degradation led to a decrease in the size of cell aggregates and the

biological functions of cell aggregates [72]. Based on the reasons, in this study, CAF aggregates were cultured until 15 days.

α-SMA is one of the most important markers for CAF. When the α-SMA level of CAF is high, it is experimentally characterized as CAF activation [46, 78, 79]. The α-SMA expression level 5 days after incubation was not significantly different. However, 10 and 15 days after incubation, the α-SMA expression level of CAF-GM-500TGF-β1 was significantly different from that of CAF-GM, CAF-GM-10TGF-β1, and CAF-GM-100TGF-β1 (Figure 4.8). In addition, the α-SMA expression level of CAF-GM-1000TGF-β1 and CAF-GM-5000TGF-β1 was much higher than that of CAF-GM-500TGF-β1. The findings clearly indicate that TGF-β1 was effective in CAF activation. However, there is no significant difference in α-SMA expression level between CAF-GM-1000TGF-β1 and CAF-GM-5000TGF-β1. There would be due to an upper limit in the CAF activation. Therefore, more than 5000 μg/ml of TGF-β1 concentration was not used to evaluate in this study. Interestingly, the addition of free TGF-β1 solution did not enable CAF to activate although the amount of TGF-β1 is the same or higher than that of TGF-β1 released. It is highly possible to say that the TGF-β1 release “in” CAF aggregates had a positive effect on activating CAF. This is because that the TGF-β1 is closely and uniformly released and exposed to cells.

Figure 4.9A shows the cancer invasion after the co-cultured of cancer cells with CAF-GM, various CAF-GM-TGF-β1, and CAF-GM + fTGF-β1. There was a good correlation between the α-SMA expression level and the cancer invasion rate (Figure 4.9B). A novel cancer invasion model using CAF aggregates incorporating GM containing a p53 inhibitor has been designed. This model was a promising tool for evaluating the cancer

invasion *in vitro*. However, the cancer invasion rate did not become higher with an increasing drug concentration. It is reported that on a high drug concentration, the cancer invasion rate was significantly higher than that on lower concentrations [97]. For further research on cancer invasion or metastasis, a cancer invasion model where the invasion rate can be regulated should be developed. It is apparent from Figure 4.9C that this cancer invasion model of CAF aggregates incorporating GM-TGF-β1 can regulate the extent of the cancer invasion by simply changing the TGF-β1 concentration contained in GM. In addition, the MMP inhibitor treatment significantly decreased the invasion rate. Moreover, the secretion level of MMP-2 had an important role in the high cancer invasion rate (Figure 4.11). Among the MMP, MMP-2 and 9 are essential to degrade the basement membrane. In this model, the secretion level of MMP-9 was not observed (data not shown). In this study, cancer cells would invade via the MMP-2 system *in vitro*. In the *in vivo* system, the cancer invasion via MMP is well known as a standard characterization. Therefore, a model to simulate the cancer invasion was designed. By the addition of free TGF-β1, the cancer invasion rate did not change, irrespective of the TGF-β1 concentrations (Figure 4.12).

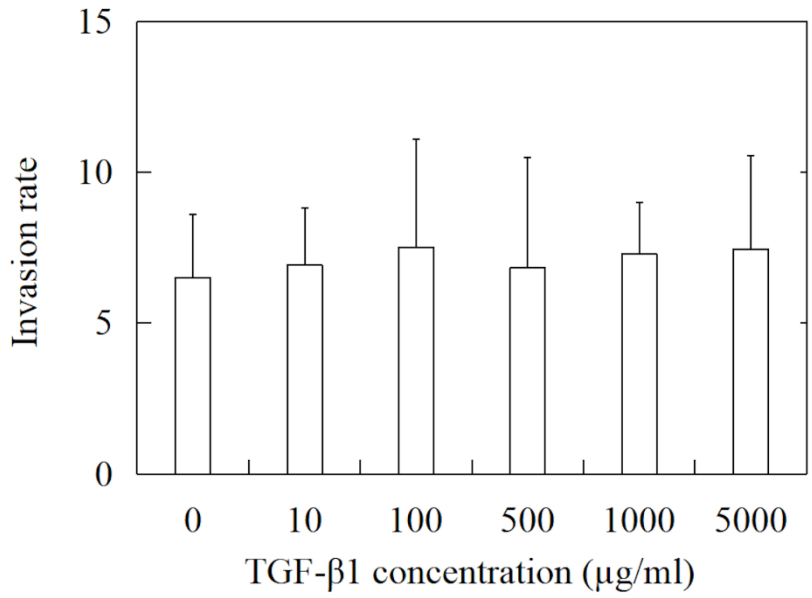


Figure 4.12. Invasion rate of cancer cells by co-cultured with CAF-GM, CAF-GM by addition of 10, 100, 500, 1000, and 5000 μg/ml TGF-β1 solution.

Again, this finding indicates the importance to release TGF-β1 in CAF aggregates for efficient CAF activation and the consequently regulated tumor invasion phenomenon.

# Chapter 5

# A co-culture system of three-dimensional tumor-associated macrophages and three-dimensional cancer-associated fibroblasts combined with biomolecule release for cancer cell migration

## 5.1. Introduction

The cancer environment is one of the essential factors to understand cancer characteristics, such as proliferation [116], invasion [117], metastasis [118], and drug resistance [63]. Stromal cells in the cancer environment are composed of cancer-associated fibroblasts (CAF), tumor-associated macrophages (TAM), endothelial cells, mesenchymal stem cells, or fat cells [46, 105]. Among these cells, CAF or TAM are major components that have been noted in the field of cancer researches [119-121]. For example, both CAF and TAM interact with cancer cells, leading to a higher production of matrix metalloproteinase (MMP) which assists the invasion of cancer cells. Because MMP can degrade collagen and laminin, which are the major components of the basement membrane (Figure 5.1) [46, 58-61, 122-124].

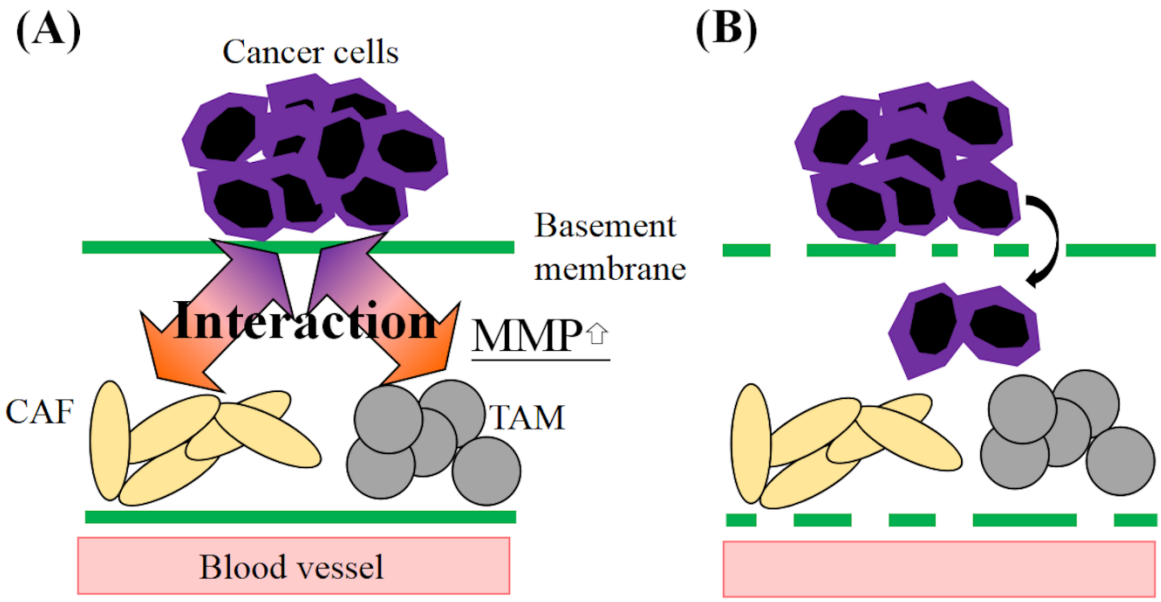


Figure 5.1. Description of cancer invasion based on the interaction between cancer and stromal cells *in vivo*. (A) Cancer cells generally exist in epithelial site and cannot invade the stromal site easily because of basement membrane presence. Both CAF and TAM of stromal cells interact with cancer cells, leading to an accelerated MMP production. The interaction ratio of CAF and TAM to cancer cells depends on tissue sites. (B) Much MMP production leads to degrade the basement membrane, which allows cancer cells to invade into the stromal site.

Although both CAF and TAM promote cancer invasion, the invasion rate of cancer cells generally depends on the type of body tissues. This is mainly due to the existence ratio of CAF and TAM [125].

Anti-cancer drug screening is normally performed by using the two-dimensional (2D) culture system of cancer cells [72, 126-129]. However, the drug efficacy of preclinical or clinical study is often different

from that of the *in vitro* drug-screening, which causes the failure of drug development [129, 130]. This is mainly because the *in vitro* culture conditions of cancer cells are quite different from those of *in vivo* cancer environment. There are two big differences; i) the cancer tissues generally consist of cancer cells and various stromal cells [46, 63]. Therefore, to mimic the cancer tissues, cancer cells should be not singly cultured, but co-cultured or tri-cultured with the stromal cells, such as CAF and TAM; ii) the 2D cell culture cannot mimic the three-dimensional (3D) cancer environment in the body. Thus, it is necessary to develop 3D cell culture technologies mimicking the body environment. In the body, it is well recognized that cells interact with other cells in a 3D manner to enhance biological functions, such as proliferation [4], cell-cell interaction [2], and enzyme secretion [131]. To this end, the 3D culture technologies [8-11], especially cancer 3D tissue engineering [132], have been reported. However, cells present in cell aggregates often lose the functions and die because of poor oxygen and nutrient supply [12, 66, 72]. In the previous study, gelatin hydrogel microspheres (GM) are incorporated in cell aggregates for enhanced cell survival [14, 72]. In addition, GM enable to release growth factors or drugs, leading to further enhanced cell functions [24, 26, 29, 30, 96]. On the other hand, GM have been used as a powerful biomaterial for tissue regeneration [72, 97-100, 133].

This study is undertaken to develop a biomaterial technology for the two issues described above. TAM aggregates incorporating GM were prepared to allow TAM to survive and enhance the functions. In addition, to further enhance the TAM functions, adenosine (A) ,which positively affects TAM functions [134-136], was impregnated in the GM for the sustained release in TAM aggregates (3D TAM-GM-A). The vascular endothelial growth factor

(VEGF) secretion was measured to evaluate the TAM function. Then, the 3D TAM-GM-A were co-cultured with liver cancer cells (HepG2) across a model basement membrane on both sides to investigate the invasion of cells. Following the co-culture of 3D TAM-GM-A and 3D CAF aggregates incorporating GM containing TGF-β1 (3D CAF-GM-TGF-β1) with lung cancer (WA-hT), breast cancer (MCF-7), and liver cancer (HepG2) cells, the effect of 3D TAM/3D CAF mixing ratio on the invasion rate of cancer cells was evaluated. The amount of MMP-2 production was examined to compare with the cancer cell invasion rate.

## 5.2. Methods

### 5.2.1. Preparation of gelatin hydrogel microspheres

Gelatin hydrogel microspheres (GM) were prepared by the chemical crosslinking of gelatin in a water-in-oil emulsion state according to the method previously reported [27]. Briefly, an aqueous solution (20 ml) of 10 wt % gelatin (isoelectric point 5.0, weight-averaged molecular weight = 100,000, Nitta Gelatin Inc., Osaka, Japan) was preheated at 40 ºC, followed by stirring at 300 rpm for 10 min to prepare the water-in-oil emulsion. The emulsion temperature was decreased at 4 ºC for the natural gelation of gelatin solution to obtain non-crosslinked hydrogel microspheres. The resulting gelatin hydrogel microspheres were washed three times with cold acetone in combination with centrifugation (5,000 rpm, 4 ºC, 5 min) to completely exclude the residual oil. Then, GM were fractionated by size using sieves with apertures of 32 and 53 μm (Iida Seisakusho Ltd, Osaka, Japan) and air dried at 4 ºC. Then, non-crosslinked and dried GM (200 mg) were treated in a vacuum oven at 140 ºC to allow to dehydrothermally crosslink for 72 hr. The picture of GM in the swollen state was taken with a microscope (BZ-X710, KEYENCE Ltd, Osaka, Japan). The size of 100 microspheres for each sample was measured using the computer program Image J (NIH Inc., Bethesda, USA) to calculate the average diameters.

### 5.2.2. Preparation of gelatin hydrogel microspheres containing adenosine

Adenosine (A) (FUJIFILM Wako Pure Chemical Corporation, Osaka, Japan) was dissolved in double-distilled water (DDW) to give solution concentrations of 1, 3, and 5 μM. The A solution (20 μl) was dropped into 2 mg of gelatin hydrogel microspheres

(GM), followed by leaving at 37 $^{O}$C overnight for the impregnation of A

into the GM to prepare gelatin hydrogel microspheres containing adenosine (GM-A). The A solution was completely absorbed into the GM through the impregnation process because the solution volume was much less than theoretically required for the equilibrated swelling of GM. GM containing 1, 3, and 5 μM of A was named as GM-1A, GM-3A, and GM-5A, respectively.

5.2.3. Evaluation of adenosine release profile

GM-1A, GM-3A, and GM-5A (2 mg) were individually incubated in phosphate-buffered saline solution (PBS, pH 7.4). At different time intervals, the buffer was removed and replaced with fresh PBS. After 24 hr, PBS was replaced with collagenase solution in PBS (10 μg/ml) to allow GM to degrade. The amount of A released from GM-A was determined using adenosine assay kit (ab211094, Abcam, Cambridge, UK).

5.2.4. Cell culture experiments

WA-hT cells of a human small cell carcinoma cell line (RIKEN, Japan) and WA-mFib cells of a cancer-associated fibroblasts (CAF) cell line derived from WA-hT were cultured in minimum essential medium (MEM) (Sigma-Aldrich Co. LLC. St. Louis, USA). MCF-7 cells of a human breast adenocarcinoma cell line (JCRB Cell Bank, Tokyo, Japan) and HepG2 cells of a human liver carcinoma cell line (JCRB Cell Bank, Tokyo, Japan) were cultured in Dulbecco's Modified Eagle's Medium (DMEM) (Thermo Inc. Waltham, USA). THP-1 cells of a human monocytes cell line were cultured in Roswell Park Memorial Institute medium-1640 (RPMI 1640) (Thermo Inc. Waltham, USA). Each culture medium was supplemented with 10 vol % fetal calf serum (FCS) (Thermo Inc., Waltham, USA) and 50 U/mL penicillin/streptomycin.

The polarization induction of THP-1 cells to TAM was performed according to the protocols previously established [134]. In brief, 100 ng/ml phorbol 12-myristate 13-acetate was added into the medium, followed by culturing THP-1 for differentiation into macrophages. After 16 hr, the macrophages obtained were stimulated with 100 ng/ml lipopolysaccharide (LPS) plus 5 μM A. TAM were maintained by culturing in the medium containing 100 ng/ml LPS and 5 μM A.

5.2.5. Preparation of different TAM aggregates and evaluation of VEGF secretion

A poly (vinyl alcohol) (PVA) sample (the degree of polymerization = 1,800, the saponification = 88 mole %, and molecular weight = $8.8\times10^4$) kindly supplied from Unitika Ltd. (Tokyo, Japan) was dissolved in PBS (pH 7.4, 1 wt %). The PVA solution was added to each well of round-bottomed (U-bottomed) 96 multi-well culture plate (200 μl/well) and incubated at 37 $^{o}$C for 15 min. Then, the solution was removed by aspiration and the wells washed twice with PBS (200 μl/well). GM, GM-1A, GM-3A, or GM-5A ($1\times10^3$ microspheres/ml, 100 μl) were suspended in the standard medium. Next, TAM suspension ($1\times10^6$ cells/ml, 100 μl) was prepared and mixed with different GM suspensions, followed by the addition to the wells PVA precoated. TAM aggregates, TAM aggregates incorporating GM, and TAM aggregates incorporating GM-A were named as 3D TAM, 3D TAM-GM, and 3D TAM-GM-A, respectively. As a control, 3D TAM-GM plus free A (5 μM) added into the culture medium were prepared and named as 3D TAM-GM+A. Experimental set-up and abbreviations are illustrated in Figure 5.2. The time schedule of A addition is shown in Figure 5.3.

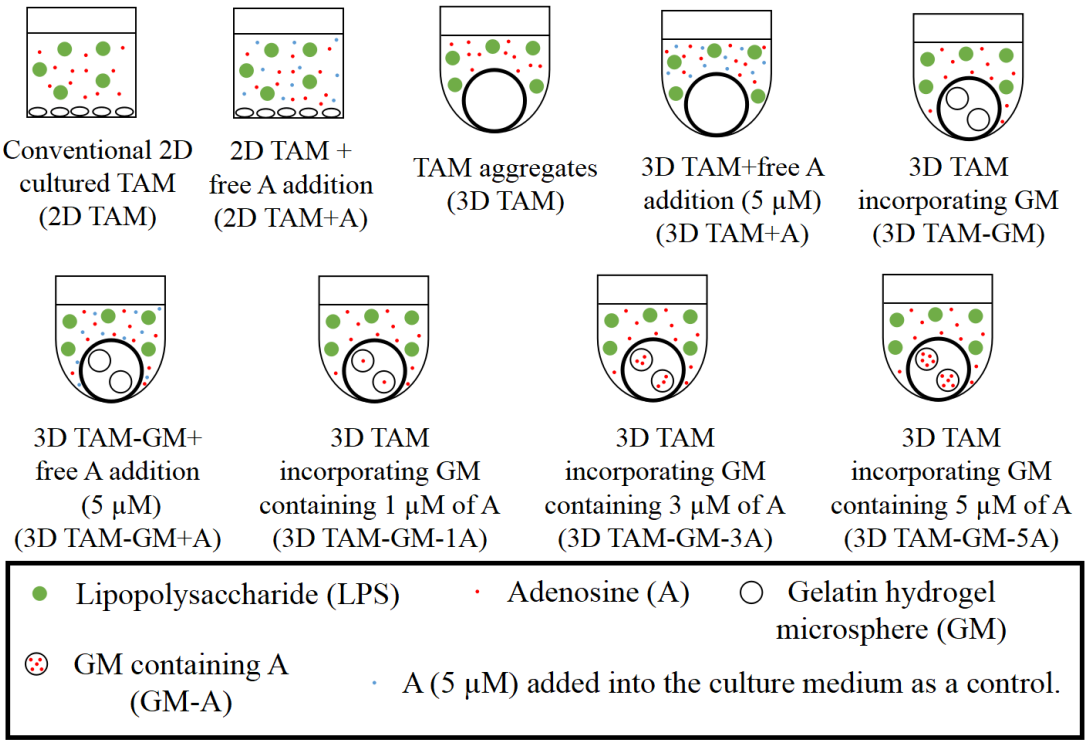


Figure 5.2. Experimental set-up of two-dimensional (2D) and three-dimensional (3D) TAM aggregates with or without GM and GM containing 1, 3, and 5 μM of adenosine. The amount of free adenosine added (free A addition) is 5 μM.

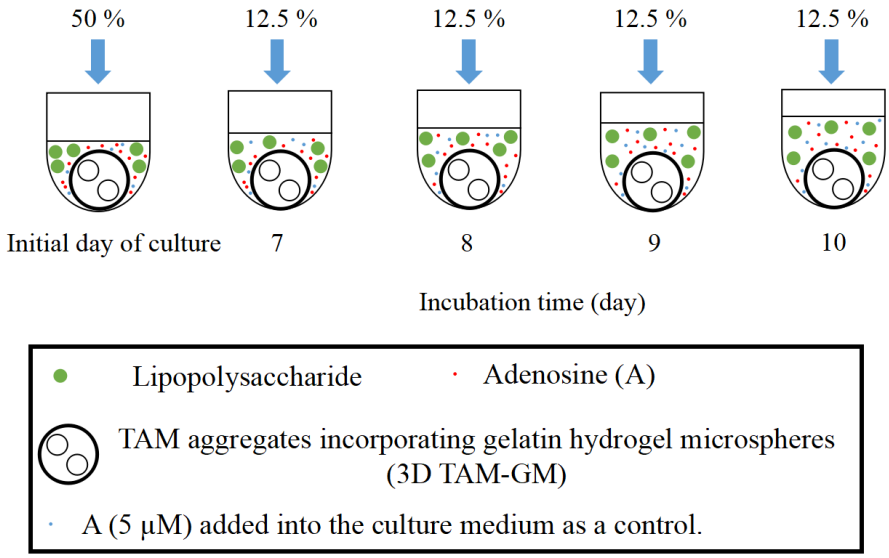


Figure 5.3. Time schedule of free A addition in the culture medium. At the initial day of culture, 50 % of total A amount contained was added. After 7 days incubation, 12.5 % of the total amount was added every day on days 7, 8, 9, and 10. The total amount of A added was the same as that of A contained in GM.

The pictures of 3D TAM, 3D TAM-GM, 3D TAM-GM-A, and 3D TAM-GM+A were taken with a microscope (CKX41, Olympus Ltd, Tokyo, Japan). The size of various TAM aggregates was measured using the computer program Image J (NIH Inc., Bethesda, USA) to calculate the average diameter.

To evaluate the TAM function, VEGF secretion at 5, 10, and 15 days after incubation was measured by using a human ELISA kit (R&D Systems Inc, Minneapolis, USA). Each experiment was independently performed at least 3 times unless otherwise mentioned.

### 5.2.6. Evaluation of 3D TAM-GM-A effect on cancer cell invasion

To evaluate the cancer invasion rate by co-culturing HepG2 cancer cells with the various types of TAM aggregates, a cancer invasion assay was performed by using Cytoselect 96 well invasion assay (Cell Biolabs, Inc., San Diego, USA). TAM aggregates cultured for 10 days were used for the assay. In brief, 2D TAM or 2D TAM+A suspensions (total cell number is 4.0 × $10^5$/well) or 3D TAM, 3DTAM+A, 3D TAM-GM, 3D TAM-GM+A, 3D TAM-GM-1A, 3D TAM-GM-3A, and 3D TAM-GM-5A (the same total cell number of 2D TAM or 2D TAM+A suspensions) were plated into the well of feeder tray. After the membrane chamber was set into the feeder tray, the HepG2 cell suspension (100 μl, 2.0 × $10^5$ cells/well in FCS-free medium) was added to the membrane chamber, followed by 24 h incubation. After completely dislodge cancer cells from the underside of the membrane, a Lysis Buffer dye solution (supplied reagent in assay kit) was added. Then, the fluorescent intensity was measured in a fluorescence spectrometer (F-2000, HITACHI Ltd, Tokyo, Japan) at excitation and emission wavelengths of 480 and 520 nm, respectively. The invasion rate of cancer cells was calculated as follows: the number of cancer cells in the underside of the membrane was divided by 2.0 × $10^5$. In addition, to evaluate the function of 3D TAM-GM-A, the amount of MMP-2 secreted in the medium was determined by the total MMP-2 quantikine ELISA kit (MMP200) (R&D Systems, Inc., Minneapolis, USA).

5.2.7. Assay of epithelial-mesenchymal transition

To evaluate the epithelial-mesenchymal transition (EMT) event, E-cadherin, N-cadherin, and Vimentin expression levels of invaded cancer cells were determined by the real-time polymerase chain reaction (RT-PCR). After the invasion assay finished, cancer cells penetrated through the

chamber membrane were collected, and then the total RNA was extracted using RNeasy Plus Mini Kit (QUIAGEN, Hilden, Germany) according to the manufacture's protocol. The complementary DNA (cDNA) was synthesized using a SuperScript VILO cDNA synthesis kit (Thermo Fisher Scientific Inc., Massachusetts, USA). The cDNA (100 ng, 1 µl), forward and reverse primers (10 µM, each 0.5 µl), and 25 µl of Power SYBR Green PCR Master Mix (Applied Biosystems, Foster City, CA) were mixed, and the RT-PCR was performed on a Prism 7500 real-time PCR thermal cycler (Applied Biosystems, Foster City, CA). The following PCR conditions were used: 95 ºC for 10 min, followed by 40 cycles of 95 ºC for 15 s and 60 ºC for 1 min. GAPDH was used as a housekeeping gene, and the expression level was analyzed by $\Delta\Delta Ct$ method comparing with the untreated cancer cells. The primer sequences for E-cadherin, N-cadherin, and Vimentin were as follows: (Forward and Reverse)

E-cadherin: 5'-CAAATCCAACAAAGACAAAGAAGGC-3'

5'-ACACAGCGTGAGAGAAGAGAGT-3'

N-cadherin: 5'-CATCATCATCCTGCTTATCCTTGT-3'

5'-GGTCTTCTTCTCCTCCACCTTCT-3'

Vimentin: 5'-TCGTGATGCTGAGAAGTTTCG-3'

5'-TCTGGATTCACTCCCTCTGGT-3'

GAPDH: 5'-GGACCTGACCTGCCGTCTAG-3'

5'-GTAGCCCAGGATGCCCTTGA-3'

5.2.8. Evaluation of 3D CAF-GM-TGF-β1 combination effect on the 3D TAM-GM-A-associated cancer cells invasion

To evaluate the influence of CAF on the 3D TAM-GM-A-associated cancer invasion, 3D aggregates of CAF incorporating GM containing 5000

μg/ml of TGF-β1 (3D CAF-GM-TGF-β1) were prepared. In one CAF aggregate, approximately 1.5 μg of TGF-β1 was incorporated. It is found that this 3D CAF-GM-TGF-β1 alone enhanced the invasion of cancer cells *in vitro*. The cancer invasion assay similar to section 5.2.6. was performed. In brief, three types of liver, breast, and lung cancer cells were individually added to the membrane chamber. The mixture of 3D CAF-GM-TGF-β1 and 3D TAM-CAF-A at different mixing ratios of 4:0, 3:1, 2:2, 1:3, and 0:4 were plated into the feeder tray. The invasion rate of cancer cells was assessed similarly.

5.2.9. Statistical analysis

All the data were statistically analyzed and expressed as the mean ± the standard error of the mean. The data were analyzed by student t-test or Tukey's test to determine the statistically significant difference while the significance was accepted at $p < 0.05$. Experiments for each sample were performed three wells independently unless otherwise mentioned.

## 5.3. Results

### 5.3.1. Characterization of GM

Figure 5.4 shows that the microscopic picture of GM. The GM were spherical and had a smooth surface. The size of GM in the swollen condition was 50.2 ± 8.51 μm.

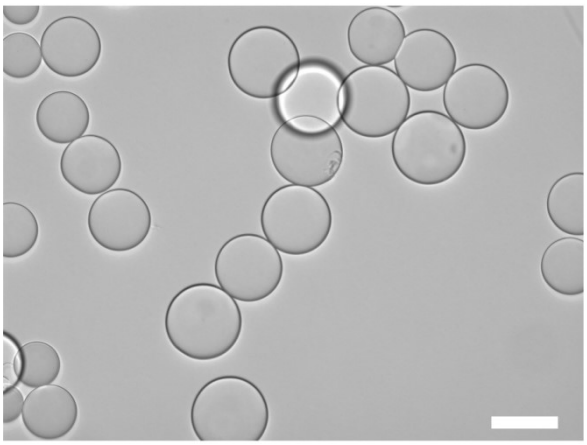

Figure 5.4. A light microscope photograph of GM dispersed in the water. Scale bar; 50 μm.

Figure 5.5 shows that the release profile of adenosine from GM-A. In PBS, a slow A release with time was observed and thereafter the release stopped. When collagenase was added into PBS, the A release was accelerated.

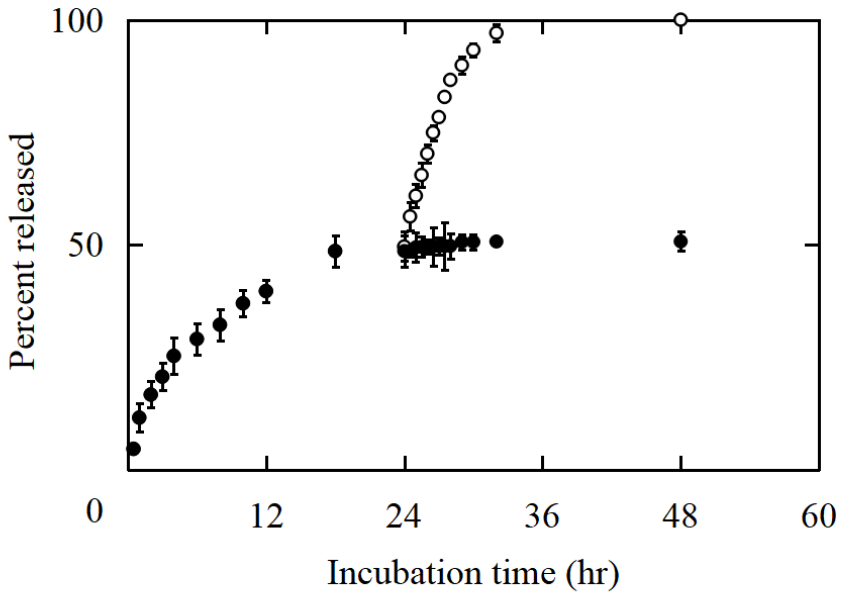


Figure 5.5. *In vitro* time profile of A from GM-5A in PBS and with (○) or without collagenase (●). Collagenase was added into PBS at 24 hr.

5.3.2. Characterization of different TAM aggregates

Figure 5.6 shows that the light microscopic pictures of 3D TAM, 3D TAM-GM, 3D TAM-GM-1A, 3D TAM-GM-3A, and 3D TAM-GM-5A. Figure 5.7 shows the time change of the size. The 3D TAM-GM were formed 7 days after incubation, irrespective of the GM type. The size of 3D TAM 5, 7, 10, and 15 days after incubation was about 200 μm, whereas that of 3D TAM-GM was about 900 μm. The formation time of 3D TAM and the size did not change by adding A into the medium, containing A into GM, and changing the A amount in GM. In addition, the size of 3D TAM-GM, 3D TAM-GM-1A, 3D TAM-GM-3A, and 3D TAM-GM-5A 15 days after incubation was smaller than that on 10 days (Figures 5.6 and 5.7).

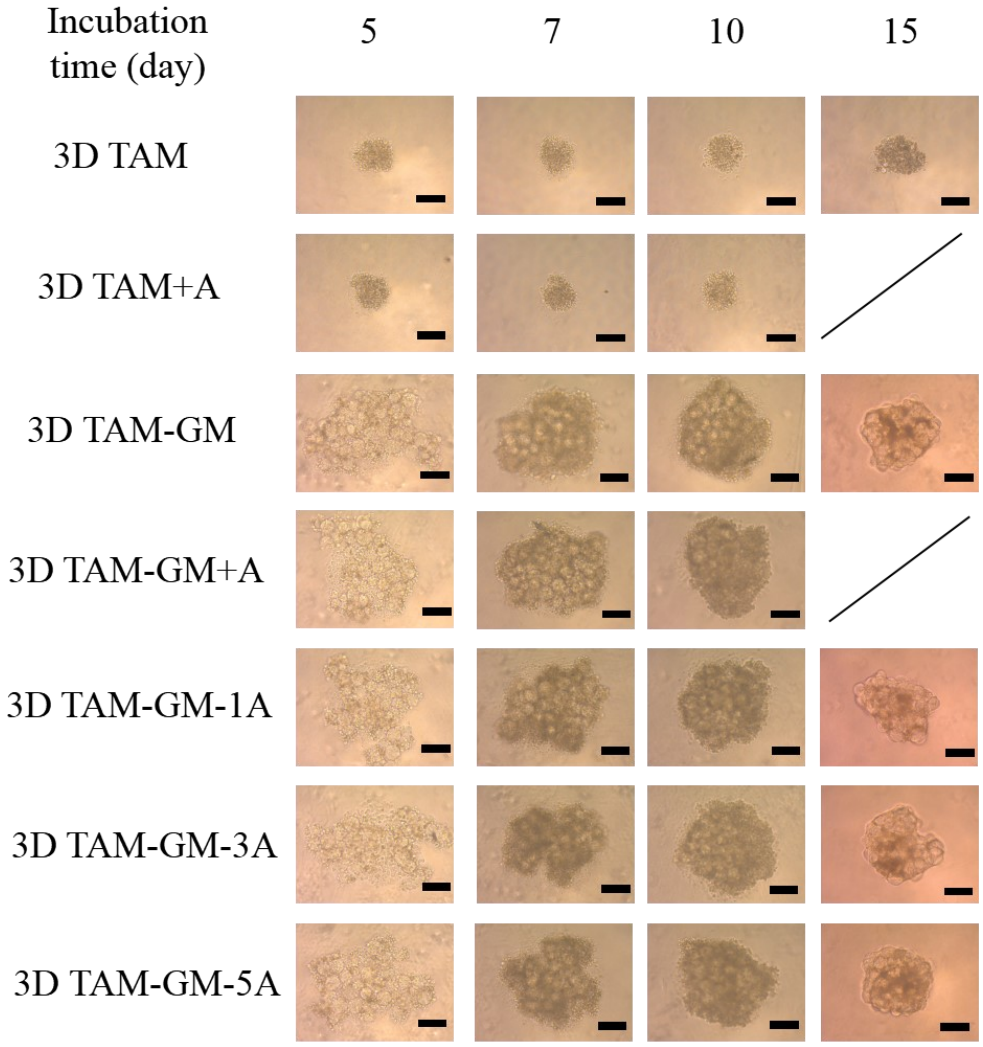


Figure 5.6. Light microscope photographs of 3D TAM, 3D TAM-GM, 3D TAM-GM-1A, 3D TAM-GM-3A, and 3D TAM-GM-5A 5, 7, 10, and 15 days after incubation or 3D TAM+A and 3D TAM-GM+A 5, 7, and 10 days after incubation. Scale bar; 200 μm.

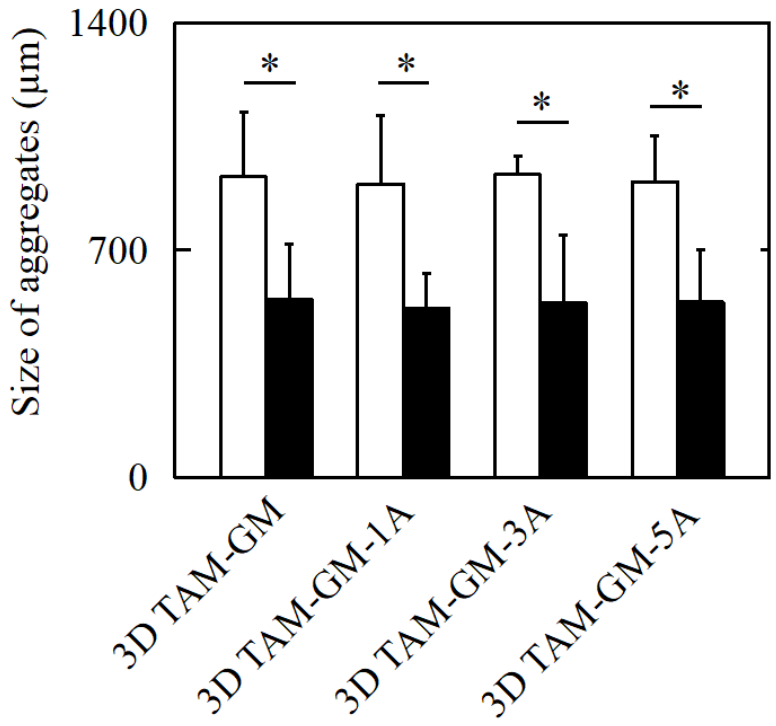


Figure 5.7. Size of 3D TAM-GM, 3D TAM-GM-1A, 3D TAM-GM-3A, and 3D TAM-GM-5A (□) 10 and (■) 15 days after incubation. $^{*}$, $p < 0.05$; significant difference between two groups.

Figure 5.8 shows the amount of VEGF secreted from various types of TAM. The secretion amount from the 3D TAM-GM-3A or 3D TAM-GM-5A was significantly higher than that from other groups although there was no significant difference between the 3A and 5A groups. Moreover, the addition of free A did not affect the amount of VEGF secreted, irrespective of culture dimension and GM type. 3D TAM-GM-3A or 3D TAM-GM-5A were cell aggregates to show a higher TAM function.

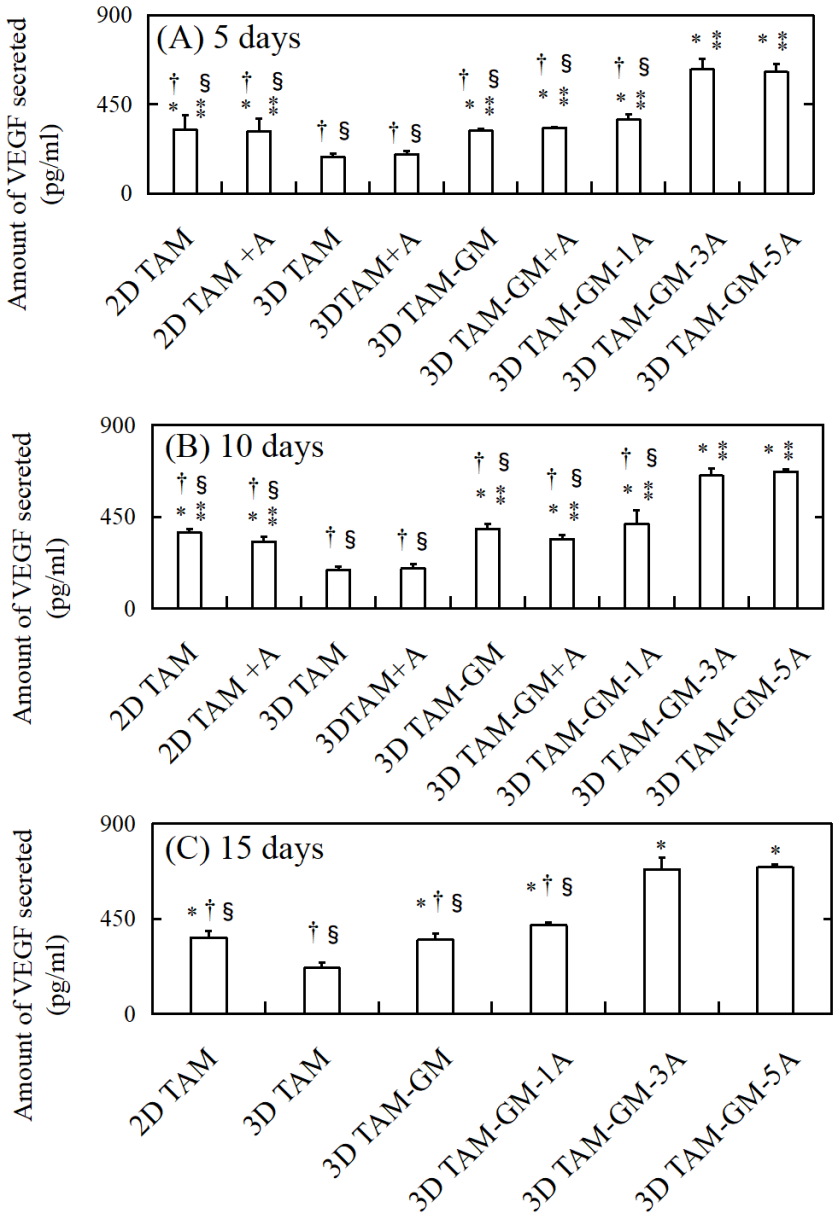


Figure 5.8. Amount of VEGF secreted from 2D TAM, 3D TAM, 3D TAM-GM, 3D TAM-GM-1A, TAM-GM-3A, and 3D TAM-GM-5A 5 (A), 10 (B), and 15 (C) days after incubation or from 2D TAM+A, 3D TAM+A, and TAM-GM+A 5 and 10 days after incubation. $^{*}$, $p < 0.05$; significant difference against the concentration of VEGF secreted from 3D TAM at the corresponding time. $^{**}$, $p < 0.05$; significant difference against the concentration of VEGF secreted from 3D TAM+A at the corresponding time.

[†], $p < 0.05$; significant difference against the concentration of VEGF secreted from 3D TAM-GM-3A at the corresponding time. [§], $p < 0.05$; significant difference against the concentration of VEGF secreted from 3D TAM-GM-5A at the corresponding time.

### 5.3.3. Cancer invasion rate

Figure 5.9 shows that the cancer invasion rate by co-culturing HepG2 cancer cells with the various types of TAM aggregates. The 3D culture, GM incorporation, GM containing 1 μM A, and the addition of free A did not affect the cancer invasion rate. However, co-culturing with 3D TAM-GM-3A or 3D TAM-GM-5A enhanced the cancer invasion rate to a significantly higher extent than other groups. There was no significant difference in the cancer invasion rate between 3D TAM-GM-3A and 3D TAM-GM-5A. A correlation between the cancer invasion rate and the amount of MMP-2 secreted was observed (Figure 5.10).

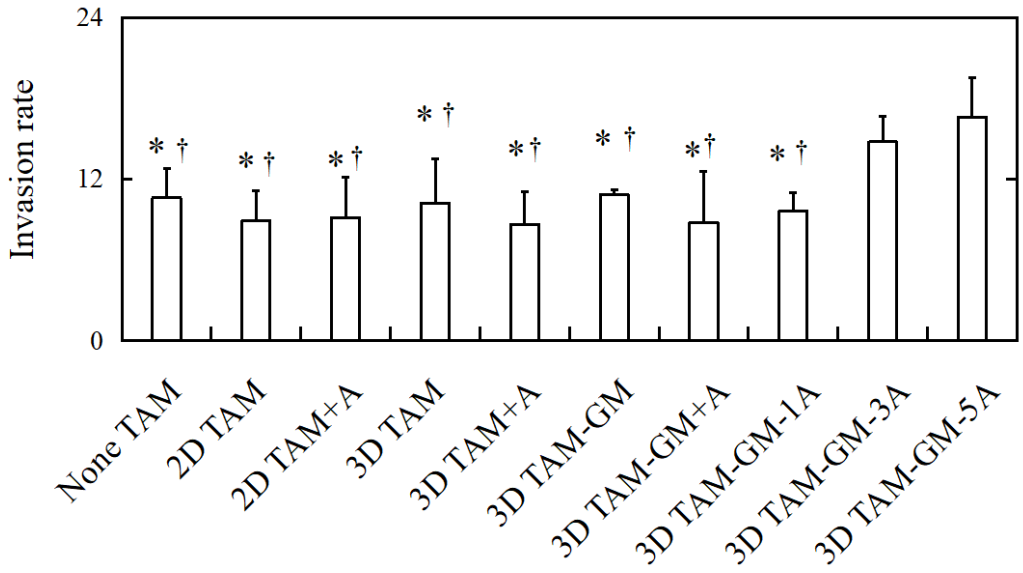


Figure 5.9. Invasion rate of HepG2 cancer cells with or without 2D TAM, 2D TAM+A, 3D TAM, 3D TAM+A, 3D TAM-GM, 3D TAM-GM+A, 3D TAM-GM-1A, 3D TAM-GM-3A, and 3D TAM-GM-5A 1 day after incubation. $^{*}$, $p < 0.05$; significant difference against the invasion rate of with 3D TAM-GM-3A. $^{\dagger}$, $p < 0.05$; significant difference against the invasion rate of with 3D TAM-GM-5A.

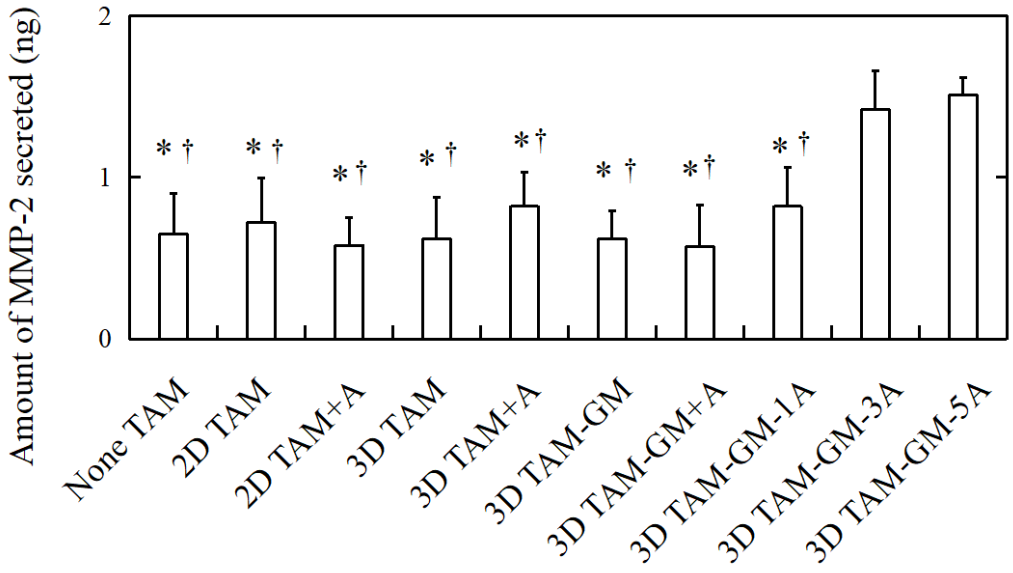


Figure 5.10. Amount of MMP-2 secreted with or without 2D TAM, 2D TAM+A, 3D TAM, 3D TAM+A, 3D TAM-GM, 3D TAM-GM+A, 3D TAM-GM-1A, 3D TAM-GM-3A, and 3D TAM-GM-5A 1 day after incubation. $^{*}$, $p < 0.05$; significant difference against the amount of MMP-2 secreted from 3D TAM-GM-3A. $^{\dagger}$, $p < 0.05$; significant difference against the amount of MMP-2 secreted from 3D TAM-GM-5A.

To evaluate the EMT event, the expression levels of E-cadherin, N-cadherin, and Vimentin of the cancer cells invaded were measured (Figure 5.11). The E-cadherin expression level of high invasive HepG2 cancer cells co-cultured with 3D TAM-GM-5A significantly decreased compared with that of low invasive HepG2 cancer cells co-cultured with 3D TAM-GM, whereas the expressions of N-cadherin and Vimentin significantly increased.

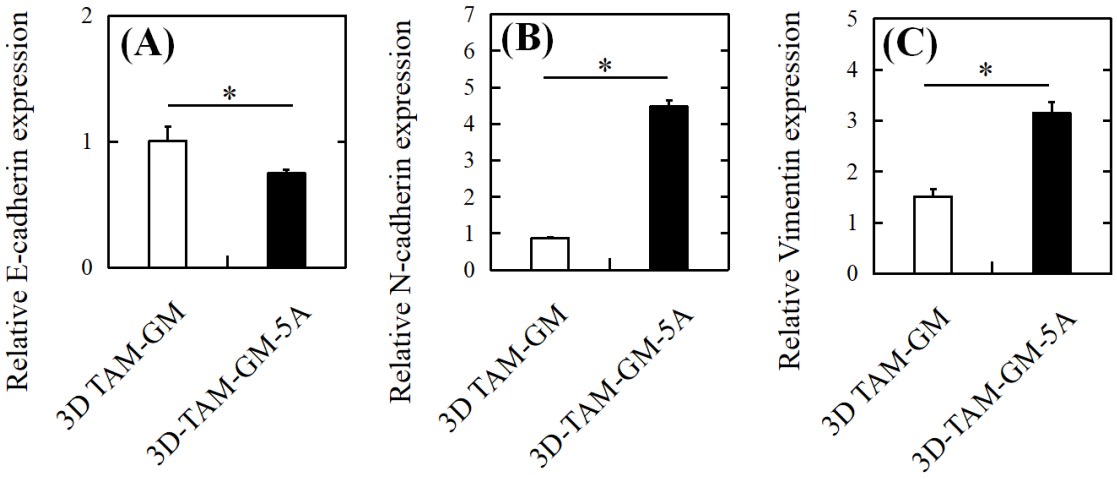


Figure 5.11. Relative expression of E-cadherin (A), N-cadherin (B), and Vimentin (C) for HepG2 cancer cells by co-cultured with 3D TAM-GM and 3D TAM-GM-5A. $^{*}$, $p < 0.05$; significant difference between two groups.

Figure 5.12 shows the cancer invasion rate by co-culturing three types of liver, breast, and lung cancer cells with a mixture of 3D CAF-GM-TGF-β1 and 3D TAM-CAF-A at different mixing ratios. The invasion rate of HepG2 was the highest when the mixing ratio of TAM to CAF was 3:1, while that of WA-hT was the highest at the ratio of 1:3 or 0:4. On the other hand, the highest invasion rate of MCF-7 was detected at the ratio of 2:2. The mixing ratio effect on the cancer invasion rate well corresponded with that on the amount of MMP-2 secreted.

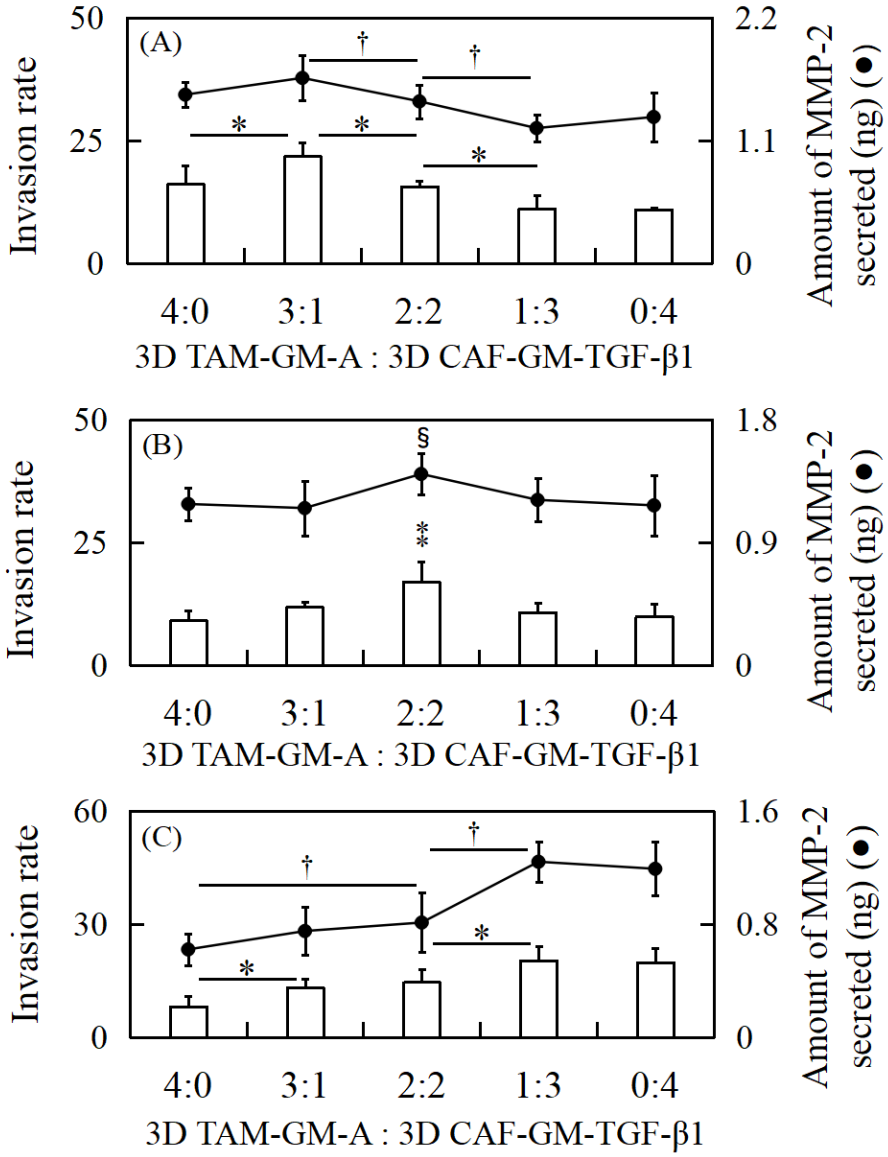


Figure 5.12. Invasion rate of HepG2 (A), MCF-7 (B), and WA-hT (C) 1 day after incubation with various mixed 3D TAM-GM-A and 3D cancer-associated fibroblasts (CAF) aggregates incorporating GM containing 5000 μg/ml of TGF-β1 (3D CAF-GM-TGF-β1) as a function of the 3D cell aggregates mixing ratios and amount of MMP-2 secreted from various mixed 3D TAM-GM-A and 3D CAF-GM-TGF-β1. $^{*}$, $p < 0.05$; significant difference in the invasion rate between two groups. $^{\dagger}$, $p < 0.05$; significant difference in the amount of MMP-2 secreted between two groups.

[‡], $p < 0.05$; significant difference against the invasion rate of MCF-7 cells for other groups. [§], $p < 0.05$; significant difference against the amount of MMP-2 secreted for other groups.

## 5.4. Discussion

Cancer invasion and metastasis are the most important problems to be solved in cancer therapy because most cancer patients die of metastasis [59, 102, 118, 131]. To further improve invasion researches, it is necessary to develop *in vitro* cell culture systems capable of invasion ability evaluation. As one trial, a cancer invasion model combined with 3D CAF-GM-TGF-β1 has been designed [131]. This model was promising to assess the invasion of cancer cells in the conventional membrane chamber assay for an anti-cancer drug screening. However, the model was effective only for a certain type of cancer cells, and there remains a technological room to be improved. In the pathological condition, it is known that the cancer environment is composed of various cell types, such as CAF, TAM, and endothelial cells [119]. For example, cancer cells are co-cultured with CAF and TAM in a 3D manner [137, 138]. However, the *in vitro* bioactivity of TAM is not always high enough to naturally interact with cancer cells. As one trial, in this study, a drug delivery system (DDS) technology is combined with the TAM culture. It is reported that A is one of the *in vivo* factors to activate the TAM function [134]. Therefore, in this study, the adenosine was impregnated in the GM, and the GM containing adenosine (GM-A) were incubated with TAM to form 3D TAM incorporating GM-A. For the preparation of TAM which have an ability of M2d type macrophages, the THP-1 cells were stimulated by both LPS and adenosine to allow them to TAM. TAM can be induced by LPS and adenosine [134-136]. Especially, to maintain and enhance the TAM function, adenosine is essential. This is because the LPS only stimulation would induce M1 macrophages whose functions are quite different from TAM functions [134]. The LPS/adenosine-induced cells from THP-1 cells were used as a TAM model

cell. Using this TAM, TAM 3D aggregates incorporating GM containing adenosine (3D TAM-GM-A) were prepared. The VEGF secretion level was evaluated since it is the most important factor to evaluate the TAM function [134, 135]. As expected, the GM-A incorporation in 3D TAM enabled TAM to enhance the function (Figure 5.8).

There have been recently reported on various microspheres of poly (lactic-*co*-glycolic acid) (PLGA) [77, 111, 112, 139], alginate [140-142], and gelatin [14, 72, 97, 131, 143] for the sustained release of drugs. In this study, gelatin is selected for microsphere preparation. This is mainly because of the lower inflammation induction and higher cell adhesion [15-17, 144, 145]. In addition, the size range of GM were adjusted to 32-53 μm. This is because this size range was suitable to form cell aggregates incorporating GM [41, 72]. On the other hand, as the dehydrothermally crosslinking time, 72 h was employed since the crosslinking time is experimentally confirmed to be appropriate for GM degradation [41].

The release test revealed that in PBS, about 50 % of adenosine was released from GM-A initially, but thereafter the release was off. By the addition of collagenase, the adenosine release with time was observed. In addition, the adenosine amount impregnated did not affect the adenosine release profile (data not shown). This implies that 50 % of adenosine was released from the GM-A as a result of GM collagenase degradation. This release mechanism is shown for other drugs previously reported for GM [26, 97]. This can be explained in the association site number of gelation with adenosine. The number of gelatin molecules is large enough to associate with adenosine molecules. Taken together, it is likely that the adenosine is released from the GM-A even in the TAM 3D aggregates.

To claim the biological efficacy of adenosine release “inside” TAM

aggregates on the TAM functions, free adenosine solution was continuously added into the culture medium. The addition schedule was determined based on the time profile of adenosine release. In Figure 5.5, 50 % of the total adenosine amount contained was initially released in PBS, followed by the controlled adenosine release as the result of GM degradation with time was observed. To manually follow the release profile, at the starting point of culture, 50 % of the total adenosine amount was added into the culture medium. In this study, TAM aggregates were formed 7 days after incubation. It is well known that cell aggregates produce enzymes, cytokines, or chemokines much more efficiently than non-aggregated cells [2, 3, 131]. Considering the GM degradation and adenosine release, in this study, 12.5 % of adenosine amount was added daily for 4 days from day 7 to day 10.

The cell number of TAM aggregates prepared was the same as that of TAM initially seeded because TAM do not have a proliferation nature [134]. The previous study demonstrates that the cell number of 3D CAF-GM-TGF-β1 was $1\times10^5$ cells to obtain a good result [131]. Based on this, in this study, the cell number of TAM aggregates was fixed to be $1\times10^5$ cells. The mixing number ratio of TAM to GM must affect the TAM activity. To check an optimal ratio, we evaluated the ATP activity of 3D TAM-GM incorporating different numbers of GM incorporated. The ATP activity of 100 GM incorporation was significantly higher than that of 50 and 150 GM (data not shown). When the number was 200, the 3D TAM-GM were not formed (data not shown). The previous study demonstrates that an excessive number of GM prevents the formation of cell aggregates because the frequency of cell-cell interaction decreases. Based on the findings, $1\times10^5$ cell number and 100 GM were selected in this study.

Figure 5.6 shows that the aggregates' morphology and the incubation time of aggregates are different between 3D TAM and 3D TAM-GM. The delayed formation of 3D TAM-GM is due to the poor cell-cell interaction. It is likely that the GM presence prevents cells to interact with each other, leading to a longer incubation time of aggregates formation. In addition, the amount of adenosine present in the GM did not affect the formation of the aggregates. The size of 3D TAM-GM with or without adenosine incorporation 15 days after incubation was smaller than that on 10 days (Figures 5.6 and 5.7). This can be explained in terms of GM degradation in 3D TAM. It was found that the GM were degraded in the cell aggregates due to the enzymes secreted from cells with time [72]. However, the space in between cells in aggregates is lost accompanied with the GM degradation, resulting in decreasing functions of cells [72]. Based on this phenomenon, cell culture experiments were finished on 15 days after incubation in this study.

The amount of VEGF secreted is an important factor to assess the TAM function [134, 135]. The VEGF secretion amount for 3D TAM was significantly lower than that for 2D TAM (Figure 5.6). This clearly indicates that the TAM function decreases. Because the low oxygen would weaken the TAM activity. However, the GM incorporation gives cells present in aggregates a better condition of oxygen. The previous study revealed that the GM incorporation can supply oxygen or nutrients to cells in aggregates efficiently, leading to enhanced cell function, compared with GM-free aggregates [14, 72]. As the result, the VEGF secretion from the 3D TAM-GM significantly increased compared with that from the 3D TAM. On the other hand, the amount of VEGF secreted from the 3D TAM-GM-3A and 3D TAM-GM-5A was significantly higher than that from the TAM-GM-1A.

This may be due to the activation effect of adenosine on TAM. However, the VEGF secretion amount did not change by the addition of free adenosine into the culture medium. These findings suggest the possibility that an increase in the adenosine concentration does not always activate the TAM function, but the adenosine supply in the sustained release fashion does. Or a shorter action distance between adenosine and cells may be another reason. Comparing the adenosine addition effect between 3D TAM and 3D TAM-GM, for the 3D TAM, the adenosine applied acts only on the surface of 3D aggregates. On the other hand, the GM incorporation would enable adenosine to penetrate into the TAM deeper through the GM water phase. Interestingly, however, the enhancement of VEGF secretion was low compared with the adenosine release in TAM aggregates. This same phenomenon was observed in previous studies [97, 131]. Taken together, to enhance the effect, it is important to give adenosine to cells closely and uniformly which can be achieved only by the combination of 3D cell culture and DDS technology. In addition, there was no significant difference in the secretion amount between the 3D TAM-GM-3A and 3D TAM-GM-5A. This may be due to a limited drug action to TAM.

It has been reported that the number of stromal cells is about more than two times as much as that of cancer cells in the body, although the ratio depends on the cancer region [46, 118]. Based on the findings, in this study, the mixing ratio of cancer cells to TAM of 1:2 was fixed. In this assay, TAM cultured for 10 days were used. Interestingly, there was no significance in the rate between the TAM-free and 2D TAM groups. This may be explained in terms of the distance between cancer cells and TAM. The distance would prevent the interaction between cancer cells and TAM. In the previous study, the distance made it difficult to interact between the cancer cells and CAF

[97]. The invasion rate of cancer cells co-cultured with TAM-GM-3A or TAM-GM-5A was significantly higher than that with TAM-free, 2D TAM, 3D TAM, 3D TAM-GM without or with free adenosine solution, and 3D TAM-GM-1A groups (other groups). In addition, the MMP-2 secretion amount upon co-culturing with TAM-GM-3A or TAM-GM-5A was significantly higher than that of other groups. Among the MMP groups, MMP-2 and 9 play important roles in the degradation of the basement membrane, leading to an enhanced membrane penetration for cancer cell invasion [46, 122, 146, 147]. However, MMP-9 was not secreted in this model (data not shown), but the MMP-2 secretion was enough to enhance the cell invasion.

To evaluate the EMT induction, the expression of genes involved in EMT, such as E-cadherin, N-cadherin, and Vimentin, was measured. It is apparent from Figure 5.11 that lower E-cadherin and higher N-cadherin and Vimentin for the 3D TAM-GM-5A than that for 3D TAM-GM was observed. In addition, there was no significant difference in the genes expression level of the low invasive cancer cells among the TAM-free, 2D TAM, 2D TAM+A, 3D TAM, 3D TAM+A, 3D TAM-GM, 3D TAM-GM+A, and 3D TAM-GM-1A groups. It is well known that there is a good correlation between the MMP-2 secretion and EMT *in vivo*. The correlation was also observed in this model. It is highly conceivable based on the results obtained that both 3D TAM-GM-3A and 3D TAM-GM-5A promote the cancer cell invasion via the MMP-2 system. However, in this model, the promoted invasion was observed only for liver HepG2 cancer cells, but not for lung WA-hT cancer cells (data not shown). Thus, as the next design of the cell culture system, it has been tried to mimic the cancer environment better by further combining the 3D CAF-GM-TGF-β1. The amount of TGF-β1 incorporated in GM was

confirmed by the previous study to be 5000 μg/ml [131]. In addition, to evaluate the mixing effect of 3D TAM-GM-A and 3D CAF-GM-TGF-β1 on the cancer invasion rate, the mixing ratio of 3D TAM-GM-A and 3D CAF-GM-TGF-β1 was changed to use while the total cell number was constant. In Figure 5.12, the invasion rate of HepG2 was the highest at the mixing TAM/CAF ratio of 3:1, while that of WA-hT was at 1:3 or 0:4. On the other hand, the highest rate was observed for MCF-7, when the ratio was equal. For example, for lung cancers, the contribution of CAF is larger than that of TAM, while the opposite CAF/TAM contribution was observed for liver cancers. On the other hand, when the existence ratio is around one, there is a similar contribution to the invasion event, which is seen for breast cancers [125]. The tendency observed was similar to that of real cancer types. This clearly indicates that to replicate the cancer cell event *in vitro*, it is of prime importance to give a suitable environment to cancer cells considering and mimicking *in vivo* environment of various cancer sites. The combination culture system of 3D TAM-GM-A and 3D CAF-GM-TGF-β1 may be one of the realistic techniques to reproduce the *in vivo* cancer environment.

There are two interesting findings to be emphasized in this study; i) "how to culture TAM for a long time period": No experimentally accepted culture method has been completely established. The technology combination of 3D cell culture and the local release of adenosine (3D TAM-GM-A) was useful to permit the TAM culture with the activity remaining; ii) "design of a cancer invasion model which mimics better the *in vivo* cancer environment": the co-culture of 3D CAF and 3D TAM combined with GM containing drugs makes it possible to reproduce the invasion behavior for cancer cells of different types. It is suggested to evaluate the

invasion rate of different cancer cells only by changing the mixing ratio of 3D CAF and 3D TAM. This study strongly demonstrates that the combination of 3D CAF and 3D TAM both activated by the local sustained release of respectively effective drugs is a new cell culture system that can *in vitro* evaluate the difference in the invasion of cancer cells.

## 6. Conclusions

In chapter 2, the effect of the shaking culture of cell aggregates incorporating gelatin hydrogel microspheres has been investigated. In the case of gelatin hydrogel microspheres-free or lower amount of the microspheres, shaking culture enables to enhance the function of cell aggregates, such as ATP activity because of oxygen supply.

In chapter 3, a novel cancer invasion model combined with three-dimensional cancer-associated fibroblasts culture and drug delivery system technology has been designed. This model may be useful to evaluate the cancer invasion ability or therapeutic efficacy *in vitro*. This study is the first report to create an invasion model *in vitro* by taking advantage of a combined three-dimensional culture system and the drug delivery system technology based on the interaction between cancer cells and stromal cells such as cancer-associated fibroblasts.

In chapter 4, a novel cancer invasion model where the cancer invasion rate can be regulated *in vitro* has been designed. The present model is promising to realize the cancer invasion whose rate can be modified by changing the TGF-β1 concentration. This model may be a useful tool to evaluate the difference in cancer invasion ability or therapeutic efficacy *in vitro*. As one experimental strategy to mimic the body environment, it would be important not only to achieve a 3D cell culture but also to allow the growth factors to act on the cells.

In chapter 5, a cell culture system to enhance the tumor-associated macrophage function based on the combination of three-dimensional cell aggregates and gelatin hydrogel microspheres for adenosine delivery has been proposed. An additional combination of three-dimensional cancer-associated fibroblasts incorporating gelatin hydrogel microspheres

containing transforming growth factor-β1 allowed cancer cells to enhance their invasion rate. This co-culture system is promising to evaluate the ability of cancer cell invasion for anti-cancer drug screening.

## 7. References


1. Nii, T.; Makino, K.; Tabata, Y. Three-Dimensional Culture System of Cancer Cells Combined with Biomaterials for Drug Screening. *Cancers (Basel)*, **2020**, *12*, 2754. DOI:10.3390/cancers12102754
2. Fukuda, J.; Sakai, Y.; Nakazawa, K. Novel hepatocyte culture system developed using microfabrication and collagen/polyethylene glycol microcontact printing. *Biomaterials*, **2006**, *27*, 1061-1070.
3. Rodriguez-Enriquez, S.; Gallardo-Perez, J.C.; Aviles-Salas, A.; Marin-Hernandez, A.; Carreno-Fuentes, L.; Maldonado-Lagunas, V.; Moreno-Sanchez, R. Energy metabolism transition in multi-cellular human tumor spheroids. *J Cell Physiol*, **2008**, *216*, 189-197.
4. Kurosawa, H. Methods for inducing embryoid body formation: in vitro differentiation system of embryonic stem cells. *J Biosci Bioeng*, **2007**, *103*, 389-398.
5. Lin, R.Z.; Chang, H.Y. Recent advances in three-dimensional multicellular spheroid culture for biomedical research. *Biotechnol J*, **2008**, *3*, 1172-1184.
6. Breslin, S.; O'Driscoll, L. Three-dimensional cell culture: the missing link in drug discovery. *Drug Discov Today*, **2013**, *18*, 240-249.
7. Hait, W.N. Anticancer drug development: the grand challenges. *Nat Rev Drug Discov*, **2010**, *9*, 253-254.
8. Benton, G.; George, J.; Kleinman, H.K.; Arnaoutova, I.P. Advancing science and technology via 3D culture on basement membrane matrix. *J Cell Physiol*, **2009**, *221*, 18-25.
9. Mohan, N.; Nair, P.D.; Tabata, Y. A 3D biodegradable protein based matrix for cartilage tissue engineering and stem cell differentiation to

cartilage. *J Mater Sci Mater Med*, **2009**, *20 Suppl 1*, S49-60.

10. Okochi, M.; Takano, S.; Isaji, Y.; Senga, T.; Hamaguchi, M.; Honda, H. Three-dimensional cell culture array using magnetic force-based cell patterning for analysis of invasive capacity of BALB/3T3/v-src. *Lab Chip*, **2009**, *9*, 3378-3384.
11. Hanjaya-Putra, D.; Gerecht, S. Vascular engineering using human embryonic stem cells. *Biotechnol Prog*, **2009**, *25*, 2-9.
12. Kellner, K.; Liebsch, G.; Klimant, I.; Wolfbeis, O.S.; Blunk, T.; Schulz, M.B.; Gopferich, A. Determination of oxygen gradients in engineered tissue using a fluorescent sensor. *Biotechnol Bioeng*, **2002**, *80*, 73-83.
13. Bradford, A. The role of hypoxia and platelets in air travel-related venous thromboembolism. *Curr Pharm Des*, **2007**, *13*, 2668-2672.
14. Hayashi, K.; Tabata, Y. Preparation of stem cell aggregates with gelatin microspheres to enhance biological functions. *Acta Biomater*, **2011**, *7*, 2797-2803.
15. Zekorn, D. Intravascular retention, dispersal, excretion and break-down of gelatin plasma substitutes. *Bibl Haematol*, **1969**, *33*, 131-140.
16. Narita, A.; Takahara, M.; Ogino, T.; Fukushima, S.; Kimura, Y.; Tabata, Y. Effect of gelatin hydrogel incorporating fibroblast growth factor 2 on human meniscal cells in an organ culture model. *Knee*, **2009**, *16*, 285-289.
17. Takahashi, Y.; Yamamoto, M.; Tabata, Y. Osteogenic differentiation of mesenchymal stem cells in biodegradable sponges composed of gelatin and beta-tricalcium phosphate. *Biomaterials*, **2005**, *26*, 3587-3596.

18. Hori, Y.; Inoue, S.; Hirano, Y.; Tabata, Y. Effect of culture substrates and fibroblast growth factor addition on the proliferation and differentiation of rat bone marrow stromal cells. *Tissue Eng*, **2004**, *10*, 995-1005.

19. Watanabe, M.; Jo, J.; Radu, A.; Kaneko, M.; Tabata, Y.; Flake, A.W. A tissue engineering approach for prenatal closure of myelomeningocele with gelatin sponges incorporating basic fibroblast growth factor. *Tissue Eng Part A*, **2010**, *16*, 1645-1655.

20. Akagawa, Y.; Kubo, T.; Koretake, K.; Hayashi, K.; Doi, K.; Matsuura, A.; Morita, K.; Takeshita, R.; Yuan, Q.; Tabata, Y. Initial bone regeneration around fenestrated implants in Beagle dogs using basic fibroblast growth factor-gelatin hydrogel complex with varying biodegradation rates. *J Prosthodont Res*, **2009**, *53*, 41-47.

21. Hiraoka, Y.; Yamashiro, H.; Yasuda, K.; Kimura, Y.; Inamoto, T.; Tabata, Y. In situ regeneration of adipose tissue in rat fat pad by combining a collagen scaffold with gelatin microspheres containing basic fibroblast growth factor. *Tissue Eng*, **2006**, *12*, 1475-1487.

22. Igai, H.; Chang, S.S.; Gotoh, M.; Yamamoto, Y.; Misaki, N.; Okamoto, T.; Yamamoto, M.; Tabata, Y.; Yokomise, H. Regeneration of canine tracheal cartilage by slow release of basic fibroblast growth factor from gelatin sponge. *ASAIO J*, **2006**, *52*, 86-91.

23. Okamoto, T.; Yamamoto, Y.; Gotoh, M.; Huang, C.L.; Nakamura, T.; Shimizu, Y.; Tabata, Y.; Yokomise, H. Slow release of bone morphogenetic protein 2 from a gelatin sponge to promote regeneration of tracheal cartilage in a canine model. *J Thorac Cardiovasc Surg*, **2004**, *127*, 329-334.

24. Kimura, Y.; Tabata, Y. Controlled release of stromal-cell-derived

factor-1 from gelatin hydrogels enhances angiogenesis. *J Biomater Sci Polym Ed*, **2010**, *21*, 37-51.

25. Esaki, J.; Marui, A.; Tabata, Y.; Komeda, M. Controlled release systems of angiogenic growth factors for cardiovascular diseases. *Expert Opin Drug Deliv*, **2007**, *4*, 635-649.
26. Tabata, Y.; Nagano, A.; Ikada, Y. Biodegradation of hydrogel carrier incorporating fibroblast growth factor. *Tissue Eng*, **1999**, *5*, 127-138.
27. Ozeki, M.; Tabata, Y. In vivo degradability of hydrogels prepared from different gelatins by various cross-linking methods. *J Biomater Sci Polym Ed*, **2005**, *16*, 549-561.
28. Nitta, N.; Ohta, S.; Tanaka, T.; Takazakura, R.; Toyama, T.; Sonoda, A.; Seko, A.; Furukawa, A.; Takahashi, M.; Murata, K., et al. An initial clinical study on the efficacy of cisplatin-releasing gelatin microspheres for metastatic liver tumors. *Eur J Radiol*, **2009**, *71*, 519-526.
29. Patel, Z.S.; Yamamoto, M.; Ueda, H.; Tabata, Y.; Mikos, A.G. Biodegradable gelatin microparticles as delivery systems for the controlled release of bone morphogenetic protein-2. *Acta Biomater*, **2008**, *4*, 1126-1138.
30. Kikuchi, T.; Kubota, S.; Asaumi, K.; Kawaki, H.; Nishida, T.; Kawata, K.; Mitani, S.; Tabata, Y.; Ozaki, T.; Takigawa, M. Promotion of bone regeneration by CCN2 incorporated into gelatin hydrogel. *Tissue Eng Part A*, **2008**, *14*, 1089-1098.
31. Kushibiki, T.; Tomoshige, R.; Iwanaga, K.; Kakemi, M.; Tabata, Y. Controlled release of plasmid DNA from hydrogels prepared from gelatin cationized by different amine compounds. *J Control Release*, **2006**, *112*, 249-256.

32. Ichinohe, N.; Kuboki, Y.; Tabata, Y. Bone regeneration using titanium nonwoven fabrics combined with fgf-2 release from gelatin hydrogel microspheres in rabbit skull defects. *Tissue Eng Part A*, **2008**, *14*, 1663-1671.

33. Patel, Z.S.; Ueda, H.; Yamamoto, M.; Tabata, Y.; Mikos, A.G. In vitro and in vivo release of vascular endothelial growth factor from gelatin microparticles and biodegradable composite scaffolds. *Pharm Res*, **2008**, *25*, 2370-2378.

34. Tabata, Y.; Hijikata, S.; Muniruzzaman, M.; Ikada, Y. Neovascularization effect of biodegradable gelatin microspheres incorporating basic fibroblast growth factor. *J Biomater Sci Polym Ed*, **1999**, *10*, 79-94.

35. Ikada, Y.; Tabata, Y. Protein release from gelatin matrices. *Adv Drug Deliv Rev*, **1998**, *31*, 287-301.

36. Xie, Y.; Hardouin, P.; Zhu, Z.; Tang, T.; Dai, K.; Lu, J. Three-dimensional flow perfusion culture system for stem cell proliferation inside the critical-size beta-tricalcium phosphate scaffold. *Tissue Eng*, **2006**, *12*, 3535-3543.

37. Yeatts, A.B.; Fisher, J.P. Bone tissue engineering bioreactors: dynamic culture and the influence of shear stress. *Bone*, **2011**, *48*, 171-181.

38. Teixeira, F.G.; Panchalingam, K.M.; Assuncao-Silva, R.; Serra, S.C.; Mendes-Pinheiro, B.; Patricio, P.; Jung, S.; Anjo, S.I.; Manadas, B.; Pinto, L., et al. Modulation of the Mesenchymal Stem Cell Secretome Using Computer-Controlled Bioreactors: Impact on Neuronal Cell Proliferation, Survival and Differentiation. *Sci Rep*, **2016**, *6*, 27791. DOI:10.1038/srep27791

39. Baraniak, P.R.; Cooke, M.T.; Saeed, R.; Kinney, M.A.; Fridley, K.M.; McDevitt, T.C. Stiffening of human mesenchymal stem cell spheroid microenvironments induced by incorporation of gelatin microparticles. *J Mech Behav Biomed Mater*, **2012**, *11*, 63-71.

40. Dang, P.N.; Dwivedi, N.; Phillips, L.M.; Yu, X.; Herberg, S.; Bowerman, C.; Solorio, L.D.; Murphy, W.L.; Alsberg, E. Controlled Dual Growth Factor Delivery From Microparticles Incorporated Within Human Bone Marrow-Derived Mesenchymal Stem Cell Aggregates for Enhanced Bone Tissue Engineering via Endochondral Ossification. *Stem Cells Transl Med*, **2016**, *5*, 206-217.

41. Tajima, S.; Tabata, Y. Preparation and functional evaluation of cell aggregates incorporating gelatin microspheres with different degradabilities. *J Tissue Eng Regen Med*, **2013**, *7*, 801-811.

42. Petty, R.D.; Sutherland, L.A.; Hunter, E.M.; Cree, I.A. Comparison of MTT and ATP-based assays for the measurement of viable cell number. *J Biolumin Chemilumin*, **1995**, *10*, 29-34.

43. Efron, N.; Morgan, P.B.; Cameron, I.D.; Brennan, N.A.; Goodwin, M. Oxygen permeability and water content of silicone hydrogel contact lens materials. *Optom Vis Sci*, **2007**, *84*, 328-337.

44. Chung, H.J.; Park, T.G. Injectable cellular aggregates prepared from biodegradable porous microspheres for adipose tissue engineering. *Tissue Eng Part A*, **2009**, *15*, 1391-1400.

45. Zhang, H.N.; Leng, P.; Wang, Y.Z.; Lu, C.Y.; Wang, X.D.; Wang, C.Y. [Repair full-thickness meniscal defects with injectable tissue engineering technique]. *Zhonghua Wai Ke Za Zhi*, **2010**, *48*, 1309-1312.

46. Shiga, K.; Hara, M.; Nagasaki, T.; Sato, T.; Takahashi, H.; Takeyama,

H. Cancer-Associated Fibroblasts: Their Characteristics and Their Roles in Tumor Growth. *Cancers (Basel)*, **2015**, *7*, 2443-2458.

47. Kalluri, R.; Zeisberg, M. Fibroblasts in cancer. *Nat Rev Cancer*, **2006**, *6*, 392-401.

48. Li, H.; Fan, X.; Houghton, J. Tumor microenvironment: the role of the tumor stroma in cancer. *J Cell Biochem*, **2007**, *101*, 805-815.

49. Kuperwasser, C.; Chavarria, T.; Wu, M.; Magrane, G.; Gray, J.W.; Carey, L.; Richardson, A.; Weinberg, R.A. Reconstruction of functionally normal and malignant human breast tissues in mice. *Proc Natl Acad Sci U S A*, **2004**, *101*, 4966-4971.

50. Grum-Schwensen, B.; Klingelhofer, J.; Berg, C.H.; El-Naaman, C.; Grigorian, M.; Lukanidin, E.; Ambartsumian, N. Suppression of tumor development and metastasis formation in mice lacking the S100A4(mts1) gene. *Cancer Res*, **2005**, *65*, 3772-3780.

51. Cornil, I.; Theodorescu, D.; Man, S.; Herlyn, M.; Jambrosic, J.; Kerbel, R.S. Fibroblast cell interactions with human melanoma cells affect tumor cell growth as a function of tumor progression. *Proc Natl Acad Sci U S A*, **1991**, *88*, 6028-6032.

52. Powell, D.W.; Mifflin, R.C.; Valentich, J.D.; Crowe, S.E.; Saada, J.I.; West, A.B. Myofibroblasts. I. Paracrine cells important in health and disease. *Am J Physiol*, **1999**, *277*, C1-9.

53. Infante, J.R.; Matsubayashi, H.; Sato, N.; Tonascia, J.; Klein, A.P.; Riall, T.A.; Yeo, C.; Iacobuzio-Donahue, C.; Goggins, M. Peritumoral fibroblast SPARC expression and patient outcome with resectable pancreatic adenocarcinoma. *J Clin Oncol*, **2007**, *25*, 319-325.

54. Wandel, E.; Grasshoff, A.; Mittag, M.; Haustein, U.F.; Saalbach, A.

Fibroblasts surrounding melanoma express elevated levels of matrix metalloproteinase-1 (MMP-1) and intercellular adhesion molecule-1 (ICAM-1) in vitro. *Exp Dermatol*, **2000**, *9*, 34-41.

55. Wilson, C.L.; Heppner, K.J.; Labosky, P.A.; Hogan, B.L.; Matrisian, L.M. Intestinal tumorigenesis is suppressed in mice lacking the metalloproteinase matrilysin. *Proc Natl Acad Sci U S A*, **1997**, *94*, 1402-1407.

56. Thomasset, N.; Lochter, A.; Sympson, C.J.; Lund, L.R.; Williams, D.R.; Behrendtsen, O.; Werb, Z.; Bissell, M.J. Expression of autoactivated stromelysin-1 in mammary glands of transgenic mice leads to a reactive stroma during early development. *Am J Pathol*, **1998**, *153*, 457-467.

57. Place, A.E.; Jin Huh, S.; Polyak, K. The microenvironment in breast cancer progression: biology and implications for treatment. *Breast Cancer Res*, **2011**, *13*, 227.

58. Boire, A.; Covic, L.; Agarwal, A.; Jacques, S.; Sherifi, S.; Kuliopulos, A. PAR1 is a matrix metalloprotease-1 receptor that promotes invasion and tumorigenesis of breast cancer cells. *Cell*, **2005**, *120*, 303-313.

59. Stetler-Stevenson, W.G.; Aznavoorian, S.; Liotta, L.A. Tumor cell interactions with the extracellular matrix during invasion and metastasis. *Annu Rev Cell Biol*, **1993**, *9*, 541-573.

60. Takahashi, M.; Fukami, S.; Iwata, N.; Inoue, K.; Itohara, S.; Itoh, H.; Haraoka, J.; Saido, T. In vivo glioma growth requires host-derived matrix metalloproteinase 2 for maintenance of angioarchitecture. *Pharmacol Res*, **2002**, *46*, 155-163.

61. Koontongkaew, S.; Amornphimoltham, P.; Monthanpisut, P.; Saensuk,

T.; Leelakriangsak, M. Fibroblasts and extracellular matrix differently modulate MMP activation by primary and metastatic head and neck cancer cells. *Med Oncol*, **2012**, *29*, 690-703.

62. Sandler, R.S.; Halabi, S.; Baron, J.A.; Budinger, S.; Paskett, E.; Keresztes, R.; Petrelli, N.; Pipas, J.M.; Karp, D.D.; Loprinzi, C.L., et al. A randomized trial of aspirin to prevent colorectal adenomas in patients with previous colorectal cancer. *N Engl J Med*, **2003**, *348*, 883-890.
63. Tredan, O.; Galmarini, C.M.; Patel, K.; Tannock, I.F. Drug resistance and the solid tumor microenvironment. *J Natl Cancer Inst*, **2007**, *99*, 1441-1454.
64. Pampaloni, F.; Reynaud, E.G.; Stelzer, E.H. The third dimension bridges the gap between cell culture and live tissue. *Nat Rev Mol Cell Biol*, **2007**, *8*, 839-845.
65. Nelson, L.J.; Walker, S.W.; Hayes, P.C.; Plevris, J.N. Low-shear modelled microgravity environment maintains morphology and differentiated functionality of primary porcine hepatocyte cultures. *Cells Tissues Organs*, **2010**, *192*, 125-140.
66. Compan, V.; Guzman, J.; Riande, E. A potentiostatic study of oxygen transmissibility and permeability through hydrogel membranes. *Biomaterials*, **1998**, *19*, 2139-2145.
67. Brancato, V.; Gioiella, F.; Profeta, M.; Imparato, G.; Guarnieri, D.; Urciuolo, F.; Melone, P.; Netti, P.A. 3D tumor microtissues as an in vitro testing platform for microenvironmentally-triggered drug delivery systems. *Acta Biomater*, **2017**, *57*, 47-58.
68. Brancato, V.; Comunanza, V.; Imparato, G.; Cora, D.; Urciuolo, F.; Noghero, A.; Bussolino, F.; Netti, P.A. Bioengineered tumoral

microtissues recapitulate desmoplastic reaction of pancreatic cancer. *Acta Biomater*, **2017**, *49*, 152-166.

69. Brancato, V.; Gioiella, F.; Imparato, G.; Guarnieri, D.; Urciuolo, F.; Netti, P.A. 3D breast cancer microtissue reveals the role of tumor microenvironment on the transport and efficacy of free-doxorubicin in vitro. *Acta Biomater*, **2018**, *75*, 200-212.
70. Rebelo, S.P.; Pinto, C.; Martins, T.R.; Harrer, N.; Estrada, M.F.; Loza-Alvarez, P.; Cabecadas, J.; Alves, P.M.; Gualda, E.J.; Sommergruber, W., et al. 3D-3-culture: A tool to unveil macrophage plasticity in the tumour microenvironment. *Biomaterials*, **2018**, *163*, 185-197.
71. Ferreira, L.P.; Gaspar, V.M.; Mano, J.F. Bioinstructive microparticles for self-assembly of mesenchymal stem Cell-3D tumor spheroids. *Biomaterials*, **2018**, *185*, 155-173.
72. Nii, T.; Makino, K.; Tabata, Y. Influence of shaking culture on the biological functions of cell aggregates incorporating gelatin hydrogel microspheres. *J Biosci Bioeng*, **2019**, *128*, 606-612.
73. Hill, R.; Song, Y.; Cardiff, R.D.; Van Dyke, T. Selective evolution of stromal mesenchyme with p53 loss in response to epithelial tumorigenesis. *Cell*, **2005**, *123*, 1001-1011.
74. Arandkar, S.; Furth, N.; Elisha, Y.; Nataraj, N.B.; van der Kuip, H.; Yarden, Y.; Aulitzky, W.; Ulitsky, I.; Geiger, B.; Oren, M. Altered p53 functionality in cancer-associated fibroblasts contributes to their cancer-supporting features. *Proc Natl Acad Sci U S A*, **2018**, *115*, 6410-6415.
75. Procopio, M.G.; Laszlo, C.; Al Labban, D.; Kim, D.E.; Bordignon, P.; Jo, S.H.; Goruppi, S.; Menietti, E.; Ostano, P.; Ala, U., et al.

Combined CSL and p53 downregulation promotes cancer-associated fibroblast activation. *Nat Cell Biol*, **2015**, *17*, 1193-1204.

76. Tabata, Y.; Ikada, Y. Synthesis of gelatin microspheres containing interferon. *Pharm Res*, **1989**, *6*, 422-427.

77. Nii, T.; Takeuchi, I.; Kimura, Y.; Makino, K. Effects of the conformation of PLGA molecules in the organic solvent on the aerodynamic diameter of spray dried microparticles. *Colloids and Surfaces a-Physicochemical and Engineering Aspects*, **2018**, *539*, 347-353.

78. Sappino, A.P.; Skalli, O.; Jackson, B.; Schurch, W.; Gabbiani, G. Smooth-muscle differentiation in stromal cells of malignant and non-malignant breast tissues. *Int J Cancer*, **1988**, *41*, 707-712.

79. Orimo, A.; Weinberg, R.A. Heterogeneity of stromal fibroblasts in tumors. *Cancer Biol Ther*, **2007**, *6*, 618-619.

80. Ji, H.; Ramsey, M.R.; Hayes, D.N.; Fan, C.; McNamara, K.; Kozlowski, P.; Torrice, C.; Wu, M.C.; Shimamura, T.; Perera, S.A., et al. LKB1 modulates lung cancer differentiation and metastasis. *Nature*, **2007**, *448*, 807-810.

81. Chueca, E.; Apostolova, N.; Esplugues, J.V.; Garcia-Gonzalez, M.A.; Lanas, A.; Piazuelo, E. Proton Pump Inhibitors Display Antitumor Effects in Barrett's Adenocarcinoma Cells. *Front Pharmacol*, **2016**, *7*, 452. DOI:10.3389/fphar.2016.00452

82. Ishii, S.; Yamashita, K.; Harada, H.; Ushiku, H.; Tanaka, T.; Nishizawa, N.; Yokoi, K.; Washio, M.; Ema, A.; Mieno, H., et al. The H19-PEG10/IGF2BP3 axis promotes gastric cancer progression in patients with high lymph node ratios. *Oncotarget*, **2017**, *8*, 74567-74581.

83. Smith, R.W.; Coleman, J.D.; Thompson, J.T.; Vanden Heuvel, J.P. Therapeutic potential of GW501516 and the role of Peroxisome proliferator-activated receptor beta/delta and B-cell lymphoma 6 in inflammatory signaling in human pancreatic cancer cells. *Biochem Biophys Rep*, **2016**, *8*, 395-402.

84. Loizou, G.D. Animal-Free Chemical Safety Assessment. *Front Pharmacol*, **2016**, *7*, 218. DOI:10.3389/fphar.2016.00218

85. Mahler, G.J.; Esch, M.B.; Stokol, T.; Hickman, J.J.; Shuler, M.L. Body-on-a-chip systems for animal-free toxicity testing. *Altern Lab Anim*, **2016**, *44*, 469-478.

86. Leist, M.; Hasiwa, N.; Rovida, C.; Daneshian, M.; Basketter, D.; Kimber, I.; Clewell, H.; Gocht, T.; Goldberg, A.; Busquet, F., et al. Consensus report on the future of animal-free systemic toxicity testing. *ALTEX*, **2014**, *31*, 341-356.

87. Pfuhler, S.; Fautz, R.; Ouedraogo, G.; Latil, A.; Kenny, J.; Moore, C.; Diembeck, W.; Hewitt, N.J.; Reisinger, K.; Barroso, J. The Cosmetics Europe strategy for animal-free genotoxicity testing: project status up-date. *Toxicol In Vitro*, **2014**, *28*, 18-23.

88. Mittal, R.; Woo, F.W.; Castro, C.S.; Cohen, M.A.; Karanxha, J.; Mittal, J.; Chhibber, T.; Jhaveri, V.M. Organ-on-chip models: Implications in drug discovery and clinical applications. *J Cell Physiol*, **2019**, *234*, 8352-8380.

89. Cochrane, A.; Albers, H.J.; Passier, R.; Mummery, C.L.; van den Berg, A.; Orlova, V.V.; van der Meer, A.D. Advanced in vitro models of vascular biology: Human induced pluripotent stem cells and organ-on-chip technology. *Adv Drug Deliv Rev*, **2019**, *140*, 68-77.

90. Zahedi-Tabar, Z.; Bagheri-Khoulenjani, S.; Mirzadeh, H.; Amanpour,

S. 3D in vitro cancerous tumor models: Using 3D printers. *Med Hypotheses*, **2019**, *124*, 91-94.

91. Boutin, M.E.; Kramer, L.L.; Livi, L.L.; Brown, T.; Moore, C.; Hoffman-Kim, D. A three-dimensional neural spheroid model for capillary-like network formation. *J Neurosci Methods*, **2018**, *299*, 55-63.
92. Alexander, F., Jr.; Eggert, S.; Wiest, J. A novel lab-on-a-chip platform for spheroid metabolism monitoring. *Cytotechnology*, **2018**, *70*, 375-386.
93. Oyama, H.; Takahashi, K.; Tanaka, Y.; Takemoto, H.; Haga, H. Long-term Culture of Human iPS Cell-derived Telencephalic Neuron Aggregates on Collagen Gel. *Cell Struct Funct*, **2018**, *43*, 85-94.
94. Yu, F.; Hunziker, W.; Choudhury, D. Engineering Microfluidic Organoid-on-a-Chip Platforms. *Micromachines (Basel)*, **2019**, *10*, 165. DOI:10.3390/mi10030165
95. Nayak, B.; Balachander, G.M.; Manjunath, S.; Rangarajan, A.; Chatterjee, K. Tissue mimetic 3D scaffold for breast tumor-derived organoid culture toward personalized chemotherapy. *Colloids Surf B Biointerfaces*, **2019**, *180*, 334-343.
96. Ogawa, T.; Akazawa, T.; Tabata, Y. In vitro proliferation and chondrogenic differentiation of rat bone marrow stem cells cultured with gelatin hydrogel microspheres for TGF-beta1 release. *J Biomater Sci Polym Ed*, **2010**, *21*, 609-621.
97. Nii, T.; Makino, K.; Tabata, Y. A Cancer Invasion Model Combined with Cancer-Associated Fibroblasts Aggregates Incorporating Gelatin Hydrogel Microspheres Containing a p53 Inhibitor. *Tissue Eng Part C Methods*, **2019**, *25*, 711-720.

98. Inoo, K.; Bando, H.; Tabata, Y. Insulin secretion of mixed insulinoma aggregates-gelatin hydrogel microspheres after subcutaneous transplantation. *Regen Ther*, **2018**, *8*, 38-45.

99. Inoo, K.; Bando, H.; Tabata, Y. Enhanced survival and insulin secretion of insulinoma cell aggregates by incorporating gelatin hydrogel microspheres. *Regen Ther*, **2018**, *8*, 29-37.

100. Tajima, S.; Tabata, Y. Preparation of EpH4 and 3T3L1 cells aggregates incorporating gelatin hydrogel microspheres for a cell condition improvement. *Regen Ther*, **2017**, *6*, 90-99.

101. Tajima, S.; Tabata, Y. Preparation of epithelial cell aggregates incorporating matrigel microspheres to enhance proliferation and differentiation of epithelial cells. *Regen Ther*, **2017**, *7*, 34-44.

102. Siegel, R.L.; Miller, K.D.; Jemal, A. Cancer Statistics, 2017. *CA Cancer J Clin*, **2017**, *67*, 7-30.

103. Shan, T.; Chen, S.; Chen, X.; Lin, W.R.; Li, W.; Ma, J.; Wu, T.; Cui, X.; Ji, H.; Li, Y., et al. Cancer-associated fibroblasts enhance pancreatic cancer cell invasion by remodeling the metabolic conversion mechanism. *Oncol Rep*, **2017**, *37*, 1971-1979.

104. Alvarez-Teijeiro, S.; Garcia-Inclan, C.; Villaronga, M.A.; Casado, P.; Hermida-Prado, F.; Granda-Diaz, R.; Rodrigo, J.P.; Calvo, F.; Del-Rio-Ibisate, N.; Gandarillas, A., et al. Factors Secreted by Cancer-Associated Fibroblasts that Sustain Cancer Stem Properties in Head and Neck Squamous Carcinoma Cells as Potential Therapeutic Targets. *Cancers (Basel)*, **2018**, *10*, 334. DOI: 10.3390/cancers10090334

105. Kalluri, R. The biology and function of fibroblasts in cancer. *Nat Rev Cancer*, **2016**, *16*, 582-598.

106. Micke, P.; Ostman, A. Tumour-stroma interaction: cancer-associated fibroblasts as novel targets in anti-cancer therapy? *Lung Cancer*, **2004**, *45*, S163-S175.

107. Casey, T.M.; Eneman, J.; Crocker, A.; White, J.; Tessitore, J.; Stanley, M.; Harlow, S.; Bunn, J.Y.; Weaver, D.; Muss, H., et al. Cancer associated fibroblasts stimulated by transforming growth factor beta1 (TGF-beta 1) increase invasion rate of tumor cells: a population study. *Breast Cancer Res Treat*, **2008**, *110*, 39-49.

108. McEarchern, J.A.; Kobie, J.J.; Mack, V.; Wu, R.S.; Meade-Tollin, L.; Arteaga, C.L.; Dumont, N.; Besselsen, D.; Seftor, E.; Hendrix, M.J., et al. Invasion and metastasis of a mammary tumor involves TGF-beta signaling. *Int J Cancer*, **2001**, *91*, 76-82.

109. Wick, W.; Platten, M.; Weller, M. Glioma cell invasion: regulation of metalloproteinase activity by TGF-beta. *J Neurooncol*, **2001**, *53*, 177-185.

110. Bratt-Leal, A.M.; Carpenedo, R.L.; Ungrin, M.D.; Zandstra, P.W.; McDevitt, T.C. Incorporation of biomaterials in multicellular aggregates modulates pluripotent stem cell differentiation. *Biomaterials*, **2011**, *32*, 48-56.

111. Cheng, C.Y.; Pho, Q.H.; Wu, X.Y.; Chin, T.Y.; Chen, C.M.; Fang, P.H.; Lin, Y.C.; Hsieh, M.F. PLGA Microspheres Loaded with beta-Cyclodextrin Complexes of Epigallocatechin-3-Gallate for the Anti-Inflammatory Properties in Activated Microglial Cells. *Polymers (Basel)*, **2018**, *10*, 519. DOI: 10.3390/polym10050519

112. Alenezi, A.; Naito, Y.; Terukina, T.; Prananingrum, W.; Jinno, Y.; Tagami, T.; Ozeki, T.; Galli, S.; Jimbo, R. Controlled release of clarithromycin from PLGA microspheres enhances bone regeneration

in rabbit calvaria defects. *J Biomed Mater Res B Appl Biomater*, **2018**, *106*, 201-208.

113. Yuan, Y.; Shi, X.; Gan, Z.; Wang, F. Modification of porous PLGA microspheres by poly-l-lysine for use as tissue engineering scaffolds. *Colloids Surf B Biointerfaces*, **2018**, *161*, 162-168.

114. Thaya, R.; Vaseeharan, B.; Sivakamavalli, J.; Iswarya, A.; Govindarajan, M.; Alharbi, N.S.; Kadaikunnan, S.; Al-Anbr, M.N.; Khaled, J.M.; Benelli, G. Synthesis of chitosan-alginate microspheres with high antimicrobial and antibiofilm activity against multi-drug resistant microbial pathogens. *Microb Pathog*, **2018**, *114*, 17-24.

115. Zeng, J.; Li, L.; Zhang, H.; Li, J.; Liu, L.; Zhou, G.; Du, Q.; Zheng, C.; Yang, X. Radiopaque and uniform alginate microspheres loaded with tantalum nanoparticles for real-time imaging during transcatheter arterial embolization. *Theranostics*, **2018**, *8*, 4591-4600.

116. Friedman, A.; Kim, Y. Tumor cells proliferation and migration under the influence of their microenvironment. *Math Biosci Eng*, **2011**, *8*, 371-383.

117. Kim, Y.; Stolarska, M.A.; Othmer, H.G. The role of the microenvironment in tumor growth and invasion. *Prog Biophys Mol Biol*, **2011**, *106*, 353-379.

118. Spano, D.; Zollo, M. Tumor microenvironment: a main actor in the metastasis process. *Clin Exp Metastasis*, **2012**, *29*, 381-395.

119. Zhou, J.; Tang, Z.; Gao, S.; Li, C.; Feng, Y.; Zhou, X. Tumor-Associated Macrophages: Recent Insights and Therapies. *Front Oncol*, **2020**, *10*, 188.

120. Patel, A.K.; Singh, S. Cancer associated fibroblasts: phenotypic and

functional heterogeneity. *Front Biosci (Landmark Ed)*, **2020**, *25*, 961-978.

121. Ireland, L.V.; Mielgo, A. Macrophages and Fibroblasts, Key Players in Cancer Chemoresistance. *Front Cell Dev Biol*, **2018**, *6*, 131. DOI:10.3389/fcell.2018.00131

122. Yang, J.; Li, X.; Liu, X.; Liu, Y. The role of tumor-associated macrophages in breast carcinoma invasion and metastasis. *Int J Clin Exp Pathol*, **2015**, *8*, 6656-6664.

123. Panchabhai, S.; Kelemen, K.; Ahmann, G.; Sebastian, S.; Mantei, J.; Fonseca, R. Tumor-associated macrophages and extracellular matrix metalloproteinase inducer in prognosis of multiple myeloma. *Leukemia*, **2016**, *30*, 951-954.

124. Liu, L.; Ye, Y.; Zhu, X. MMP-9 secreted by tumor associated macrophages promoted gastric cancer metastasis through a PI3K/AKT/Snail pathway. *Biomed Pharmacother*, **2019**, *117*, 109096. DOI:10.1016/j.biopha.2019.109096

125. Komohara, Y.; Takeya, M. CAFs and TAMs: maestros of the tumour microenvironment. *J Pathol*, **2017**, *241*, 313-315.

126. Astashkina, A.; Mann, B.; Grainger, D.W. A critical evaluation of in vitro cell culture models for high-throughput drug screening and toxicity. *Pharmacol Ther*, **2012**, *134*, 82-106.

127. Marino, S.; Bishop, R.T.; de Ridder, D.; Delgado-Calle, J.; Reagan, M.R. 2D and 3D In Vitro Co-Culture for Cancer and Bone Cell Interaction Studies. *Methods Mol Biol*, **2019**, *1914*, 71-98.

128. Chitcholtan, K.; Asselin, E.; Parent, S.; Sykes, P.H.; Evans, J.J. Differences in growth properties of endometrial cancer in three dimensional (3D) culture and 2D cell monolayer. *Exp Cell Res*, **2013**,

*319*, 75-87.

129. DiMasi, J.A.; Grabowski, H.G.; Hansen, R.W. The cost of drug development. *N Engl J Med*, **2015**, *372*, 1972.

130. Baras, A.I.; Baras, A.S.; Schulman, K.A. Drug development risk and the cost of capital. *Nat Rev Drug Discov*, **2012**, *11*, 347-348.

131. Nii, T.; Makino, K.; Tabata, Y. A cancer invasion model of cancer-associated fibroblasts aggregates combined with TGF-beta1 release system. *Regen Ther*, **2020**, *14*, 196-204.

132. Burdett, E.; Kasper, F.K.; Mikos, A.G.; Ludwig, J.A. Engineering tumors: a tissue engineering perspective in cancer biology. *Tissue Eng Part B Rev*, **2010**, *16*, 351-359.

133. Tajima, S.; Tabata, Y. Preparation of cell aggregates incorporating gelatin hydrogel microspheres containing bone morphogenic protein-2 with different degradabilities. *J Biomater Sci Polym Ed*, **2018**, *29*, 775-792.

134. Huang, X.; Li, Y.; Fu, M.; Xin, H.B. Polarizing Macrophages In Vitro. *Methods Mol Biol*, **2018**, *1784*, 119-126.

135. Ferrante, C.J.; Pinhal-Enfield, G.; Elson, G.; Cronstein, B.N.; Hasko, G.; Outram, S.; Leibovich, S.J. The adenosine-dependent angiogenic switch of macrophages to an M2-like phenotype is independent of interleukin-4 receptor alpha (IL-4Ralpha) signaling. *Inflammation*, **2013**, *36*, 921-931.

136. Murray, P.J.; Allen, J.E.; Biswas, S.K.; Fisher, E.A.; Gilroy, D.W.; Goerdt, S.; Gordon, S.; Hamilton, J.A.; Ivashkiv, L.B.; Lawrence, T., et al. Macrophage activation and polarization: nomenclature and experimental guidelines. *Immunity*, **2014**, *41*, 14-20.

137. Kuen, J.; Darowski, D.; Kluge, T.; Majety, M. Pancreatic cancer

cell/fibroblast co-culture induces M2 like macrophages that influence therapeutic response in a 3D model. *PLoS One*, **2017**, *12*, e0182039. DOI:10.1371/journal.pone.0182039

138. Liu, X.Q.; Kiefl, R.; Roskopf, C.; Tian, F.; Huber, R.M. Interactions among Lung Cancer Cells, Fibroblasts, and Macrophages in 3D Co-Cultures and the Impact on MMP-1 and VEGF Expression. *PLoS One*, **2016**, *11*, e0156268. DOI:10.1371/journal.pone.0156268

139. Jung, H.; Jang, H.E.; Kang, Y.Y.; Song, J.; Mok, H. PLGA Microspheres Coated with Cancer Cell-Derived Vesicles for Improved Internalization into Antigen-Presenting Cells and Immune Stimulation. *Bioconjug Chem*, **2019**, *30*, 1690-1701.

140. Mi, X.; Wang, X.; Xu, C.; Zhang, Y.; Tan, X.; Gao, J.; Liu, Y. Alginate microspheres prepared by ionic crosslinking of pickering alginate emulsions. *J Biomater Sci Polym Ed*, **2019**, *30*, 1083-1096.

141. Uyen, N.T.T.; Hamid, Z.A.A.; Tram, N.X.T.; Ahmad, N. Fabrication of alginate microspheres for drug delivery: A review. *Int J Biol Macromol*, **2020**, *153*, 1035-1046.

142. Chen, K.; Zhang, H. Alginate/pectin aerogel microspheres for controlled release of proanthocyanidins. *Int J Biol Macromol*, **2019**, *136*, 936-943.

143. Zhang, S.; Dai, W.; Lu, Z.; Lei, Z.; Yang, B.; He, B.; Zhou, H.; Cao, J. Preparation and evaluation of cefquinome-loaded gelatin microspheres and the pharmacokinetics in pigs. *J Vet Pharmacol Ther*, **2018**, *41*, 117-124.

144. Nakamura, K.; Saotome, T.; Shimada, N.; Matsuno, K.; Tabata, Y. A Gelatin Hydrogel Nonwoven Fabric Facilitates Metabolic Activity of Multilayered Cell Sheets. *Tissue Eng Part C Methods*, **2019**, *25*,

344-352.

145. Nakamura, K.; Nobutani, K.; Shimada, N.; Tabata, Y. Gelatin Hydrogel-Fragmented Fibers Suppress Shrinkage of Cell Sheet. *Tissue Eng Part C Methods*, **2020**, *26*, 216-224.

146. Chu, W.K.; Hsu, C.C.; Huang, S.F.; Hsu, C.C.; Chow, S.E. Caspase 12 degrades IkappaBalpha protein and enhances MMP-9 expression in human nasopharyngeal carcinoma cell invasion. *Oncotarget*, **2017**, *8*, 33515-33526.

147. Muscella, A.; Vetrugno, C.; Cossa, L.G.; Marsigliante, S. TGF-beta1 activates RSC96 Schwann cells migration and invasion through MMP-2 and MMP-9 activities. *J Neurochem*, **2020**, *153*, 525-538.

## 8. List of Publications

Chapter 2. Teruki Nii; Kimiko Makino; Yasuhiko Tabata. Influence of shaking culture on the biological functions of cell aggregates incorporating gelatin hydrogel microspheres. *J Biosci Bioeng*, **2019**, *128*, 606-612.

Chapter 3. Teruki Nii; Kimiko Makino; Yasuhiko Tabata. A Cancer Invasion Model Combined with Cancer-Associated Fibroblasts Aggregates Incorporating Gelatin Hydrogel Microspheres Containing a p53 Inhibitor. *Tissue Eng Part C Methods*, **2019**, *25*, 711-720.

Chapter 4. Teruki Nii; Kimiko Makino; Yasuhiko Tabata. A cancer invasion model of cancer-associated fibroblasts aggregates combined with TGF-beta1 release system. *Regen Ther*, **2020**, *14*, 196-204.

Chapter 5. Teruki Nii; Toshie Kuwahara; Kimiko Makino; Yasuhiko Tabata. A Co-Culture System of Three-Dimensional Tumor-Associated Macrophages and Three-Dimensional Cancer-Associated Fibroblasts Combined with Biomolecule Release for Cancer Cell Migration, Tissue Eng Part A, **2020**, *26*, 1272-1282.

Other Publications

1. Teruki Nii; Kimiko Makino; Yasuhiko Tabata. Three-Dimensional Culture System of Cancer Cells Combined with Biomaterials for Drug Screening. *Cancers (Basel)*, **2020**, *12*, 2754. DOI:10.3390/cancers12102754

2. Teruki Nii; Issei Takeuchi; Yukie Kimura; Kimiko Makino. Effects of the

conformation of PLGA molecules in the organic solvent on the aerodynamic diameter of spray dried microparticles. *Colloids and Surfaces a-Physicochemical and Engineering Aspects*, **2018**, *539*, 347-353.

3. Issei Takeuchi; Yumi Tetsuka; Teruki Nii; Masayuki Shinogase; Kimiko Makino. Inhalable nanocomposite particles using amino acids with improved drug content and humidity resistance, *Colloids and Surfaces a-Physicochemical and Engineering Aspects*, **2017**, 529, 387-393.

## 9. Acknowledgements

The author wishes to express his special thanks to Professor Kimiko Makino at Faculty of Pharmaceutical Sciences, Tokyo University of Science, for my chief examiner and advisor.

The author also thanks to my sub-chief examiners, Professor Tatsuya Higashi, Professor Makiya Nishikawa, Professor Toshiyuki Kaji, Professor Chikamasa Yamashita, and Professor Noriyasu Hada for their many instructive and important advice.

The present research was carried out under the continuous guidance of Professor Yasuhiko Tabata at the Institute of Frontier Life and Medical Sciences, Kyoto University, and Professor Kimiko Makino. The author is deeply indebted to Professor Tabata and Professor Makino for their constant guidance, encouragement, valuable discussion, and detailed criticism of the manuscript throughout the present work. The completion of the present research has been an exciting project and one which would not have been possible without their guidance.

The author wishes to express his special thanks to Dr. Jun-Ichiro Jo, Associate Professor of the Institute of Frontier Life and Medical Sciences, Kyoto University, for his thoughtful guidance, helpful suggestion, and intimate advice.

The author likes to take an opportunity to extend his heartily thanks to Ms. Chiaki Okada and Mrs. Kaori Takahashi, Secretary to Professor Yasuhiko Tabata and other members of Professor Tabata's Laboratory and Professor Makino's Laboratory for their kind help and kindness.

Finally, the author is deeply indebted to his parents, Keigo and Fumie.

Teruki Nii